SYSTEMS ANALYSIS OF ENGINEERED AND NATURAL MICROBIAL CONSORTIA

by

Hans Christopher Bernstein

A dissertation submitted in partial fulfillment
of the requirements for the degree

of

Doctor of Philosophy

in

Engineering

MONTANA STATE UNIVERSITY
Bozeman, Montana

May 2013

APPROVAL

of a dissertation submitted by

Hans Christopher Bernstein

This dissertation has been read by each member of the dissertation committee and has been found to be satisfactory regarding content, English usage, format, citation, bibliographic style, and consistency and is ready for submission to The Graduate School.

Dr. Ross P. Carlson

Approved for the Department of Chemical and Biological Engineering

Dr. Jeffrey Heys

Approved for The Graduate School

Dr. Ronald W. Larsen

STATEMENT OF PERMISSION TO USE

In presenting this dissertation in partial fulfillment of the requirements for a doctoral degree at Montana State University, I agree that the Library shall make it available to borrowers under rules of the Library. I further agree that copying of this dissertation is allowable only for scholarly purposes, consistent with "fair use" as prescribed in the U.S. Copyright Law. Requests for extensive copying or reproduction of this dissertation should be referred to ProQuest Information and Learning, 300 North Zeeb Road, Ann Arbor, Michigan 48106, to whom I have granted "the exclusive right to reproduce and distribute my dissertation in and from microform along with the non-exclusive right to reproduce and distribute my abstract in any format in whole or in part."

Hans Christopher Bernstein

May 2013

DEDICATION

This thesis is dedicated to my loving wife, Katharina Frank Bernstein. It's been a long road and Katha has supported me from my undergraduate degree through this Ph.D. work. This accomplishment is as much hers as my own.

ACKNOWLEDGEMENTS

I would like to acknowledge my main Ph.D. advisor, Dr. Ross Carlson, for giving me a shot at graduate school when others would not. However, I am near certain he is satisfied about his decision. For if he had not picked me up as a student; then he may have perished by accidently locking himself in a bathroom at the Goldschmidt conference, in the Czech Republic. You never know when you may need a graduate student to kick a door down. I have also received support and encouragement from my secondary thesis advisors, Drs. Jeff Heys, Brent Peyton and Robin Gerlach. Finally, I would also like to thank Dr. Bill Inskeep for additional support through the NSF-IGERT fellowship program and by acting as my field-research mentor.

TABLE OF CONTENTS

TABLE OF CONTENTS – CONTINUED

TABLE OF CONTENTS – CONTINUED

TABLE OF CONTENTS – CONTINUED

TABLE OF CONTENTS – CONTINUED

LIST OF TABLES

LIST OF FIGURES

LIST OF FIGURES - CONTINUED

LIST OF FIGURES - CONTINUED

LIST OF FIGURES - CONTINUED

ABSTRACT

Microorganisms are ubiquitous and typically exist within complex interacting communities or consortia. Microbial consortia are capable of cooperating in a coordinated fashion to extract mass and free energy from their environment. Chemical and biological engineers have long been keen to harness microbial processes for the development of technologies with applications ranging from energy capture to environmental remediation to human health. The pursuit of novel microbial biotechnologies has given rise to the relatively new discipline of microbial consortia engineering, which differs from and expands upon more traditional monoculture based practices. Many successful examples of applied and/or engineered microbial consortia mimic fundamental ecological strategies observed from nature, highlighting the importance for engineers to study natural biological phenomena. The overarching goal for this dissertation was to observe and quantitatively characterize interactions and physical phenomena occurring within select microbial consortial systems. The technical research presented here explores microbial consortia on three main fronts: (i) metabolically engineered heterotrophic systems, (ii) photoautotrophic-heterotrophic biofilm systems and (iii) naturally occurring thermo-acidophilic microbial mat systems. The metabolically engineered systems were designed to mimic a common ecological strategy involving syntrophic metabolite exchange via primary-productivity coupled with secondary consumption of potentially inhibitory byproducts (*i.e.,* acetic acid). This system exhibited enhanced biomass productivity as compared to monoculture controls. The primary-productivity concept was also explored, in a more traditional sense, by characterizing production, consumption and exchanges of oxygen within photoautotrophic-heterotrophic biofilm systems. Tight spatial coupling of oxygenic-photosynthesis and aerobic-respiration was observed in both biofuel producing and waste-water remediating biofilm communities. The role of oxygen as an important terminal electron acceptor was also investigated in pristine Fe(III)-oxide microbial mats from geothermal springs located in Yellowstone National Park (USA). For these systems, oxygen availability defines ecological niche environments that spatially govern specific community member abundances and activities. Classical chemical engineering reaction and diffusion analysis was used to model concentration dependent oxygen consumption kinetics and establish that these mats are likely mass transfer limited. Both primary-productivity and microbially mediated oxygen reactions are interrelated, cross-cutting themes throughout this dissertation. The research described here is interdisciplinary chemical engineering that utilizes fundamental microbial ecology as a foundational platform.

1. GENERAL INTRODUCTION

The primary subject matter for this dissertation relates to interactions and observable phenomena within microbial consortia. Microorganisms rarely exist as isolated monocultures in nature and are often evolved towards specific interspecies interactions and dependencies. Even in such cases that microbes exist in the monoculture or single species-state, differentiated functionality can often be observed due to heterogeneous environmental constraints. For example, a single species or consortium growing within a biofilm can experience very different environmental constraints due to intrinsic gradients of mass and/or energy sources resulting in tightly coupled community-like interactions (Stewart and Franklin 2008; Ward et al. 2006). This type of environmentally imposed functional differentiation often occurs within gradients of oxygen availability (Bernstein et al. 2013; Glud et al. 2002). Oxygen is a key environmental parameter that often dictates microbial ecological phenomena. Hence, much of the research described in this dissertation considers oxygen as an important cross-cutting theme for microbial consortia. This dissertation explores microbial consortia on three main fronts: (i) metabolically engineered heterotrophic systems, (ii) photoautotrophic-heterotrophic biofilm systems and (iii) naturally occurring thermo-acidophilic microbial mat systems. The overarching goal for this work was to observe and quantitatively characterize the interactions and physical phenomena occurring in these microbial consortia.

Microbial ecology is a firmly established scientific discipline that has been adopted by interdisciplinary chemical and biological engineers for applications such as

biochemical/biofuel production, environmental remediation, enhanced mineral extraction and human health (Bernstein and Carlson 2012; Brenner et al. 2008; Rawlings and Johnson 2007). Microbial consortia engineering has recently become a distinct area of research that is based on assembling microbial communities by enabling, encouraging or enforcing interactions between individual cell populations and their environment. Successfully engineered consortial designs typically borrow ecological principles observed in nature, highlighting the need and importance of fundamental scientific characterization from natural microbial ecosystems. The research described in this dissertation evaluates both engineered and naturally occurring microbiological systems on the molecular, cellular and community scale using fundamental microbial ecology as a foundation.

Chapter 2, in this thesis, contains a detailed introduction and literature review on microbial consortia in the context of cell factories (Bernstein and Carlson 2012). Cell factories are, living biological catalyst materials and are important to many chemical and biological engineering processes. This review chapter also highlights some fundamental ecological principles that serve as platforms for microbial consortia engineering. It defines specific types of consortia and describes some previously investigated biotechnology applications. Project specific introduction material and relevant literature reviews are contained in each technical chapter presented in this dissertation.

Synthetic microbial consortia are defined as communities of microorganisms composed of genetically manipulated or metabolically engineered strains (Bernstein and Carlson 2012). Step-wise experimental methodology for the design, construction and

characterization of synthetic microbial consortia has been presented in Chapter 3 which is formatted for publication in a Methods in Molecular Biology book titled, *Engineering Multicellular Systems* (in-press). These methods have been expanded upon those reported in Chapter 4 of this thesis which served as the preceding foundation study for engineering synthetic microbial consortia of *Escherichia coli* for syntrophic metabolite exchange. The synthetic *E. coli* consortia studies mimicked a naturally occurring ecological theme of primary-productivity complemented by secondary-consumption. The secondary-consumption employed in these systems involved oxidation of potentially inhibitory organic acid byproducts (*i.e.,* acetic acid) which relates back to oxygen as an important biological substrate and terminal electron acceptor. Microbial primary-productivity is an important re-occurring concept and another cross-cutting theme in this dissertation.

Natural primary-productivity is typically described as a trophic-station involving autotrophy and frequently photoautotrophy; capable of converting energy from photons into chemical free energy and reducing carbon dioxide into biomolecules. Primary-production within photoautotrophic microbial consortia in biofilms was also investigated in this thesis. The electron donor for these systems is water which results in molecular oxygen as a byproduct formed from oxygenic-photosynthesis. The production and spatial distribution of oxygen inside a photoautotrophic biofilm can be used to quantify oxygenic-photosynthesis, or water splitting reactions catalyzed by photosystem II (Glud et al. 2004). Both Chapter 5 and Appendix-A describe research that spatially analyzes rates of photosynthesis, aerobic-respiration and photosynthesis-coupled respiration in biofilms. For the phototroph studies described in this thesis, oxygen has been identified

as a key exchange metabolite that connects photoautotrophy with aerobic-heterotrophy. Microbial production, consumption and exchange of oxygen is a ubiquitous ecological phenomenon in almost all terrestrial and aquatic environments and has been considered here as an important design feature for engineered systems (*i.e.,* biofuel production and waste-water remediation platforms).

Oxygen availability often defines specific ecological niche environments within microbial consortia, particularly in biofilms (Bernstein et al. 2013; de Beer et al. 1994; Ward et al. 2006). This thesis contains a fundamental scientific study that investigates the role of oxygen as the principle terminal electron acceptor for thermo-acidophilic Fe(III)-oxide microbial mat communities (Chapter 6). The microbial mats form in geothermal springs located in Yellowstone National Park (USA) and are considered pristine, extremophilic ecosystems. *In situ* oxygen microsensor measurements were combined with classical chemical engineering reaction and diffusion modeling to investigate the oxygen reaction kinetics and degree of mass transfer limitation influencing these biomineralizing microbial communities.

The technical research presented in this dissertation explores microbial consortia on three main fronts: (i) metabolically engineered heterotrophic systems, (ii) photoautotrophic-heterotrophic biofilm systems and (iii) naturally occurring thermo-acidophilic microbial mat systems. The overarching goal for this work was to observe and quantitatively characterize the interactions and physical phenomena occurring in these microbial consortia. Both primary-productivity and biologically mediated oxygen reactions were used as cross-cutting themes for this work. This scientific research has

been performed through interdisciplinary chemical and biological engineering approaches that utilize fundamental microbial ecology as a foundation.

2. MICROBIAL CONSORTIA ENGINEERING FOR CELLULAR FACTORIES: IN VITRO TO IN SILICO SYSTEMS

Contribution of Authors and Co-Authors

Manuscript in Chapter 2

Author: Hans C. Bernstein

Contributions: Conception and critical analysis of review article, data collection and analysis, manuscript drafting and editing.

Co-Author: Dr. Ross P. Carlson

Contributions: Conception and critical analysis of review article, manuscript drafting and editing.

Manuscript Information Page

Hans C. Bernstein and Ross P. Carlson*
Journal Name: Computational and Structural Biotechnology Journal
Status of Manuscript:
__Prepared for submission to a peer-reviewed journal
__Officially submitted to a peer-reviewed journal
__Accepted by a peer-reviewed journal
_X_ Published in a peer-reviewed journal

Computational and Structural Biotechnology Journal
Published in CSBJ Volume 3, October 2012

*Department of Chemical and Biological Engineering, Montana State University, Bozeman, MT.
rossc@biofilm.montana.edu

2.1. Abstract

This mini-review discusses the current state of experimental and computational microbial consortia engineering with a focus on cellular factories. A discussion of promising ecological theories central to community resource usage is presented to facilitate interpretation of consortial designs. Recent case studies exemplifying different resource usage motifs and consortial assembly templates are presented. The review also highlights *in silico* approaches to design and to analyze consortia with an emphasis on stoichiometric modeling methods. The discipline of microbial consortia engineering possesses a widely accepted potential to generate highly novel and effective bio-catalysts for applications from biofuels to specialty chemicals to enhanced mineral recovery.

2.2. Introduction

Microbial consortia engineering (MCE) has become an established scientific discipline, populated by biologists, engineers, computer scientists and ecologists (Brenner et al. 2008; Brune and Bayer 2012; Momeni et al. 2011; Sabra et al. 2010). The methodology is based on assembling microbial consortia through enabling, encouraging or enforcing interactions between distinct cell populations and their environment. A common aim of MCE is to capitalize on both the capabilities of individual microbes and their interactions to create useful systems-level emergent properties like enhanced productivity, stability or metabolic functionality (Brenner et al. 2008).

The soundness of the consortia concept for bioprocessing applications is supported by observations in nature. Naturally occurring ecosystems, optimized by eons

of evolution, are almost ubiquitously organized as mixed communities. The consortia-based cell factory concept is in stark contrast with the traditional, albeit successful, bioprocess focus on monocultures and 'superbugs' capable of a wide range of concurrent processes. Engineering a single microbe to simultaneously optimize multiple metabolic tasks represents a major challenge under most situations (Brenner et al. 2008). In fact, the concept of a robust superbug, capable of all functions simultaneously, violates a widely held ecological theory related to stable, competitive ecological function; optimization of one trait typically comes at the price of other traits due to tradeoffs in metabolic resource allocation (Kneitel and Chase 2004; Law 1979; McMahon et al. 2007). Well-designed consortia will almost certainly outperform traditional monocultures. The discipline of MCE possesses a widely accepted potential to generate highly novel and effective bio-catalysts for applications from biofuels to specialty chemicals to enhanced mineral recovery although translation from laboratories to industrial facilities remains a challenge.

2.3. Ecology as the Foundation for Engineered Consortia

Microbial consortia production systems must account for the environmental relationships, distribution and abundance of participating members. Bioengineers are beginning to mine decades of rich ecological theory and experiments to design these templates (Klitgord and Segrè 2011; McMahon et al. 2007; Taffs et al. 2009). Ecological expertise provides a rational framework for dissecting nature's solutions for enabling persistence in diverse environments and for designing theory-based engineered systems.

Two established ecological theories are highlighted here because they provide promising design principles for consortial systems.

The first ecological concept is a broadly unifying theory based on resource consumption, competition and niche partitioning known as resource ratio theory (RRT) (Tilman 1982); RRT has been described as one of the most successful theories in ecology (Miller et al. 2005). This theory is used both qualitatively and quantitatively to assess outcomes between organisms competing for shared, limiting resources. These resource-based interactions can lead to either coexistence or exclusion of competitors. A recent example illustrates how photoautotrophic communities competing for three essential resources (light, nitrogen, phosphorous) can create distinct environmental resource niches which permit coexistence of multiple microbes or the competitive exclusion of all but a single microbe (Brauer et al. 2012). RRT has been adapted to consider the benefits of resource trading in consortia, highlighting conditions where coexistence is more competitive than monoculture strategies (De Mazancourt and Schwartz 2010). A major theme from RRT adapted for cooperation is a positive feedback mechanism that creates what has been termed a super-competitor unit; a design goal of many engineered systems (De Mazancourt and Schwartz 2010). A super-competitor unit is a consortium that possesses the emergent system property of enhanced resource utilization and therefore depletes resources more efficiently than the respective monocultures.

Another ecological theory relevant to MCE is the maximum power principle (MPP) initially proposed by Lotka (1922) and invoked in numerous studies including DeLong (2008) (DeLong 2008; Lotka 1922a; Lotka 1922b). While modifications to the

current interpretations of MPP have been proposed (Sciubba 2011), the general principle is valuable for analyzing consortial interactions. MPP asserts that biological systems harvest and utilize resources to build and maintain structures and gradients that permit further harvesting of resources. It also dictates that biological systems maximize fitness by maximizing power which is analogous to metabolic rate or the capacity to capture and utilize energy (measured in units of power [$J\ s^{-1}$]). If a consortium has a higher metabolic rate than the respective monocultures, it will have greater fitness because it possesses a superior ability to acquire available energy. For example based on MPP theory, a consortium that utilizes multiple substrates in parallel would have a higher metabolic rate and therefore fitness than a monoculture that utilized the same substrates sequentially. This common consortia design of parallel substrate utilization is discussed in more detail below. Both RRT and MPP are useful for examining design principles for engineering consortial interactions and provide a solid theoretical framework for testing performance.

2.4. Consortial Interaction Motifs

Natural consortia interaction strategies typically enable efficient resource usage. At the foundation of many cooperative interactions is division of labor through functional differentiation and specialization (Briones and Raskin 2003; Crespi 2001). Division of labor permits parallel or sequential processing of resources and is often credited with improving accessibility of resources to the community leading to enhanced productivity, nutrient cycling and stability against perturbation. Sequestering different reaction types within designated cells can aid overall resource usage efficiency increasing reaction

specificity and reducing the formation of side-products by localizing the reactions to favorable environments. Division of labor also permits concurrent optimization of multiple tasks, a trait useful for multistep-processes like degradation of complex biological material.

A common consortial interaction strategy that occupies a subspace of the classic division of labor motif can be termed synergistic division of resources in engineered systems. Chemical species serving as the carbon or energy source (electron donors or electron acceptors) are partitioned between community members in a noncompetitive manner based on metabolic functionality. This template permits parallel processing of substrates and has been used to construct consortia which simultaneously ferment pentose and hexose sugars, a functionality that is often unattainable in monocultures due to catabolite repression (Eiteman et al. 2008; Eiteman et al. 2009; Unrean and Srienc 2010).

Another common interaction motif is commensalism, where one community member's activity provides an ecological niche for others at no benefit or cost to itself. Commensalism is frequent in biofilms where, for instance, the consumption of oxygen by one community member establishes an oxygen gradient creating microenvironments suitable for anaerobic microbes (Bernstein et al. 2012; Brenner and Arnold 2011; Rosche et al. 2009). Another form of commensalism occurs through metabolite exchange when a producer organism secretes byproducts at no benefit or cost to itself which permits sequential consumption by other community members (Ren et al. 2007).

Mutualistic motifs are often observed in nature and are defined as relationships that benefit all participants. In cellular factory applications, mutualism can involve

syntrophy, defined here as resource exchanges or cross-feeding (Bernstein et al. 2012; Bizukojc et al. 2010; Ducat et al. 2012; Niederholtmeyer et al. 2010; Shou et al. 2007; Wintermute and Silver 2010a). Mutualistic designs have been utilized in numerous biotechnology studies including consolidated bioprocessing of cellulose coupled with biofuel production (Sabra et al. 2010; Zeidan et al. 2010; Zuroff and Curtis 2012). For instance, it is commonly demonstrated in producer-consumer relationships where an organic acid consuming community member scavenges inhibitory byproducts from a producer population (Bernstein et al. 2012; Bizukojc et al. 2010). Figure 2.1 illustrates some common ecological motifs utilized in MCE.

Consortial cellular factory systems are typically designed to express cooperative relationships while excluding competitive, predatory or cheater behaviors. However, interesting synthetic systems have been built to explore these naturally occurring themes (Balagadde et al. 2008).

2.5. Consortia Types and Case Studies

The current review discusses a variety of published consortia studies. To organize the current state of the discipline, the published systems are divided into three major classifications: artificial, synthetic, and natural consortia along with one hybrid classification: semi-synthetic consortia (Figure 2.2). This section highlights recent applications of the resource usage motifs and consortial design strategies through brief descriptions of case studies as well as tables highlighting additional noteworthy studies.

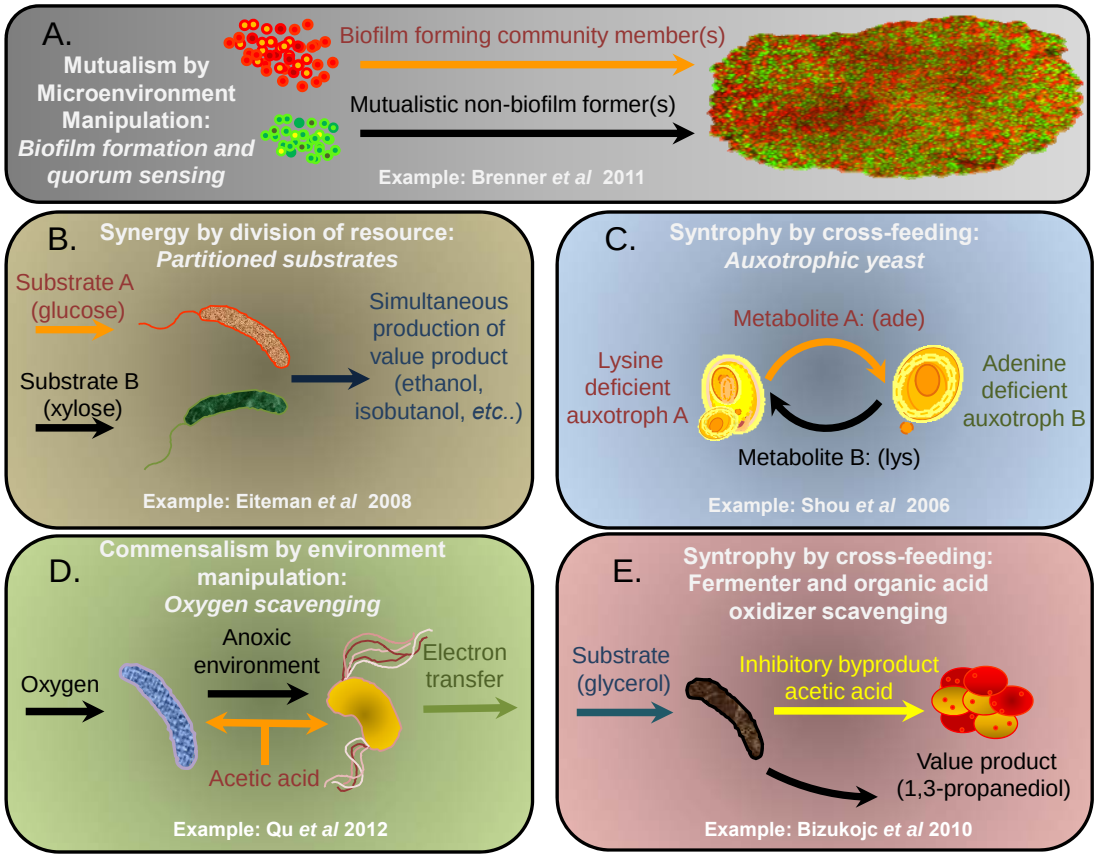

Figure 2. 1. Illustrated examples of microbial consortia organized by common interaction motifs. A) A form of mutualism by microenvironment manipulation where one population has the ability to attach to surfaces and create an environment in which a mutualistic, non-biofilm forming strain can coexist and help support growth of system. For the example presented in Brenner et al. (2011), this is accomplished via quorum sensing with synthetic cocultures. B) An example of consortial co-fermentation of hexose and pentose sugars which highlights synergy by division of resources. C) An example of syntrophic cross-feeding in synthetic auxotrophic cocultures. D) Oxygen consumption by *Escherichia coli* (blue) aids exoelectrogenic activity of *Geobacter sulfurreducens* (orange) by creating an anoxic environment. This is an example of commensalism by environment manipulation. E) An applied example of syntrophy by cross-feeding coupled with organic acid detoxification.

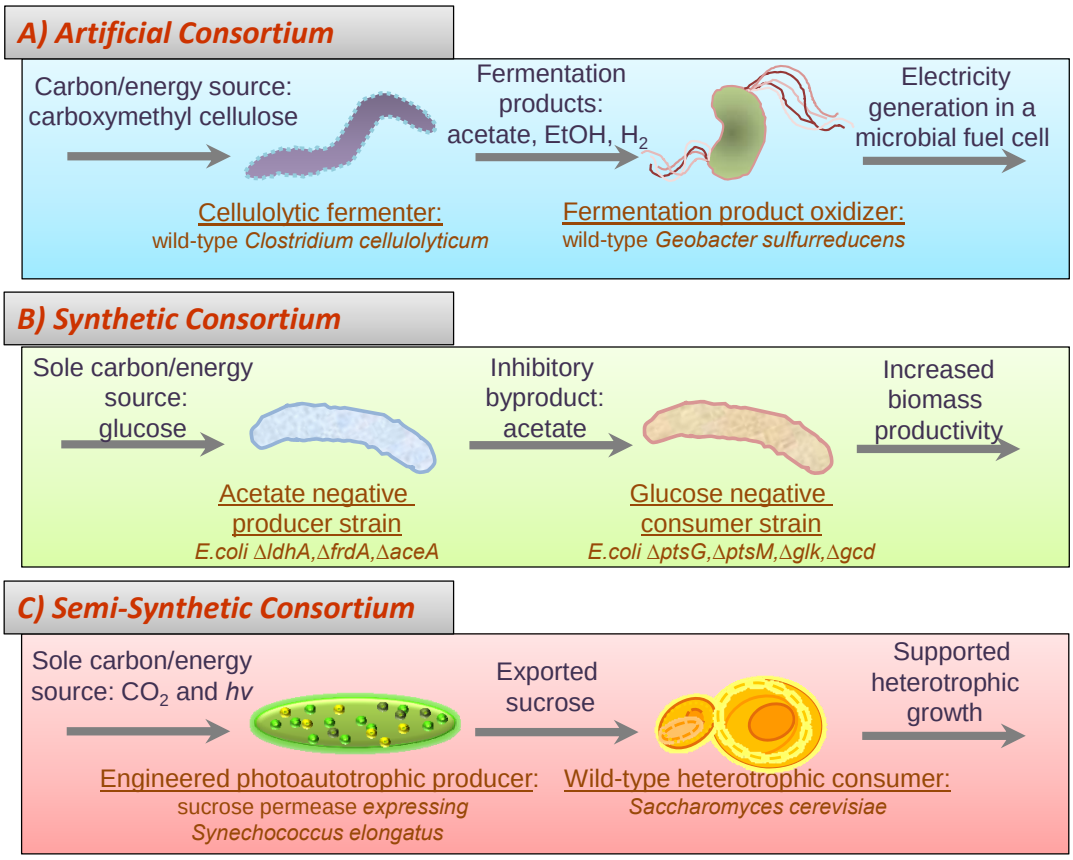

Figure 2. 2. Illustrated examples of engineered consortia categorized as A) artificial, B) synthetic and C) semi-synthetic systems. Artificial communities are composed of wild-type populations which do not coexist naturally. Synthetic microbial communities are composed of two or more metabolically engineered cell populations. Semi-synthetic communities combine metabolically engineered cells with wild-type populations. Illustrations are drawn from cited literature examples; A) Ren et al. 2007, B) Bernstein et al. 2012 and C) Ducat et al. 2012

2.5.1. Artificial Consortia

The term 'artificial' microbial consortium (AMC) is used here to describe systems composed of two or more wild-type populations whose interactions do not typically occur naturally. Assembling AMCs require *a priori* knowledge of each population's native eco-physiology; software has been developed to facilitate the pairing of potentially compatible microbes (Freilich et al. 2011; Klitgord and Segrè 2010). Industrially relevant

AMCs have been applied in multiple areas including renewable energy, food processing and bioremediation (Boonchan et al. 2000; Lee et al. 2010; Zhang and Hu 2012). The majority of AMC technologies, with the exception of biogas production, employ binary cultures while a few studies report purposefully engineered interactions between more than two microbial strains (Kim et al. 2008).

Industrial interest in alternative energy has driven MCE applications in the areas of biofuels and microbe-mediated electricity generation. Consolidated bioprocessing technologies for conversion of cellulosic feed stocks into biofuels, typically ethanol, commonly employ consortial designs (Zuroff and Curtis 2012). An AMC example from Xu *et al.* (2011) utilized a thermophilic coculture, consisting of *Clostridium thermocellum* and *Clostridium thermolacticum,* to convert either cellulose or glucose/xylose mixtures into ethanol with higher yields than the respective monocultures (Xu and Tschirner 2011). The two strains express complimentary cellulose degrading enzymes increasing the accessibility of resources to the binary culture and when fed mixtures of sugars, *C. thermocellum* catabolized glucose while *C. thermolacticum* catabolized pentose increasing consortia metabolic rate relative to the monocultures.

Microbial fuel cells (MFC) are a popular bioenergy platform. A study from Qu *et al.* (2012) demonstrated that a coculture of *Escherichia coli* and exoelectrogenic Geobacter sulfurreducens could produce more electrical power in an MFC than a monoculture of G. sulfurreducens (Qu et al. 2012). E. coli *functioned as an oxygen scavenger and consumed oxygen that leaked into the MFC, a potential problem with anaerobic MFCs (Lin et al. 2004; Nevin et al. 2011; Qu et al. 2012). This novel AMC*

based on commensalism created an environment more conducive for electrical power generation by the oxygen sensitive G. sulfurreducens.

Microalgae are becoming popular biofuel hosts because many photosynthetically fix carbon dioxide into energy rich lipids that can serve as biodiesel precursors (Chisti 2007a; Gardner et al. 2012a; Valenzuela et al. 2012). Biomass recovery from aqueous media accounts for a large portion of algal-biofuel production costs (Chisti and Yan 2011; Uduman et al. 2010); an AMC utilized by Zhang and Hu (2012) addresses this challenge using a coculture of microalgae and fungi. *Chlorella vulgaris* was grown photoautotrophically and the filamentous fungi *Aspergillus niger* was added to aid algal biomass collection by causing flocculation (Zhang and Hu 2012). The study does not report a mechanism for syntrophy but photoautotroph-heterotroph pairs are often based on mutually beneficial production and consumption of oxygen and organic acids. Additional examples of AMCs are highlighted in Table 2.1.

2.5.2. Synthetic and Semi-Synthetic Consortia

A ‘synthetic’ microbial consortium (SMC) is defined here as a system of metabolically engineered microbes which are modified through manipulations of genetic content and/or regulatory processes to establish, encourage or enforce an interaction typically coordinating resource usage. Hybrid systems comprised of wild-type and metabolically engineered populations are defined here as a ‘semi-synthetic’ consortium (semi-SMC). Synthetic and semi-synthetic microbial consortia have been built on many different interaction motifs including metabolite exchange, quorum sensing and synergistic division of resources (Bernstein et al. 2012; Brenner et al. 2007; Ducat et al.

2012; Eiteman et al. 2008; Shou et al. 2007). Some of the earliest reported SMCs were designed for bioremediation technologies (*see* Table. 2.2) (Cowan et al. 2000; Gilbert et al. 2003; Kapley et al. 1999). Several more recent studies describe SMC constructed as artificial ecosystems that have potential to be further developed as bioprocessing platforms (Bernstein et al. 2012; Brenner et al. 2007; Ducat et al. 2012) while other SMCs have been used directly as catalysts for synthesis of compounds such as lactate or methyl halides (Bayer et al. 2009; Eiteman et al. 2008; Eiteman et al. 2009).

Table 2. 1. Specific examples of artificial microbial consortia, respective interaction type and brief description. Examples are ordered based on date of publication.

Consortium Composition and Environmental Context	**Interaction Type**	**Application and Major Conclusions**	**Reference**
Marine fungus, *Pestolotia sp.*, cocultured with gram negative bacteria	Competitive interactions	Production of antibiotic, pestalone, by *Pestolotia sp.* in the presence of the bacterial strain CNJ-328	(Cueto et al. 2001)
Microbial fuel cell cocultures; *Clostridium cellulolyticum* and *Geobacter sulfurreducens*	Commensalism through metabolite exchange	Cellulose degradation by *C. cellulolyticum* produced acetate, ethanol and hydrogen used by exoelectrogenic oxidizer *G. sulfurreducens*	(Ren et al. 2007)
Papaya juice fermentation with *S. cerevisiae* and *Williopsis saturnus*	Mutualistic division of resource	Fermentation products including complex aroma compounds were produced during coculturing for papaya wine production	(Lee et al. 2010)
Fermentation of date palm spoilage by *Clostridium acetobutylicum* and	Commensalism through micro-environment manipulation	Oxygen removed from culture by *B. subtilis* encouraged fermentation of date palm spoilage by *C. acetobutylicum* to acetone, ethanol and butanol	(Abd-Alla and Elsadek El-Enany 2012)

A semi-SMC study by Ducat *et al* (2012) (Ducat et al. 2012) engineered the photoautotrophic cyanobacterium *Synechococcus elongatus* to secrete sucrose which was

consumed by a wild-type *Saccharomyces cerevisiae* population (Figure 2.2). This study reported increased cyanobacteria productivity and carbon fixation rates when sucrose was exported. The effect was attributed to sucrose serving as an electron sink relieving an over reduced cyanobacterial central metabolism. Extracellular sucrose concentrations were reported at >10 mM.

Bernstein *et al.* (2012) constructed a SMC system which established a syntrophic producer-consumer relationship between two *E. coli* strains (Bernstein et al. 2012; Bhardwaj et al. 2012). This study engineered a glucose utilizing producer strain and a glucose negative consumer strain which scavenged metabolic byproducts like acetate (Bernstein et al. 2012b). This interaction motif is analogous to strategies commonly found in naturally occurring consortia. Total biomass productivity increased in the SMC compared with monoculture controls even though the SMC 'metagenome' was identical to the wild-type monoculture genome. The partitioning and specialization of metabolic function along with a positive feedback mechanism of byproduct detoxification was vital for efficient resource usage. This system also produced spatial partitioning of strains when grown as a biofilm. The glucose negative consumer strain localized primarily to the oxic air interface where it could oxidize non-fermentable byproducts while the glucose positive strain, unconstrained by external electron acceptor availability, was found in micro-oxic and anoxic regions of the biofilm.

The use of SMC to convert renewable resources like cellulosic biomass into value-added bio-products has been the focus of several studies (Zuroff and Curtis 2012). Bayer *et al.* (2009) (Bayer et al. 2009) report a novel semi-SMC technology which

produced methyl-halides and synthetic gasoline from cellulosic feed stocks. This study expressed a methyl halide transferase enzyme in a recombinant *S. cerevisiae* strain. The recombinant *S. cerevisiae* was co-cultured with cellulytic *Actinotalea fermentans*. *A. fermentans* catabolized cellulose into inhibitory-acetate and ethanol; the recombinant *S. cerevisiae* converted the acetate into methyl-halides which concurrently detoxified the local culturing environment. Another novel aspect of this study was the coupling of biotic methyl-halide synthesis with abiotic chemical catalysis. Zeolite catalysts converted the methyl halides into gasoline-like hydrocarbons. Additional examples of SMC systems are summarized in Table 2.2.

Table 2. 2. Specific examples of synthetic and semi-synthetic microbial consortia, respective interaction type and brief description. Examples are ordered based on date of publication.

Consortium Composition and Environmental Context	**Interaction Type**	**Application and Major Conclusions**	**Reference**
Biofilm coculture of engineered *E. coli* and *Pseudomonas putida*	Mutualism: microenvironment manipulation and byproduct scavenging	Multistep detoxification of insecticide by *E. coli* SD2 and *P. putida* KT2440 pSB337 in biofilm	(Gilbert et al. 2003)
Biofilm coculture of *E. coli* expressing engineered quorum sensing systems	Mutualism though quorum sensing dependency	Developed a quorum sensing circuit-based consensus consortium and engineered co-localization in biofilms	(Brenner et al. 2007)
Cocultures of auxotrophic *E. coli* deletion mutants	Syntrophy through metabolite exchange	Demonstrated emergent benefits though mutualistic cross feeding of essential metabolites	(Wintermute and Silver 2010c)
Fluidic micro-droplets containing *E. coli* auxotrophic consortia	Syntrophy through auxotrophic amino acid exchange	Established microfluidic method for rapid screening and compartmentalization of dependent consortia strains	(Park et al. 2011)

2.5.3. Natural Consortia

The classification of 'natural' microbial consortia (NMC) is considered self-explanatory. These systems have extensive industrial applications including bioremediation, wastewater treatment, and biogas synthesis (Wagner and Loy 2002; Watanabe 2001). Highlighted case studies of NMC are not presented here because of an excellent literature base describing their use (*e.g.*, Handelsman 1998) (Handelsman et al. 1998). It is worth highlighting a study by Swenson *et al.* (2000) that actively guided the development of natural consortia toward a desirable functionality (Swenson et al. 2000a,b). This approach selects successive generations of laboratory ecosystems possessing improvements in desired functionality. The process, consisting of parental and selected offspring generations, is analogous to monoculture-based adaptive evolution experiments except it is performed at the ecosystem level. The approach has been used to alter ecosystem degradation of industrial chemicals and to enhance plant growth.

2.6. Microbial Consortia in Industry

While the field of MCE has gained popularity in recent years, the use of consortia for industrial purposes is well established. Microbial consortia have been used for commercial production of fermented food products such as vinegar, soy sauce, cheese, and bread for millennia (Caplice and Fitzgerald 1999). In addition, consortia-based industrial processes are established in a range of applications including municipal and industrial waste water treatment (Angenent et al. 2004), biogas production (Bagi et al. 2007) and environmental remediation (Sabra et al. 2010). Consortia are also used in the

mining industry to extract minerals from ore (Rawlings 2002). More detailed reviews on existing consortia-based industrial processes can be found in Sabra *et al.* (2010) and Bader *et al.* (2010) (Bader et al. 2010; Sabra et al. 2010).

2.7 *In silico* Analysis of Microbial Consortia

The highly coupled nature of microbial metabolisms and the numerous possible interactions complicates quantitative theoretical examination of microbial communities. Computational analyses are typically required to integrate the large number of metabolic components including hundreds of enzyme catalyzed reactions and interactions into testable formats. Computer models are important design tools and preliminary testing methods for consortial interactions which can save time and money. Traditional microbial ecology modeling approaches have used differential equations, game theory and stochastic methods to gain systems-based insight (Gore et al. 2009; Holmes et al. 1994; Wimpenny and Colasanti 1997). Here, the focus is on recent developments in stoichiometric metabolic models which have expanded from their traditional examination of single organisms to microbial communities (Carlson and Taffs 2009; Hanly and Henson 2011; Stolyar et al. 2007; Taffs et al. 2009; Zhuang et al. 2011).

Stoichiometric modeling methods are attractive due to their applicability to the growing ‘omics’ databases and because they do not require extensive condition-dependent kinetic parameter sets. These models require only stoichiometric knowledge of system relevant metabolic reactions and the assumption of a pseudo steady-state. The two most widely applied stoichiometric modeling approaches include (i) objective function

and constraint-based linear programming (LP) often known as flux balance analysis (FBA) and (ii) unbiased, pathway analysis known as elementary flux mode analysis (EFMA) (Carlson 2007; Carlson 2009; Orth et al. 2010; Schuster et al. 1999a). Both genome-scale and focused central carbon metabolism stoichiometric models have proven useful as metabolic engineering design tools.

Table 2. 3. Specific examples of in silico microbial consortia, in silico modeling methodology and brief description. Examples are ordered based on date of publication.

Consortium Composition and Environmental Context	***In Silico* Modeling Technique**	**Application and Conclusions**	**Reference**
Synthetic and semi-synthetic cocultures of *E. coli* deletion mutants grown in batch simulations	Genome scale dynamic-FBA	Systematic evaluation of gene deletions revealed semi-synthetic cocultures optimized for biomass yields and growth rates	(Tzamali and Reczko 2008)
Mixed microbial cultures from activated sludge in batch reactor simulations	Dynamic-FBA	Comparison of bioplastic production on substrates acetate and propionate	(Dias et al. 2008)
Syntrophic artificial coculture with *Clostridium butyricum* and *Methanosarcina mazei*	LP/FBA	1,3-propanediol producer *C. butyricum* and syntrophic byproduct scavenging by methanogenic *M. mazei*	(Bizukojc et al. 2010)
Syntrophic interactions in microbial consortia including a coculture and phototrophic biofilm system described in articles (Stolyar et al. 2007; Taffs et al. 2009)	Multiple Objective-FBA	Established a new FBA framework (OptCom) which permits multiple levels/objectives to investigate consortial interactions	(Zomorrodi and Maranas 2012)

Stolyar *et al.* (2007) (Stolyar et al. 2007) reported the earliest use of stoichiometric models to study microbe interactions. This FBA study built metabolic models to analyze mutualistic metabolite exchange between a sulfate reducer

Desulfovibrio vulgaris and methanogen *Methanococcus maripaludis*. This study accurately predicted the relative abundances of *D. vulgaris* and *M. maripaludis* in an experimental coculture.

Another example of FBA being adapted to consortia is found in Hanly *et al.* (2011) (Hanly and Henson 2011). The study used a dynamic modeling extension of FBA to simulate two different cocultures engineered for a synergistic division of resources motif to co-ferment xylose and glucose mixtures into ethanol (Hanly and Henson 2011). One study examined a synthetic coculture of *E. coli* mutants while the second system examined a semi-synthetic coculture comprised of a xylose utilizing *E. coli* mutant and a wild-type glucose utilizing S. cerevisiae. *The* E. coli *coculture simulations were contrasted with experimental data reported by Eiteman* et al. *(2008) (Eiteman et al. 2008).*

Community elementary flux mode analysis (cEFMA) has been shown to have its own attributes in the context of metabolic network modeling. Taffs et al. (2009) examined mass and energy flows through microbial community models of a well-studied phototrophic, biofilm community (Taffs et al. 2009; Ward et al. 2006). This work developed and compared three distinct methods for evaluating multi-species or multi-functional guild interactions including the use of (i) compartmentalized networks which explicitly accounted for reaction and metabolite partitioning between each specific microbial species, (ii) a collective ecosystem/metagenomic-level metabolic representation which pooled the metabolic potential of the entire consortium into a single mass-balanced unit with no attempt to assign functionality to individual microbe species, and (iii) a

nested, multi-round analysis which first data mined individual microbe-level metabolic models for ecologically relevant strategies, these strategies then served as input reactions for a second round of analysis on a community-level. Each approach had its theoretical and computational advantages and disadvantages but interestingly, a comparison of results across the methods provided additional system insight. For instance, it was possible to quantify efficiency costs associated with the logistics of partitioning ecosystem functionally and then linking the microbes using metabolite exchange. Figure 2.3 illustrates the three distinct cEFMA modeling approaches developed in this study.

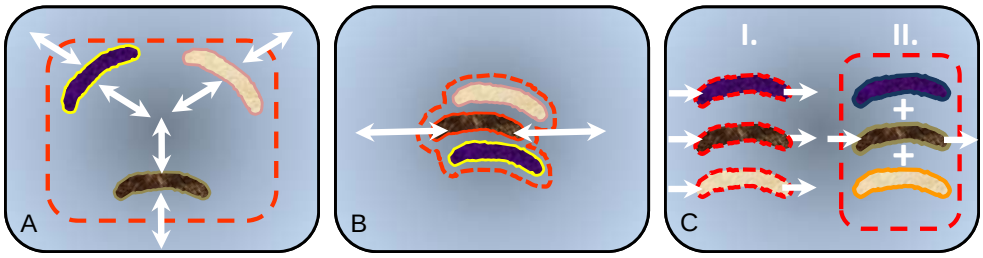

Figure 2. 2. Illustrated diagram representing three computational methods utilized in community elementary flux mode analysis (cEFMA) from Taffs et al. (2009). The dotted red lines indicate system boundaries for simulations where the interior is constrained by steady-state assumptions and the exteriors account for metabolic sources and sinks. The strategies are categorized as A) compartmentalized method in which reactions and metabolites are partitioned into specific species and metabolites can be exchanged through a mass balanced extracellular compartment, B) pooled method which combines all ecosystem relevant reactions and metabolites into a single network model without assignment to specific species and C) nested method which first computes and identifies ecologically relevant results for individual species-level models and then uses these results to perform a second, community-level simulation.

2.8 Broader Impact and Future Directions

MCE has become an established academic discipline and the collective capabilities of biologists, engineers, computer scientists and ecologists will continue to push the envelope of this multi-disciplinary field. Additional novel synthetic consortial capabilities will emerge as practical genetic systems become available for unique microorganisms, new ecological theories are tapped, and as consortia construction and control techniques mature permitting systems to be assembled from increasing numbers of interacting components. These advances will obviously be supported by continuing developments in computational systems biology and 'omics' based technologies. New MCE technologies will benefit from sustained societal driving forces ranging from fundamental scientific exploration to requirements for new technologies related to sustainable food production, improved resource acquisition like metals from ore, enhanced nutrient cycling of nitrogen, phosphorous and carbon, effective anthropogenic waste management and competitive bioenergy production. Microbial consortia cell factories and MCE have a promising future.

2.9. Acknowledgments

This work was funded by National Institute of Health grant (EB006532) and the National Science Foundation-Integrative Graduate Education and Research Training (IGERT) Program (DGE 0654336) for support to H.C.B.

2.10. Citation

Bernstein H.C., Carlson R.P. (2012) Microbial Consortia Engineering for Cellular Factories: *in vitro* to *in silico* systems. Computational and Structural Biotechnology Journal. 3 (4): e201210017. doi: http://dx.doi.org/10.5936/csbj.201210017

3. DESIGN, CONSTRUCTION AND CHARACTERIZATION METHODOLOGIES FOR SYNTHETIC MICROBIAL CONSORTIA

Contribution of Authors and Co-Authors

Manuscript in Chapter 3

Author: Hans C. Bernstein

Contributions: Conception and critical analysis of methods, data collection and analysis, manuscript drafting and editing.

Co-Author: Dr. Ross P. Carlson

Contributions: Manuscript drafting and editing.

Manuscript Information Page

Hans C. Bernstein and Ross P. Carlson*
Book Name: Methods in Molecular Biology, Engineering Multicellular Systems
Status of Manuscript:
__Prepared for submission to a peer-reviewed journal
__Officially submitted to a peer-reviewed journal
_X_Accepted by a peer-reviewed journal
__Published in a peer-reviewed journal

Springer
Submitted in August 2012

*Department of Chemical and Biological Engineering, Montana State University, Bozeman, MT.
rossc@biofilm.montana.edu

3.1. Abstract

Engineered microbial consortia are of growing interest to a range of scientists including: bioprocess engineers, systems biologists and microbiologists because of their ability to simultaneously optimize multiple tasks, to test fundamental systems-science and to understand the microbial ecology of environments like chronic wounds. Metabolic engineering, synthetic biology and microbial ecology provide a sound scientific basis for designing, building, and analyzing consortium-based microbial platforms.

The following chapter outlines strategies and protocols useful for i) *in silico* network design, ii) experimental strain construction, iii) consortia culturing including biofilm growth methods and iv) physiological characterization of consortia. The laboratory and computational methods given here may be adapted for synthesis and characterization of many other engineered consortia designs.

3.2. Introduction

Microbes do not typically exist as monocultures in nature, instead most microbial processes are multicellular. Synthetic consortia with engineered division of labor are being utilized to explore fundamental concepts associated with different types of microbial interactions (Kneitel and Chase 2004; McMahon et al. 2007). Many synthetic consortia are built around a naturally occurring strategy of syntrophy, a category of microbial cross-feeding interactions that are mutually beneficial (Bernstein et al. 2012; Brenner et al. 2008; Taffs et al. 2009; Wintermute and Silver 2010a; Wintermute and Silver 2010b; Zuroff and Curtis 2012). This chapter illustrates consortia-focused

methodologies for system design, engineering and analysis based on a previously described synthetic binary consortium composed of *Escherichia coli* deletion mutants (Bernstein et al. 2012). The engineered coculture utilizes a nature-inspired motif of strain cross-feeding which utilizes positive feedback to encourage mutualistic interactions. The consortium is composed of a glucose-positive *E. coli 'producer strain'* and a specialized byproduct consuming *E. coli 'scavenger strain'*. The functionality of this system differs from a wild-type *E. coli* monoculture system by enabling simultaneous consumption of both glucose and inhibitory byproducts such as acetate. Figure 3.1 illustrates the example engineered community metabolite exchange theme. Wild-type *E. coli*, in the presence of glucose, will preferentially consume glucose before catabolizing byproducts such as acetate due to catabolite repression (Wolfe 2005). Acetate is an inhibitory metabolite that negatively influences growth, lowers process yields due to a combination of toxicity and a diversion of substrate carbon away from desired products. Acetate accumulation represents a significant problem in large-scale bioprocess applications. The scavenger strain relieves system wide inhibition and captures substrate carbon that would otherwise be lost.

The following chapter describes approaches useful for constructing and analyzing synthetic consortia. The chapter topics include i) *in silico* metabolic network analysis, ii) experimental strain construction via gene deletions, iii) consortia culturing including chemostat and biofilm growth methods and iv) physiological characterization of consortia using HPLC, microscopy and microelectrodes. The methods presented can be used as a starting point to synthesize and characterize a wide variety of synthetic consortia.

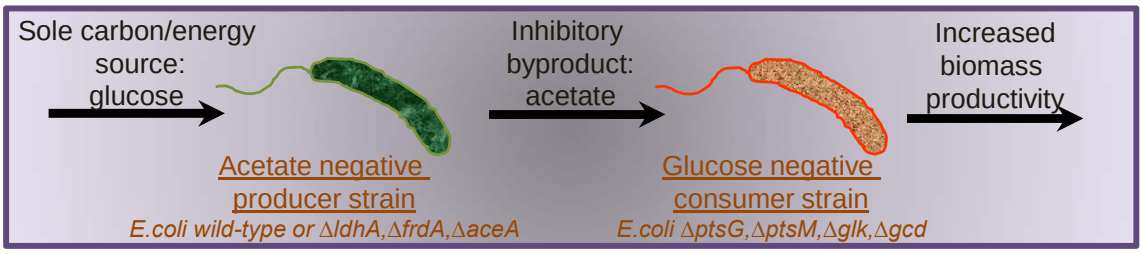

Figure 3. 1. Schematic diagram illustrating the engineered coculture described in Bernstein et al. (2012). The glucose positive strain's byproducts feed the scavenger strain. Engineered E. coli serve as a convenient host system for synthetic consortia due to their metabolic flexibility, extensive literature base and well established genetic systems.

3.3. Materials for *In Silico*, Stoichiometry-Based Metabolic Pathway Analysis.

3.3.1. Stoichiometric Modeling Software

Numerous software platforms exist for performing elementary flux mode analysis including: Cell Net Analyzer (CNA; Max Planck Innovation GmbH) (Klamt et al. 2003), Elementary Flux Mode Tool (EFMTool; ETH-CSB Zurich) (Terzer and Stelling 2006; Terzer and Stelling 2008) and METATOOL (Pfeiffer et al. 1999). Additional useful systems biology tools like COBRA (http://opencobra.sourceforge.net) and CoPasi (www.copasi.org) are also available.

3.3.2. Matrix Manipulation Software

In silico network analysis output is succinctly represented as matrices. Efficient matrix manipulation software packages such as MATLAB or open source GNU octave are recommended. For modestly sized models, spreadsheet applications like MS Excel are sufficient.

3.3.3. Stoichiometric Model

Obtain or build a stoichiometric reaction model for central carbon metabolism of interest (Carlson and Srienc 2004; Carlson 2007). In addition to manuscripts and book chapters, public model repositories contain numerous microbial models (*e.g.,* www.ebi.ac.uk/biomodels-main) (*see* Note 1).

3.4 P1 Phage Transduction and Antibiotic Resistance Cassette Curing Materials

3.4.1. Antibiotic Stock Solutions
(1000x running concentration)

100 mg/ml kanamycin, 100 mg/ml chlorotetracycline and 100 mg/ml ampicillin.

3.4.2. Luria-Bertani (Low Salt-LB) Medium Variants

LB supplemented with 25 mM Na_3Citrate; LB containing 200 µg/mL heat-inactivated (autoclaved) chlorotetracycline and 100 µg/ml ampicillin; LB agar (14 g/L agarose) containing 25 mM Na_3Citrate and 100 µg/ml kanamycin; LB agar containing 100 µg/ml ampicillin; Z-broth: LB containing 5mM $CaCl_2$ (1 M $CaCl_2$ stock solution autoclaved separately and added to LB after autoclaving).

3.4.2. Citrate Buffer

0.1 M citrate buffer pH 5.5.

3.4.3. P1 Phage Lysate

Derived from *E. coli* MG1655 wild-type or desired *E. coli* host strain) and chloroform.

3.4.4. E. coli Keio Knock-Out Collection
(Thermo Scientific)

Desired deletion mutants containing a FRT-flanked kanamycin cassette (or appropriate antibiotic selection marker) gene replacement (Baba et al. 2006; Datsenko and Wanner 2000). Temperature sensitive *pFTA* plasmid (Pósfai et al. 1997), electroporator (or materials for chemical transformation) and SOC medium (Life Technologies, CA). Appropriate PCR primers which flank desired gene deletion(s) (*see* Note 2).

3.5. Culturing Materials and Reactors

3.5.1. Culturing Medium

M9 minimal media, pH = 6.8-7.0 (6 g/L $NaHPO_4$, 3 g/L KH_2PO_4, 1 g/L NH_4Cl, 0.5 g/L NaCl, 1 ml/L of 1 M $MgSO_4 \cdot 6H_2O$ and 10 ml/L of trace metal stock solution (0.55 g/L $CaCl_2$, 0.1 g/L $MnCl_2 \cdot 4H_2O$, 0.17 g/L $ZnCl_2$, 0.043 g/L $CoCl_2 \cdot 6H_2O$, 0.06 g/L $Na_2MoO_4 \cdot 2H_2O$, 0.06 g/L $Fe(NH_4)_2 (SO_4)_2 \cdot 6H_2O$, 0.2 g/L $FeCl_3 \cdot 6H_2O$)) (Miller 1972). Carbon sources should be added to final concentrations of 4 and 2 g/L for glucose and sodium acetate respectively. Stock solutions of carbon sources, 1 M $MgSO_4 \cdot 6H_2O$ and trace metals should be autoclaved separately. M9 solid agar petri-dishes containing appropriate carbon source can be prepared by adding 14 g/L agarose to basic salt solution prior to autoclaving. Additional solutions are added after autoclaving as with M9 broth.

3.5.2. Reactors for Batch
and Continuous Culturing

1 L glass vessel (straight lipped beaker) equipped with: aseptic sampling port(s), gas diffuser, magnetic stir-bar agitator, flow inlet port (for continuous operation), and a dipstick outlet port (for continuous operation) (*see* Note 3). 250 ml Erlenmeyer shake flasks for preliminary, screening batch growth experiments.

3.5.3. Colony Biofilms

M9 agar plates (1% carbon source w/v), sterile 0.22 μm pore-25 mm diameter polycarbonate membranes (GE Water and Process Technologies, K02BP02500), sterile forceps, sterile phosphate buffer saline solution (PBS; pH = 7.4), tissue homogenizer (e.g. Polyscience Tissue Homogenizer model K-120; Polysciences) and sterile homogenizing blade(s).

3.6. HPLC Materials and Standards

3.6.1. HPLC

Agilent 1200 series HPLC (or equivalent) equipped with a variable wave length and refractive index detector (VWD and RID respectively).

3.6.2. Column and Mobile Phase

HPX-87H column (BioRad) and filtered (0.45 μm) 0.005 M H_2SO_4 in DI or nanopure water for mobile phase.

3.6.3. Standards and Dilution Matrix

All standards should be made in M9 media with no added carbon source or $MgSO_4$. The primary, multi-component standard solution used for calibration curve(s) contain: 5 g/L glucose and 3 g/L of the following salts: lactate, formate, succinate, acetate, fumarate (optional) and ethanol (optional) (*see* Note. 4). Acidifying dilution matrix: a 2X mobile phase solution (0.01 M H_2SO_4 in DI or nanopure) containing 5 g/L fucose as the internal standard.

3.7. Microscopy Preparation Materials

3.7.1. Microscope and Image Analysis Software

An epi-fluorescent microscope (Nikon Eclipse E-800 or equivalent) equipped with standard FITC and TRITC filters and appropriate objectives. Imaris (Bitplane) and Metamorph (Molecular Devices) image analysis software (or equivalent) (*see* Note 5).

3.7.2. Cryosectioning

A Leica CM 1850 cryostat (or equivalent that can be operated at −20 °C), TissueTek O.T.C. tissue embedding medium, dry ice and razor blade(s). Thin, rectangular stainless-steel coupon(s) typically 25 x 75 x 1 mm. Positively-charged microscope slides (VWR Superfrost Plus; 25 x 75 x 1 mm).

3.7.3. Fluorescent Reporter Protein Plasmids

Plasmids such as pRSET-mcitrine and pRSET-td-tomato (Dr. Tsien, UC, San Diego) or equivalents that constitutively express fluorescent yellow–green proteins and red fluorescent proteins.

3.8. Oxygen Microsensor Materials and Standards

3.8.1. Oxygen Microsensors (Microelectrodes)

Clark-type oxygen sensors equipped with guard cathode designed with ≤ 5 second response time and < 5% stirring sensitivity (OX microsensors Unisense A/S, DK). Tip diameter(s) should be 10-50 μm depending on required spatial accuracy.

3.8.2. Amplification Hardware and Data Acquisition Software

Unisense multimeter (or equivalent amplifier) coupled with SensorTrace (Unisense A/S, DK) data collection software.

3.8.3. Positioning Equipment

Standard micromanipulator with manual XYZ positioning (at least mm scale accuracy), motorized stage (at least Z-direction with μm scale accuracy), mounting stage and motor controller (must be compatible with positioning software).

3.8.4. Calibration Standards

Anoxic standard prepared from DI water containing 100 mM NaOH and 100 mM ascorbic acid. The oxic standard can be prepared from air saturated DI water (sparged with 1 liter per minute (LPM) air) (*see* Note 16).

3.9. *In Silico* Design and Testing Methodology

Engineered microbial communities can be modeled *in silico* prior to synthesis and characterization. *In silico* results can provide a rational basis for identifying gene deletion or over-expression targets that encourage or enforce interactions between strains. The authors typically utilize the unbiased, stoichiometric network analysis approach known as elementary flux mode analysis (EFMA) to construct *in silico* metabolic representations of relevant metabolisms (Schuster et al. 1999; Taffs et al. 2009). EFMA defines a network's metabolic potential based on a complete listing of the simplest, non-divisible biochemical pathways (flux distributions). Using the simplest pathways as building blocks, it is possible to perform a 'bottom-up' systems biology analysis of individual microbe and community metabolisms. Stoichiometric models do not require extensive enzyme parameter sets like most kinetic (differential equation-based) models.

Stoichiometric models typically start from annotated genome databases and literature reviews. The size and scope of the models can vary depending on research goal. The central metabolism is often sufficient to represent basic physiological characteristics although larger models termed 'genome-scale' are growing in popularity. The authors

recommend software like CNA (*see* Section 3.3.1) for building and testing stoichiometric models.

Stoichiometric models, like EFMA, typically assume a steady-state for intracellular metabolites. Intracellular metabolite synthesis and consumption are balanced *via* user-defined, exchange metabolites which represent potential physiological substrates and byproducts. Typical substrates would be electron donors and acceptors such as glucose and oxygen respectively and typical byproducts would be organic acids such as acetic acid. Designation of metabolic sources and sinks plays a critical role in model output and must be considered carefully.

To create consortia models, individual microbe models are constructed with each organism's metabolites and reactions partitioned to the appropriate mass balanced compartment. Individual microbe models are linked through an extracellular mass balanced, exchange space where metabolites are permitted to be transported from one organism to another. For example, a binary consortium model would possess four independently mass balanced compartments: microorganism 1, microorganism 2, a balanced extracellular exchange compartment, and the unbalanced extracellular source/sink compartment (*see* Figure 3.2). For alternative consortia modeling approaches see Taffs *et al.* (Taffs et al. 2009).

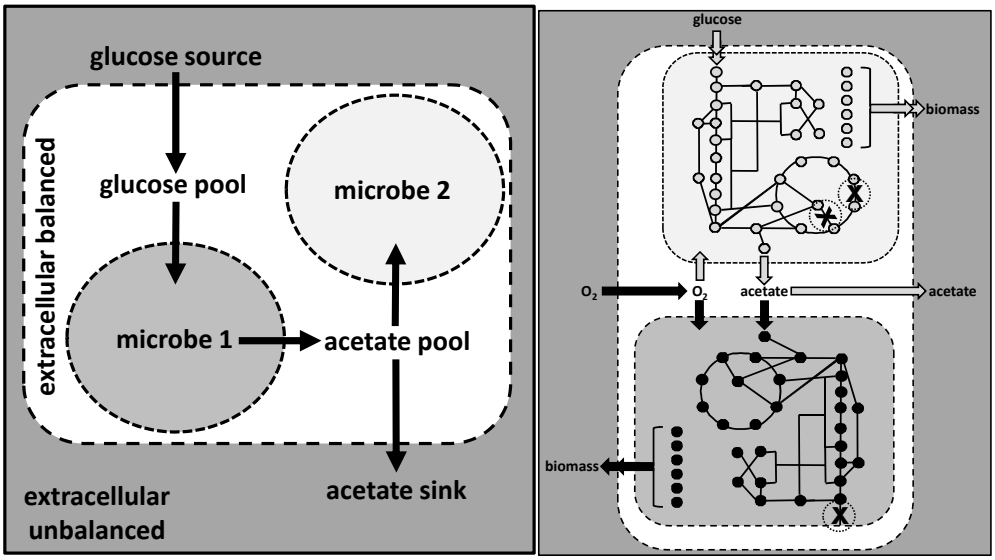

Figure 3. 2. A) Illustration of four different mass balanced compartments in a 2 microbe community elementary flux mode (cEFM). B) Illustration of an interacting cEFM model based on a metabolic design analogous to systems studied in Bernstein et al. The light gray microbe has gene knockouts in frdA and aceA while the dark gray organism has ptsG, ptsM and glk gene knockouts associated with glucose uptake, which are indicated with a single 'X'.

Consortium metabolic models are analyzed for mathematically defined metabolic pathways (elementary flux modes) using software highlighted in Section 2.1.3a. The output can be succinctly represented as a mathematical matrix where the rows represent distinct elementary flux modes and the columns represent model reactions, matrix elements represent relative fluxes through each model reaction. Zero elements indicate the model reaction is not utilized by the particular elementary flux mode.

EFMA identifies all biologically relevant, mathematically unique combinations of reactions that produce a mass balanced metabolic pathway (flux distribution). By systematically sorting these pathways using matrix manipulations, it is possible to identify which reactions are or are not required for a desired consortium functionality.

Knowing which reactions are not required, it is possible to identify rational targets for gene deletions (*see* Figure 2.1.2). Examples of output analysis for gene deletion targets can be found in (Carlson and Srienc 2004; El-Mansi et al. 2011).

3.10. Deletion Mutant Construction Methodology

The following section details a method for creating gene deletions in *E. coli* using a P1 phage transduction technique and the Keio *E. coli* mutant library. This method has been developed by combining previously reported transduction techniques (Baba et al. 2006; Datsenko and Wanner 2000; Pósfai et al. 1997). These steps may be repeated to generate mutants with multiple gene deletions. Figure 3.3 illustrates the mechanistic steps taking place during a P1-phage transduction.

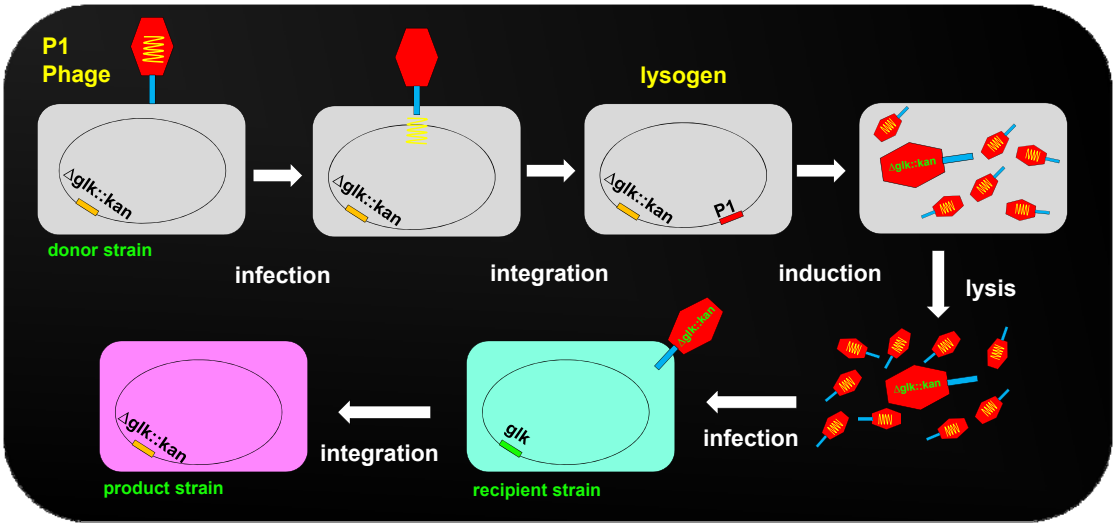

Figure 3. 3. Schematic drawing illustrating the mechanistic steps of P1-phage transduction in *E. coli*. This illustration uses the single deletion of glucose kinase (glk) as an example. Modified from schematic illustrated Medchrome: Medical and Health Articles.

i. Add 100 µl of stock P1 phage lysate (approximately 108-109 pfu/ml) to 10 ml of an overnight donor strain grown in Z-broth and diluted to OD600 = 0.5. The donor strain is typically a Keio knock-out collection strain containing a kanamycin resistance cassette. Create a control, donor strain culture with no added P1 phage. The control is compared to the P1 phage containing culture to estimate efficacy of phage lysis.

ii. Incubate the two cultures (donor strain + P1, control) for 4-6 hours at 37ºC until visually obvious cell lysis has occurred in the P1+ culture as compared to control culture. Alternatively, the P1+ culture OD600 can be followed with time (see Note 6).

iii. Centrifuge lysed P1+ culture (2000 g, 10 minutes) and transfer supernatant into sterile tubes (1.5 ml Eppendorf tube or equivalent).

iv. Add 100 µl of chloroform, vortex and store at 4ºC. P1 phage are in the aqueous phase.

v. Concentrate 6 ml of a fresh overnight recipient strain culture (target strain to receive the gene-deletion) grown in Z-broth by centrifugation (2000 g, 10 minutes).

vi. Resuspend cell pellet in 4 ml of fresh Z-broth.

vii. Prechill and maintain citrate buffer on ice (0-4ºC).

viii. Inoculate concentrated recipient strain with 100 µl of P1 phage solution (from Step 3.10.iv) and incubate at 37ºC for 20 minutes with gentle inversions to facilitate phage adsorption.

ix. Add 8 ml of cold-citrate buffer and pellet cells via centrifugation (2000 g, 10 minutes).

x. Remove unadsorbed phage by washing and centrifuging twice with 10 ml of cold-citrate buffer.

xi. Resuspend washed cells in 10 ml of LB supplemented with 25 mM Na_3Citrate and incubate for 60 minutes in a shaker at 37ºC (see Note 7).

xii. Recover cells by centrifugation (2000 g, 10 minutes) and repeat cold citrate buffer wash twice (see Step 3.10.x).

xiii. Resuspend washed cells in 300 µl citrate buffer and plate 100-300 µl of cell suspension on LB agar supplemented with 25 mM Na_3Citrate and 100 µg/ml kanamycin (or appropriate selective antibiotic). Incubate agar plates overnight at 37ºC. This step will isolate the desired E. coli deletion mutant containing the kanamycin cassette resistance marker in place of the targeted gene. Store strain in a cryogenic vial with 20% sterile glycerol at -80ºC.

xiv. Begin kanamycin resistance cassette curing process by transforming the product strain from Step 3.10.xiii with pFTA plasmid using either electroporation or chemical transformation. Immediately incubate transformant culture in SOC medium (~3 ml SOC per 100 µl transformant culture; for electroporation) at 30ºC for 30 minutes (see

Note 7 and 8). Plate 100 µl aliquot of transformed culture on LB agar + 100 µg/ml ampicillin and incubate at 30ºC.

xv. Inoculate 5 ml of LB containing 200 µg/ml heat-inactivated (autoclaved) chlortetracycline and 100 µg/L ampicillin with pFTA transformed colonies from previous step. Incubate overnight (5-10 hours) at 30ºC. This step will cure the chromosomally integrated kanamycin resistance gene by inducing expression of the pFTA flippase gene.

xvi. Spread-plate multiple volumes (from 5-100 µl) of overnight culture from previous step on LB agar (no antibiotics) to ensure growth of individual colonies. Incubate at 37ºC (see Note 8).

xvii. Screen 8-10 colonies from previous step for loss of kanamycin resistance cassette by replica plating colonies on LB agar with and without 100 µg/ml kanamycin, incubate plates at 37ºC. Successfully cured strains will not grow on LB agar plates containing kanamycin.

xviii. Verify successful chromosomal gene deletions via PCR with appropriate primers. Compare size of PCR product against both the *E. coli* wild-type control and the recombinant strain containing the kanamycin cassette (product from Step 3.10.xiii) (see Note 9). Store PCR verified product in a cryogenic vial with 20% sterile glycerol at -80ºC.

3.11. Batch and Continuous Culturing Methodology

This section describes a method used previously to characterize synthetic *E. coli* binary cultures (Bernstein et al. 2012). Achieving chemostasis in continuous cultures while maintaining two (or more) stable microbe populations can be challenging and typically requires *a priori* knowledge for growth kinetic parameters such as the maximum specific growth rates for each community member. Here, the authors recommend performing batch characterization prior to continuous growth experiments. The bioreactor based culturing method is based on a reactor type that can be assembled in the laboratory (*see* Note 3 *and* Figure. 3.4). Shake flasks are also convenient for initial culture characterization (*see* Note 10).

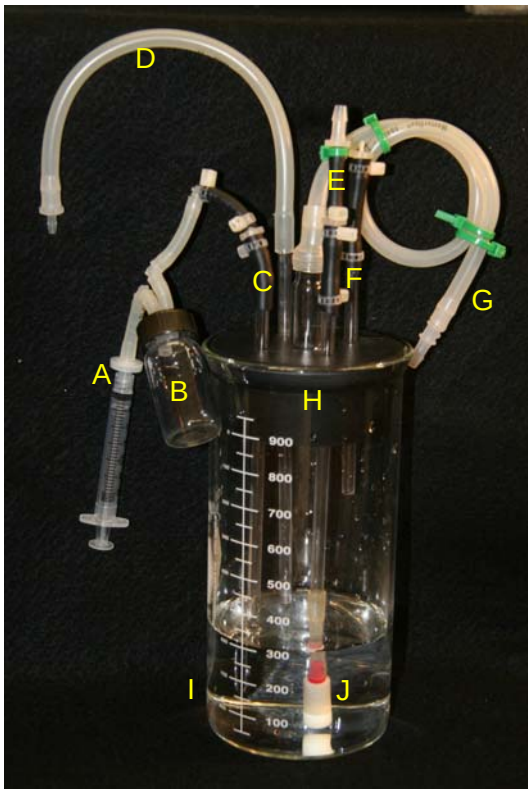

Figure 3. 4. Photograph of reactor system which can be assembled in the laboratory. A) 5 mL syringe connected via luer lock to a 0.45 µm liquid filter. The in-line liquid filter may be sterilized with the reactor. B) 20 mL collection vial with gasket sealed lid which connects (air-tight) to the syringe and sample port. C) Sample port extended into culture liquid volume via glass rod dip-stick. D) Out-channel port connected to adjustable glass dip-stick which sets reactor liquid volume during continuous operation. E) Aeration or sparge port connected to glass dip-stick coupled with porous air stone submerged in culture liquid volume. F) In-channel port connected to glass dip-stick held above culture liquid volume. G) Off-gas port coupled with tube coil to prevent air-borne contamination. H) Rubber stopper (appropriate size for 1 L cylindrical flask) with bored holes to accommodate glass tube inserts. I) 1 L cylindrical glass flask. J) Porous air stone positioned above magnetic stir bar.

i. Prepare liquid inocula from fresh overnight cultures grown in M9 plus appropriate carbon source (*i.e.,* strain specific carbon sources such as glucose or acetate). Bring fresh overnight cultures into exponential growth phase by transferring 1-3 ml to fresh media, follow growth with OD600 (see Note 10). Collect by centrifugation (2000 g, 10 minutes)

exponentially growing cells from strains cultured on carbon sources different than the chemostat feed medium, resuspend in experimental feed media (example: when chemostat feed is M9 + 4 g/L glucose; centrifuge glucose-negative mutant cells cultured with acetate medium, decant medium and resuspend in M9 + 4 g/L glucose). Dilute all cultures to an OD600 of 0.1 in experimental feed medium (see Note 13). Mix culture inocula (typically in a 1:1 volume ratio for binary cultures). 5-12 ml of OD600 = 0.1 inocula is required for reactor volumes of 300-500 ml.

ii. Fill sterile reactor vessel with 300 ml sterile M9 (containing appropriate carbon source; see Section 3.5.1). Save 5 ml of feed medium as a sterile control for downstream analysis (see Section 3.12). Inoculate reactors with binary mixture.

iii. Incubate inoculated reactor at 37ºC while agitating with a magnetic stir-bar (150 rpm). Start air sparge immediately (see Note 11). Chemostat operation is typically preceded by a batch-phase incubation long enough for the culture to obtain a cell density comparable to the known/expected steady-state value (typically 5-24 hours depending on carbon source and respective growth rates).

iv. To start chemostat operation, initiate medium feed at a volumetric flow rate appropriate for the desired dilution rate (dilution rate (D) = volumetric medium flow rate/reactor culture volume) (see Note 10). Reactor volume

must be kept constant; this is achieved with an adjustable dip-stick connected to the outflow (see Note 3 and Figure 3.4).

v. Aseptically sample reactor at regular time intervals (typically every 1-2 doubling times). Collect a sample volume large enough for OD600, pH and HPLC measurements (typically 3-5 mL; see Note 12). Some applications may also require additional sample preparation for qPCR, microscopy, etc. Reactor chemostasis can be assumed when measurements stay within +/-5% of the steady-state mean values for ≥3 residence times (residence time = 1/D).

vi. At the conclusion of chemostat operation, aseptically collect the entire culture volume. A cell dry weight vs. OD600 calibration curve can be constructed by dividing the reactor culture into 4 portions and diluting each volume with sterile experimental feed medium to obtain 4 different OD600 values. Record OD600 values, aliquot 50 ml to separate centrifuge tubes and collect cell pellets via centrifugation (2000 g, 20 minutes). Wash cell pellets twice in sterile DI water at room temperature to remove salts. Resuspend washed cells in 5 ml of sterile DI water. Transfer resuspended pellets to clean, pre-weighed 10 ml glass test tubes. It is often necessary to rinse the tube which contained the cell pellet again (once or twice with 2 ml) to successfully transfer all biomass.

vii. Incubate glass test tubes (containing 9 ml of cell suspension in DI water) in drying oven at 95-99^{0}C until dry, typically 24 hours. Allow glass test

tubes to reach room temperature. Weigh tubes containing dried cells and subtract the pre-weighed values. Use these data in combination with their respective OD600 values for constructing a cell dry weight vs. optical density standard curve for each reactor condition (see Note 13). Other methods may be used to determine the relative abundance of each community member (see Note 14).

3.12. Extracellular Metabolite Analysis (HPLC)

Comprehensive characterization of microbial consortial behavior requires the quantitative assessment of external metabolites including substrates and byproducts. High performance liquid chromatography (HPLC) is an appropriate tool for assaying many common substrates and secreted metabolites. Other methods such as gas chromatography or colorimetric assays may also be appropriate. Here, the authors present a brief description of an HPLC method used to simultaneously quantify analytes: glucose, lactate, succinate, formate, fumarate, acetate and ethanol.

i. Pre-filter all chemostat and calibration samples with a 0.45 μm syringe filter to remove particulates.
ii. Dilute calibration standard (see Section 3.6.3) in blank media (M9 with no carbon source) to a minimum of four different concentrations (see Note 4). Avoid setting concentrations below or near HPLC detection limits.

iii. Mix samples in a 1:1 ratio (v/v) with acidifying dilution matrix (see Section 3.6.3) in HPLC vials. Ensure enough sample volume for triplicate injections.

iv. HPLC method (Agilent 1200 series HPLC coupled with a Bio-Rad HPX-87H column): I) set mobile phase flow rate to 0.6 mL/min, II) set injection volume to 20 μL, III) set column and detector temperature to 40^0C (see Note 4), IV) set VWD to 210 nm, V) ensure RID is flushed with mobile phase and VI) set individual injection run time to 20% more than the retention time for the last analyte measured.

v. Inject experimental samples and standards in triplicate and ensure calibration standards are ordered from least to highest concentrations to reduce carry-over. Process chromatograms by normalizing the integrated area associated with each analyte by the corresponding signal for the internal standard (typically fucose measured on the RID).

vi. Net culture specific rate for production of byproduct α can be calculated using the following relationship: $qi = D*(C_{\alpha,out}-C_{\alpha,in})/(x)$ where D is the dilution rate(hr^{-1}), Cα is the concentration of byproduct α leaving (out) and entering (in) reactor, and x is the biomass concentration (g dry biomass/L). Culture yields can be defined using two different methods. Biomass yield on glucose can be calculated as $Y_{x/glc} = (x_{out}-x_{in})/(C_{glc,in}- C_{glc,out}) = D/q_{glc}$ where x is the biomass concentration (g dry biomass/L), C_{glc} is the appropriate glucose concentration (g glucose/L), D is the dilution rate (hr^-

^{1}), and q_{glc} is the specific glucose consumption rate (g glucose/(g dry biomass * hr)).

3.13. Colony Biofilm Culturing

Microorganisms in biofilms often display phenotypes distinct from planktonic cells. The colony biofilm (CBF) method is a no shear biofilm culturing technique which exhibits a relatively high degree of reproducibility. Colony biofilms (*see* Figure 3.5) serve as an excellent test system for engineered cross-feeding relationships due to the close physical proximity of the immobilized cells. Standardized methods for the CBF system and drop-plate enumeration techniques have been described previously (Hamilton 2003; Herigstad et al. 2001).

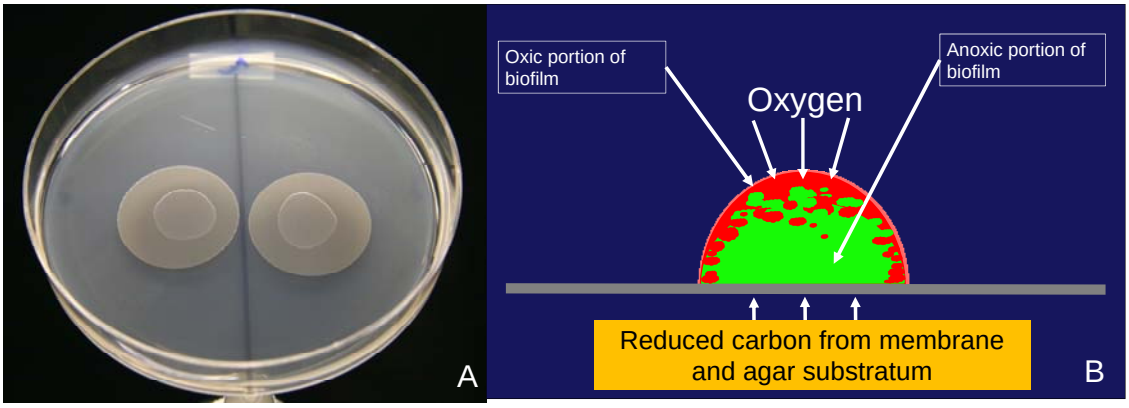

Figure 3. 5. A) Two colony biofilms cultured on M9 minimal media agar containing 2 g/L sodium acetate. B) Schematic drawing of a colony biofilm illustrating the intrinsic nutrient gradients and inherent heterogeneity associated with aerobic culturing.

i. Generate CBF inocula according to Section 3.11.i.

ii. Prepare the CBF substratum by aseptically placing 1-3 polycarbonate membranes (see Section 3.5.3) onto M9 agar plates (standard 100 x 15 mm agar plates, with appropriate carbon source) using sterile forceps. Do not exceed three CBFs per plate.

iii. Carefully pipette 100 µl of inoculum onto the center of each membrane. Allow agar/substratum to absorb liquid from inocula before transferring plates to 37^0C incubator (this helps eliminates risk of inocula culture spreading from membrane). Once biofilms are firmly attached to membranes (1-5 hours incubation), the plates may be incubated upside down to prevent accumulation of condensate.

iv. Incubate CBFs for desired time periods while aseptically transferring them to fresh M9 agar plates every 24 hours with sterile forceps.

v. To begin processing CBF sample, aseptically transfer membrane with attached biofilm into a test tube with 5 mL sterile PBS. Vortex vigorously for 30 seconds to remove cells from membrane. Carefully remove membrane from cell suspension with sterile forceps.

vi. Disaggregate cells with a tissue homogenizer at 16,000 rpm for 30 seconds. Use separate sterile homogenizing blades and/or treat with 70% ethanol for 15 seconds followed by sterile PBS rinse between each sample.

vii. The 5 ml, homogenized biofilm suspensions represent the zero dilution samples. Serially dilute samples 1:10 with sterile PBS (1 ml sample added to 9 ml PBS). Vigorously vortex each dilution sample prior to the next

sequential transfer to ensure proper mixing. *E. coli* CBFs cultured for 0-168 hours under this method are typically enumerated with the 3rd-9th dilution samples.

viii. Carefully pipette ten, individual 10 µl drops from each dilution onto LB agar (typically one agar plate can be sectioned into halves or thirds to accommodate drops from multiple dilutions) (see Note 14). Incubate drop-plates at 37^0C for 6-12 hours and enumerate colony forming units. Back-calculate through dilutions to determine number of colony forming units per original biofilm.

3.14. Microscopy Preparation Methods

Microscopy can be a valuable tool for characterizing engineered microbial consortia grown as biofilm or planktonic communities. Here, we focus on some microscopy preparation techniques useful for spatially characterizing colony biofilm (CBF) binary cultures expressing fluorescent reporter proteins (*see* Note 15). Figure 3.6A shows an example for a CBF composed from an engineered *E. coli* binary culture.

i. Culture CBFs according to methods described in Section 3.13. Use strains containing different reporter plasmids (see Section 3.7.3). Culture biofilms on agar plates containing 100 µg/ml ampicillin.

ii. Transfer each membrane containing mature biofilm to a thin rectangular stainless-steel coupon kept at room temperature with biofilm side facing up.

iii. Cover top of biofilm with tissue embedding medium (avoid bubbles)(O.C.T., TissueTek) and immediately press the bottom of the stainless-steel coupon onto dry ice. Do this quickly to minimize the spreading of the tissue embedding medium prior to freezing.

iv. Carefully remove membrane containing the frozen, embedded CBF from steel coupon with clean forceps (avoid tearing membrane). Removal is sometimes aided by applying a small amount of torque to the coupon prior to lifting.

v. Place CBF upside-down (membrane side up) on a flat dry ice surface. Carefully trim excess membrane from edges of the embedded area with razor blade. Clear trimmings before proceeding to next step.

vi. Cover bottom side of the trimmed CBF with tissue embedding medium (avoid air bubbles). Make sure the entire bottom and perimeter of CBF is covered and allow sample to freeze. Sample may now be stored for short periods of time at -80^{0}C.

vii. Transfer embedded CBF sample to a cryostat (see Section 3.7.2) and incubate at -20^{0}C for 30 min.

viii. After incubation cut embedded CBF sample in half with a clean razor blade. Append one of the cut samples (cut edge facing out) to a cold (-20^{0}C) specimen disc with tissue embedding medium.

ix. Begin cryo-sectioning sample by cutting away the rough-cut edge until the entire cross-section of the embedded CBF sample can be cut into single 5 µm slices.

x. Transfer selected 5 µm cross-section slices to surface of Plus slide(s) (see Section 3.7.2). Samples are now ready to be viewed/imaged with the chosen microscopy technique (see Note 5).

3.15. Oxygen Microsensor Analysis

Biofilms are heterogeneous accretions of cells within extracellular polymeric substances (EPS) and possess gradients of chemical species (*i.e.,* oxygen). Microbial community members often localize activity and physical location to specific regions along the oxygen gradient. Microsensor profiling can be an excellent tool for spatially characterizing microscale environmental conditions. Oxygen microsensors are well established and are a reasonably low impact method for spatially quantifying concentration gradients (Revsbech 1989b; Revsbech and Jorgensen 1986b) and are especially powerful when combined with microscopy (methods highlighted in Section 3.14; Figure 3.6B).

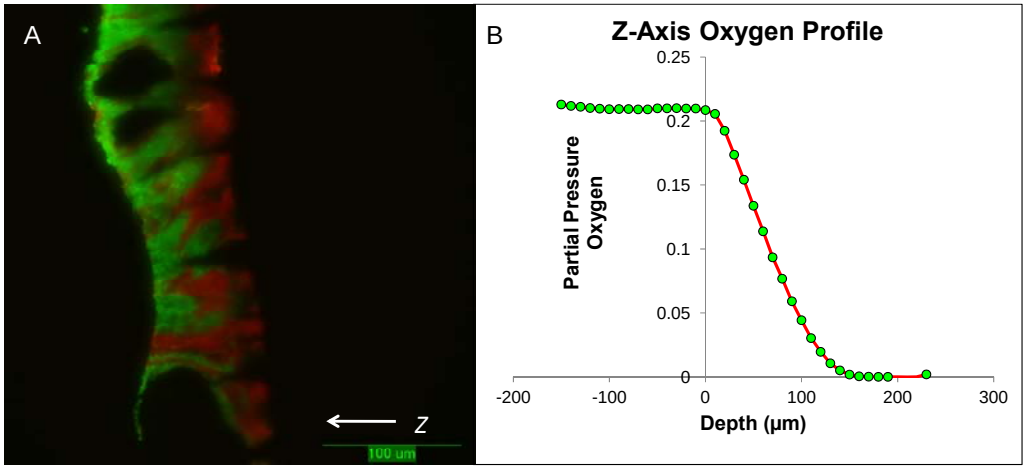

Figure 3. 6. A) Epi-fluorescence micrograph of cryo-sectioned colony biofilm composed of two engineered *E. coli* mutants; obligate glucose consumer (green) and glucose negative byproduct oxidizer (red) B) Oxygen microprofile measured in an analogous colony biofilm. The microprofile clearly shows portions of biofilm where aerobic and anaerobic microenvironments exist.

i. Culture CBFs according to methods described in Section 3.13.

ii. Pre-polarize oxygen microsensors at least 5 hours before use or until response to ambient air conditions become constant. This step removes the oxygen which may have accumulated in the sensors.

iii. Perform a 2-point calibration on sensor(s) immediately before use (see Section 3.8.4 and Note 16). Frequently check the calibration against known standards during the experiment to avoid error associated with signal drift.

iv. Position the calibrated microsensor (mounted on motorized micromanipulator) just above the biofilm surface (typically 20-100 µm). Verify that the signal is appropriate for the partial pressure of ambient air before profiling.

v. Begin profiling biofilm. Take measurements at regular time intervals appropriate to the sensor's specified response time. Set step size (distance traveled between measurements) for 1-2 times the tip-diameter of the sensor for best-case spatial resolution.

vi. Repeat profiles in multiple positions as necessary to account for biofilm heterogeneity. Process profiles in SensorTrace software or export data for custom processing (see Note 15 and 17).

3.16. Notes

Note 1.There are multiple software packages for performing EFMA which are continuously updated. Instructions and tutorials are typically included in the supporting literature. An example consortium model file with tutorial and descriptions of data processing procedures can be found in el-Mansi et al (El-Mansi et al. 2011). This two microbe model can be analyzed using the stand alone pathway analysis software METATOOL and a spreadsheet program like MS Excel (Pfeiffer et al. 1999).

Note 2. PCR primers should be designed to flank the gene to be deleted. Using DNA sequences from the coding regions of flanking genes often avoids non-unique DNA sequences found between genes. Internet based resources like EcoGene (EcoGene.org) are helpful.

Note 3. Here, the materials and methods for an inexpensive, bioreactor that can be assembled in the laboratory are presented. Figure 3.4 illustrates the custom built reactor and basic components. Incubators, peristaltic pumps and magnetic stir-plates were used

for temperature, flow and agitation control respectively. Similar reactors are commercially available from various suppliers such as DASGIP Technology (Eppendorf) or B. Braun.

Note 4. Standards for HPLC analytes ethanol and fumarate are optional. Due to evaporation, ethanol is difficult to accurately measure in moderately to heavily sparged reactors. Due to its chemical structure, fumarate may cause complications with signal overlap when using HPLC-VWD chromatographs. Column incubation temperature can significantly affect the retention time of different analytes and can be modified to decrease signal overlap. More information on the Bio-Rad HPX-87H column (and other Aminex resin-based columns) can be found at the manufacturer's website (bio-rad.com).

Note 5. The microscopy performed in the example study (Bernstein *et al.* 2012) was done with an epi-fluorescent microscope equipped with standard TRITC and FITC filters; however, in many cases scanning confocal laser microscopy may be a better option for high quality images especially for cryo-sectioned biofilms. Image analysis techniques may vary depending on application. Our studies typically use Imaris (Bitplane) and Metamorph (Molecular Devices) image analysis software.

Note 6. Once lysis has occurred, the P1-lysate should be processed within a couple hours else phage resistant microbe variants will proliferate.

Note 7. This incubation step allows time for antibiotic resistance gene expression. Typically the incubation times are 30 and 60 minutes for ampicillin and kanamycin respectively.

Note 8. Maintenance of the FT-A plasmid (*pFTA*) is temperature sensitive. Cultures containing it must be kept at or below 30ºC. Incubation at 37ºC will yield cultures which no longer replicate *pFTA* and lose their ampicillin resistance.

Note 9. Successful gene deletions can typically be verified by kanamycin resistance screening in combination with PCR. However, appropriate physiological tests (*i.e.,* presence/absence of function associated with gene deletion) should also be performed when possible.

Note 10. Transition times associated with lag, exponential and stationary growth phases for engineered *E. coli* mutants may not be consistent among each other or with wild-type cultures. It is recommended that estimates for the maximum specific growth rates (and associated doubling times) be obtained through batch studies prior to chemostat growth. Simple shake flask experiments are useful for obtaining preliminary growth rate estimates. The authors typically set the dilution rates to ≤ 90% of the measured maximum specific growth rate of the slowest growing community member to avoid chemostat *wash-out*.

Note 11. High to moderate rates of air sparging (> 0.5 volumes per min; VPM) may cause significant evaporation resulting in temperature changes within the reactor. A solution is to use an in-line humidifier incubated at the same temperature as the reactor. Higher rates of air sparging require higher humidifier volumes. Typically, 1 L of sterile DI water, incubated at 37^0C is sufficient for up to 4 days of air sparging at or below 1 liter per minute (LPM).

Note 12. For batch reactor operation, sample the minimum required volume for physiological measurements. Attempt to cumulatively sample less than 10% of the culture volume over the course of the experiment. For chemostat operation, sample reactor regularly until OD_{600}, pH and HPLC analyte measurements remain relatively constant. A practical definition of reactor chemostasis and metabolic steady-state is when respective measurements stay within +/-5% of the steady-state mean value(s) for ≥ 3 residence times (residence time = 1/D).

Note 13. Optical density (OD_{600}) is a measurement based primarily on light scattering which changes with cell density and cell geometry. Two important factors should be noted when taking optical density measurements and building cell dry weight standard curves; I) OD_{600} values above 0.3 are less accurate and should be diluted (typically 10 fold dilutions) to ensure a linear relationship with cell density, II) cell dry weight standard curves often change with different physiological conditions and gene deletions. It is important to use cells taken from chemostats at chemostasis (steady-state) and only apply standard curves to their respective growth condition and strain composition.

Note 14. Bulk enumeration values are typically reported in colony forming units (CFU) per biofilm. The drop plate enumeration technique may be modified to approximate individual populations from the biofilm or reactor culture. This can be done with antibiotic selection markers or with strain-specific physiological conditions. An example would be enumerating two sets of drop plates using two strain specific carbon sources such as glucose and acetate (specific to the example given in Bernstein *et al.*

2012). Relative abundances of community members in a biofilm or liquid culture may also be determined *via* microscopy methods if the strains are expressing reporter genes.

Note 15. Many other biofilm techniques (including microscopy and reaction-diffusion analyses) have been developed at the Center for Biofilm Engineering, Montana State University and can be found in *Biofilms: The Hypertextbook* (www.biofilmbook.com).

Note 16. Clark-type oxygen microsensors respond linearly with the partial pressure of oxygen. There are multiple methods for calibration. Factors such as temperature, ionic strength and solubility should be carefully considered before choosing a calibration medium. Avoid calibrating in liquid for obtaining concentration values from gas phase and *vice versa*. The authors recommend performing all calibrations in terms of partial pressure or % saturation which can be converted to concentration values when the appropriate medium physical properties are known.

Note 17. Oxygen microprofiles in colony biofilms (or any immobilized biological matrix) can be interpreted with classical reaction and diffusion theory. Biofilm transport theory has been described in many scientific studies and remains a field of keen interest (Beyenal et al. 2004; Stewart 2003; Xu et al. 1998).

3.17. Acknowledgements

This work was funded by National Institute of Health grant (EB006532) and the National Science Foundation-Integrative Graduate Education and Research Training (IGERT) Program (DGE 0654336) for support to H.C.B. The authors would also like to

acknowledge Reed Taffs, James Folsom, Trevor Zuroff and Betsey Pitts for their efforts associated with developing and iterating on the methods described here.

4. SYNTHETIC *ESCHERICHIA COLI* CONSORTIA ENGINEERED FOR SYNTROPHY DEMONSTRATE ENHANCED BIOMASS PRODUCTIVITY

Contribution of Authors and Co-Authors

Manuscript in Chapter 4

Author: Hans C. Bernstein

Contributions: Conception and critical analysis of research, data collection and analysis, manuscript drafting and editing.

Co-Author: Steven D. Paulson

Contributions: Data collection

Co-Author: Dr. Ross P. Carlson

Contributions: Conception and critical analysis of research, manuscript drafting and editing.

Manuscript Information Page

Hans C. Bernstein, Steven D. Paulson and Ross P. Carlson*
Journal Name: Journal of Biotechnology
Status of Manuscript:
__Prepared for submission to a peer-reviewed journal
__Officially submitted to a peer-reviewed journal
__Accepted by a peer-reviewed journal
_X_ Published in a peer-reviewed journal

Elsevier
Published in January 2011

*Department of Chemical and Biological Engineering, Montana State University, Bozeman, MT.
rossc@biofilm.montana.edu

4.1. Abstract

Synthetic *Escherichia coli* consortia engineered for syntrophy demonstrated enhanced biomass productivity relative to monocultures. Binary consortia were designed to mimic a ubiquitous, naturally occurring ecological template of primary productivity supported by secondary consumption. The synthetic consortia replicated this evolution-proven strategy by combining a glucose positive *E. coli* strain, which served as the system's primary producer, with a glucose negative *E. coli* strain which consumed metabolic byproducts from the primary producer. The engineered consortia utilized strategic division of labor to simultaneously optimize multiple tasks enhancing overall culture performance. Consortial interactions resulted in the emergent property of enhanced system biomass productivity which was demonstrated with three distinct culturing systems: batch, chemostat and biofilm growth. Glucose-based biomass productivity increased by ~15, 20 and 50% compared to appropriate monoculture controls for these three culturing systems respectively. Interestingly, the consortial interactions also produced biofilms with predictable, self-assembling, laminated microstructures. This study establishes a metabolic engineering paradigm which can be easily adapted to existing *E. coli* based bioprocesses to improve productivity based on a robust ecological theme.

4.2. Introduction

Naturally occurring microbial populations are optimized by selective pressures and evolution to competitively utilize available resources. Co-occurring species

frequently benefit from functional differentiation and metabolite exchange in an ecological strategy termed syntrophy. This consortial strategy is often credited with enabling efficient nutrient cycling and stability against perturbations (Girvan et al. 2005; Kato et al. 2008). Consortial metabolic interactions, generated by eons of selective pressure, can serve as templates for metabolic engineers to build enhanced bioprocess platforms.

The consortia concept is in stark contrast with the traditional bioprocess focus on monocultures and the creation of 'superbugs' capable of a wide range of concurrent heterologous processes. Engineering a single microbe to simultaneously optimize multiple tasks which are not consistent with its native functionality represents a major challenge (Brenner et al. 2008). In fact, the 'superbug' concept contradicts a common ecological theory regarding stable, competitive ecological functioning; optimization of one trait comes at the price of other traits due to tradeoffs in resource allocation (Carlson and Taffs 2010; Kneitel and Chase 2004). When analyzed from an ecological perspective, bioprocesses based on robust consortia should outcompete a single 'superbug' at performing multiple, complex tasks (McMahon et al. 2007).

Natural consortia typically host numerous functional guilds including consumers that specialize in catabolizing byproducts of the system's primary producers (Bateson and Ward 1988). By consuming byproducts, the consumer guild reduces feedback inhibition and metabolite toxicity while capturing reduced carbon and energy that would otherwise be lost. Monoculture-based industrial bioprocesses do not typically exhibit this functionality and often accumulate undesirable levels of byproducts such as acetic acid.

Acetic acid is inhibitory, reduces culture yields and can stall *Escherichia coli* growth at ~5 g/L (De Mey et al. 2007; Lasko et al. 2000; Majewski and Domach 1990). Byproducts like acetate also represent a waste of substrate carbon which further reduces process productivity, selectivity and yields.

Numerous metabolic engineering studies have explored strategies for reducing acetate accumulation, although each has drawbacks (De Mey et al. 2007). Deletion of the *pta-ack* pathway, which converts acetyl-CoA into acetate, reduced acetate accumulation but also prevented synthesis of acetyl-phosphate, an important global metabolic regulator (De Mey et al. 2007; Klein et al. 2007; McCleary et al. 1993; Yang et al. 1999). Other strategies have converted acetate into less toxic compounds like isoamyl acetate or acetoin (Aristidou et al. 1994; Dittrich et al. 2005). However, these compounds still represent a loss of substrate and increase host metabolic burden by requiring expression of additional recombinant pathways.

The current study designs, constructs and characterizes synthetic *E. coli* binary consortia based on the proven ecological template of syntrophy. Syntrophy can be defined broadly as any type of cross feeding between microorganisms (McInerney et al. 2009). Here, syntrophy used to describe nutritional exchanges between individual consortia members which are mutually beneficial (Wintermute and Silver 2010a). The consortia mimic the common ecological motif of a primary producer/consumer relationship (Taffs et al. 2009). Glucose-consuming *E. coli* strains serve as the systems' primary producer while a metabolically engineered glucose-negative strain concurrently consumes primary producer byproducts, improving net biomass production by reducing

inhibitory byproduct levels and by utilizing substrate carbon that would otherwise be wasted. Overall consortia functionality differs from wild-type *E. coli* monoculture functionality by enabling the simultaneous consumption of both glucose and inhibitory byproducts. Wild-type *E. coli*, due to catabolite repression, will preferentially consume glucose before catabolizing byproducts such as acetate (Nicolaou et al. 2010; Wolfe 2005). Engineered consortia that simultaneously convert glucose and xylose have been reported but they do not utilize syntrophic metabolite exchange (Eiteman et al. 2008; Eiteman et al. 2009; Minty and Lin 2010; Trinh et al. 2006). Additional engineered consortia studies have examined interactions between strains that complement auxotrophic deficiencies but with these systems; accumulation of inhibitory, yield lowering byproducts is still a major challenge (Wintermute and Silver 2010b). The current study focuses on a bioprocess ready platform that demonstrates engineered syntrophy enhancing system performance in batch, continuous, and biofilm based culturing strategies, establishing a new paradigm for metabolic engineering.

4.3. Materials and Methods

4.3.1. Bacterial Strains

E. coli K-12 MG1655 strains were used for all experiments. *E. coli* MG1655 gene deletion strains were constructed using the KEIO mutant library and successive rounds of P1 viral transductions (Baba et al. 2006; Datsenko and Wanner 2000). Gene deletions were confirmed via PCR and physiological studies.

4.3.2. Medium

All reported growth experiments were performed in M9 media (6 g/L $NaHPO_4$, 3 g/L KH_2PO_4, 1 g/L NH_4Cl, 0.5 g/L NaCl, 1 ml/L of 1 M $MgSO_4 \cdot 6H_2O$ and 10 ml/L of trace metal stock solution (0.55 g/L $CaCl_2$, 0.1 g/L $MnCl_2 * 4H_2O$, 0.17 g/L $ZnCl_2$, 0.043 g/L $CoCl_2 \cdot 6H_2O$, 0.06 g/L $Na_2MoO_4 \cdot 2H_2O$, 0.06 g/L $Fe(NH_4)_2(SO_4)_2 \cdot 6H_2O$, 0.2 g/L $FeCl_3 \cdot 6H_2O$)). Utilized carbon sources and concentrations are given below. All stock solutions were either autoclaved or filter sterilized separately (Miller 1992). Initial medium pH was adjusted to 6.8. Cell enumeration was performed on non-selective Luria-Burtani (LB) media. When necessary, agar was added at 14 g/L.

The experimental glucose concentrations (4 g/L) for batch and chemostat studies were designed to 1) permit comparison with a previously reported study (Trinh et al., 2006), 2) establish glucose-limited chemostat conditions with stabile, predictable steady-state conditions and 3) facilitate comparison of batch and chemostat culture properties.

4.3.3. Batch Culturing

Batch experiments were performed using either shake flasks or batch reactors. Shake flask cultures were grown in 250 ml baffled shake flasks containing 50 ml of M9 minimal media containing an appropriate carbon source (4 g/L glucose or 2 g/L sodium acetate). Shake flasks were incubated at 37°C and agitated at 150 RPM. Samples from the shake flasks were collected aseptically. Total sample volumes collected remained less than ~10% of the total initial culture volume.

Batch reactors (1 L) were operated with 300 ml of M9 with an appropriate reduced carbon source. Batch reactors were incubated at 37°C, agitated with magnetic stir

bars at 250 RPM and sparged with air at 1 L/min. Reactors were inoculated with 12 ml of culture, diluted to 0.2 OD_{600}, per strain. Inocula were prepared with fresh overnight cultures grown in M9 minimal media containing either 4 g/L glucose or 2 g/L sodium acetate, depending on strain. Samples were collected aseptically at regular time intervals and analyzed for OD_{600}, pH and extracellular metabolite concentrations.

4.3.4. Chemostat Culturing

Chemostat reactors (1 L) were operated with 300 ml of M9 medium with an appropriate reduced carbon source (4 g/L glucose or 2 g/L sodium acetate). Chemostats were incubated at 37°C and agitated with magnetic stir bars at 250 RPM. High-aeration conditions had an air sparge rate of 1 L min^{-1} while low-aeration cultures had an air sparge rate of 0.15 L min^{-1}.

Dilution rates (D) were set at 0.1 hr^{-1} to accommodate the specific growth rate of the acetate specialist strain. Chemostat inocula were prepared in the same manner as reported for batch reactors except 5 ml of inoculum was used for each reactor. Binary systems were inoculated with an initial 1:1 ratio of each strain. Reactors were operated until they achieved steady-state. Steady-state was defined as less than 5% changes in OD_{600}, pH and glucose after a minimum run of 6 residence times. All chemostat experiments were run in triplicate. Biomass concentrations (X) were determined from OD_{600} vs. cell dry weight (CDW) correlations specific to each reactor condition and strain composition. CDW samples were collected by centrifuging 50 ml of culture broth (1800 g for 20 min). Cell pellets were washed with sterile de-ionized water twice, dried for 24

hours at 99°C in 10 ml glass test tubes, and weighed when the samples reached room temperature.

4.3.5. Colony Biofilm Culturing

Colony biofilm cultures were grown according to previously described methods (Anderl et al. 2000; Anderl et al. 2003; Hamilton 2003; Walters et al. 2003; Zuroff et al. 2010). Colony biofilm culturing systems consisted of M9 agar plates (1% glucose(m/V)) and sterile 0.22 μm pore, 25 mm diameter polycarbonate membranes (GE Water and Process Technologies, K02BP02500). Membranes were aseptically placed on agar plates and inoculated with 100 uL of an exponentially growing culture (diluted to $OD_{600} = 0.1$) per strain. Inocula were prepared by collecting exponentially growing cells with centrifugation (1800 g for 10 min) and resuspending in fresh media containing only glucose. Biofilms were incubated at 37°C and aseptically transferred to fresh agar plates every 24 hours. After 72 hours, colony biofilms were aseptically transferred to 5 mL of sterile phosphate buffered saline (PBS) and vortexed vigorously for 30 seconds to separate cells from the membrane. The membrane was discarded and the biofilm suspension was disaggregated for 30 seconds using a tissue homogenizer. The homogenized cell suspension was serially diluted and number of colony forming units (CFU) per biofilm was determined using the drop-plate method (Herigstad et al. 2001).

4.3.6. Reporter Protein Based Analysis of Colony Biofilms

Consortia members were transformed with fluorescent reporter protein expressing plasmids to enable visualization of strain position within intact biofilms. Plasmids

pRSET-mcitrine and pRSET-td-tomato were used to constitutively express fluorescent yellow-green proteins and red fluorescent proteins respectively (Dr. Tsien, UC, San Diego). Reporter expressing strains were cultivated according to the colony biofilm methods described previously for 7 days. Mature biofilms were covered with TissueTek O.T.C. tissue embedding medium and frozen on dry ice. Embedded biofilms were cut into 5 μm thick sections using a Leica CM 1850 cryostat operated at -20°C. Sectioned samples were imaged using epi-fluorescent microscopy (Nikon Eclipse E-800) and standard FITC and TRITC filters. Images were analyzed quantitatively for spatially dependent strain abundance using Imaris (Bitplane) and Metamorph (Molecular Devices) image analysis software.

4.3.7. Extracellular Metabolite Analysis

Extracellular metabolite concentrations (glucose, acetate, lactate, fumarate, succinate and formate) were measured using an Agilent 1200 HPLC. Samples were filtered (0.45 μm) to remove debris; 20 μl filtrate samples were injected on an HPX-87H column (Bio-Rad) at 40°C, with a 0.005M H_2SO_4 mobile phase (0.6 ml/min) and analyzed with a variable wave length detector (VWD) and a refractive index detector (RID). Glucose concentrations were determined using the RID and calibration curves while organic acid concentrations were measured using the VWD (210 nm) and the RID with appropriate calibration curves.

4.4. Results

4.4.1. Construction and Adaptation of Glucose Negative, Acetate Specialist Strain

A glucose negative *E. coli* MG1655 strain (*ΔptsGΔptsMΔglkΔgcd*) was designed using a previously described *E. coli* stoichiometric model (Carlson, 2009) and built using the KEIO deletion library (materials and methods). The deletion mutant, designated strain 403, was adapted for growth on acetate over 100 generations in a chemostat (D = 0.1/hr, M9 medium with 2 g/L sodium acetate, pH 6.8). Following adaptation, culture samples were streaked for isolation on M9 and acetate agar plates.

Specific growth rates (μ) for five adapted isolates were compared to the un-adapted parent deletion mutant (strain 403). All five isolates exhibited an improved specific growth rate on M9 + 2 g/L sodium acetate as compared to the parent strain (Table 4.1). Isolate 5 exhibited the largest increase in maximum specific growth rate (μ_{max} = 0.152 hr^{-1} +/- 0.009) as compared to the parent deletion mutant (μ_{max} = 0.116 hr^{-1} +/- 0.007). This isolate was designated strain 403G100 and was used for all reported experiments.

Strain 403G100 preferentially consumed acetate even when cultured in M9 medium containing both sodium acetate and glucose (Fig. 4.1). Consistent with design, the strain did not grow in M9 medium containing glucose as the sole reduced carbon source.

Table 4. 1. Growth rate properties of *E. coli* deletion mutant 403 (ΔptsGΔptsMΔglkΔgcd) following 100 generation acetate-limited chemostat adaptation. Five isolates recovered from the adaptation experiment were analyzed for improved growth on minimal M9 + acetate medium. % increased growth rate refers to improvement in isolate specific growth rate relative to non-adapted parent deletion mutant. Specific growth rates are reported ± 1 standard deviation from replicate shake flask cultures. Isolate 5 (strain 403G100) was used for all reported batch, chemostat and biofilm studies.

Strain	Specific Growth rate (hr^{-1})	Doubling Time (hr)	% Increased Growth Rate
403 Isolate 1	0.140 ± 0.003	4.95	21%
403 Isolate 2	0.138 ± 0.012	5.02	19%
403 Isolate 3	0.132 ± 0.010	5.25	14%
403 Isolate 4	0.128 ± 0.009	5.42	10%
403G100 Isolate 5	0.152 ± 0.009	4.56	31%
403 Original	0.116 ± 0.007	5.98	NA

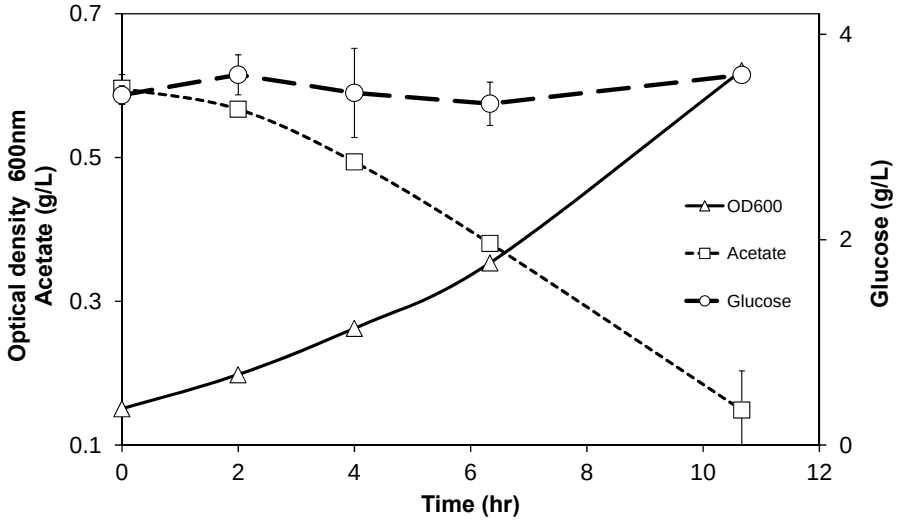

Figure 4. 1. Preferential acetate catabolism by glucose negative strain 403G100 cultured in M9 medium containing glucose and sodium acetate. Strain 403G100 did not grow in M9 medium containing glucose as the sole electron donor. Error bars represent ± 1 standard deviation from two independent shake flask experiments.

4.4.2. Binary Consortium
Batch Growth Characterization

A synthetic binary consortium, comprised of glucose negative 403G100 and wild-type MG1655, was characterized and compared to monoculture properties using batch growth (Fig. 4.2 and 4.3). Wild-type monoculture controls reached a final cell density of 1.04 ± 0.02 g CDW/L over 30 hours while the glucose negative strain 403G100 monoculture controls showed negligible growth on glucose (Fig. 4.2B). The binary consortium produced higher final biomass titers, reaching a final cell density of 1.20 ± 0.04 gCDW/L, a ~15% increase as compared to the monocultures. Consortium and wild-type monoculture volumetric glucose consumption rates were effectively identical; both cultures consumed all glucose within 12 hours (Fig. 4.2A). The consortium produced ~15% more biomass in the same 12 hour exponential growth phase as compared to the wild-type monoculture resulting in a ~15% higher volumetric biomass productivity ($P_{batch} = \Delta x/\Delta t$). Reported values are means from three independent experiments ± one standard deviation. Wild-type monoculture growth rates, glucose yields and acetate yields are consistent with previous publications for this *E. coli* K-12 laboratory culture (Trinh et al. 2006; Trinh et al. 2008).

The binary consortium had an increased biomass yield on glucose and a corresponding reduction in byproduct accumulation as compared to the wild-type monoculture (Fig. 4.3A). Binary cultures consistently synthesized more biomass per acetate produced during batch growth (Fig. 4.3B). The reduction in acetate accumulation kept the binary consortium pH higher than the wild-type monoculture likely reducing metabolic stress. In addition, unlike the monoculture, the consortium did not require a

metabolically expensive diauxie-based enzyme shift from glucose catabolism to acetate catabolism further improving glucose yields.

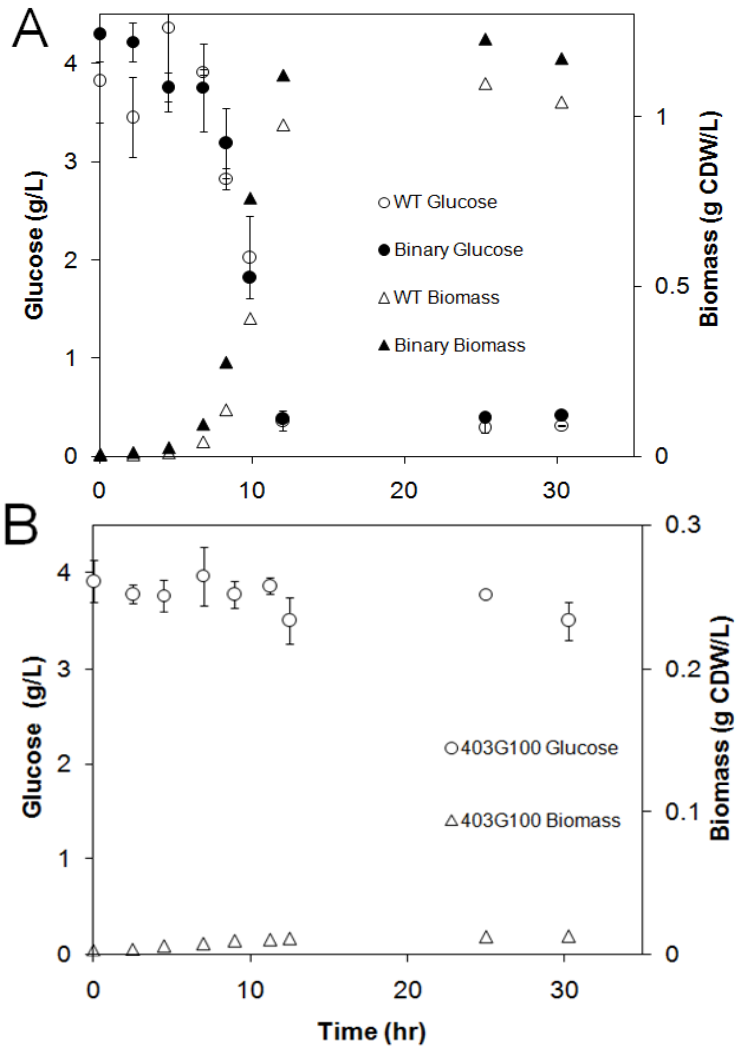

Figure 4. 2. Binary consortium and monoculture batch growth. A) Binary consortium (403G100 + WT) and wild-type monoculture batch growth glucose and biomass concentration time profiles. All experiments were performed with M9 medium supplemented with glucose as the sole reduced carbon source. Error bars represent ± 1 standard deviation from three independent batch experiments. B) Strain 403G100 monocultures did not demonstrate significant growth or glucose consumption. All error bars represent ± 1 standard deviation from three technical replicates of measurements.

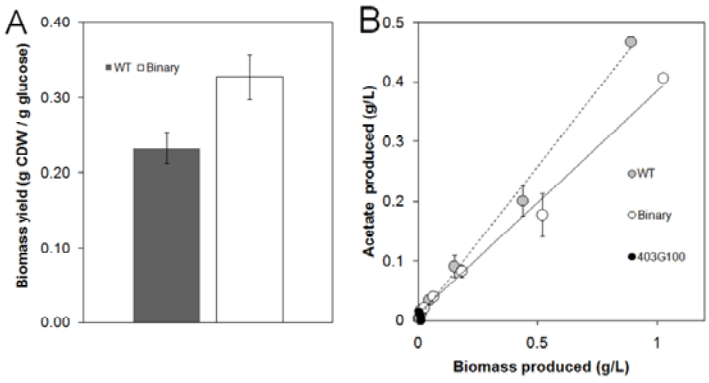

Figure 4. 3. Binary consortium (403G100 + WT) and monoculture batch growth physiological parameters. A) Biomass yield on glucose (g CDW/G glucose) for the engineered binary consortium and wild-type monoculture control. Glucose negative strain 403G100 did not produce significant growth on glucose. Error bars represent ± 1 standard deviation from three independent batch experiments. B) Exponential growth phase acetate accumulation plotted as a function of biomass from a representative batch growth experiment. Error bars represent ± 1 standard deviation from three technical replicates of measurements.

4.4.3. Binary Consortium

Continuous Growth Characterization

Synthetic consortium properties (wild-type + strain 403G100) were compared to monoculture controls under steady-state chemostat growth (D=0.1/hr). The chemostat dilution rate was selected to accommodate planktonic strain 403G100 growth (μ_{max} = 0.116 hr^{-1}). The experiments were performed using two distinct aeration regimes, high-aeration and low-aeration (3.3 vpm and 0.5 vpm respectively, vpm = culture volumes per minute). The two aeration regimes were selected because the major metabolite exchanged by the binary culture is thought to be acetate and acetate secretion is negatively correlated to oxygen availability (Alexeeva et al. 2002).

Under both aeration regimes, the binary culture exhibited a ~20% higher steady state biomass concentration which corresponded with a ~20% lower specific glucose

uptake rate as compared to the wild-type monocultures (Figs. 4.4 and 4.5). Consequently, the binary consortia biomass productivity ($P_{chemostat}$ = xD) was ~20% higher than the monocultures under both aeration regimes.

As expected, high-aeration (3.3 vpm) cultures had higher biomass productivities than low-aeration (0.5 vpm) cultures. Low-aeration growth conditions resulted in ~3-fold higher specific glucose uptake rates and ~3-fold lower biomass productivity, as compared to the high-aeration cultures. Wild-type monoculture yields and specific glucose uptake rates for the high-aeration chemostats were comparable to previously reported aerobic chemostat values (Trinh et al. 2006; Trinh et al. 2008).

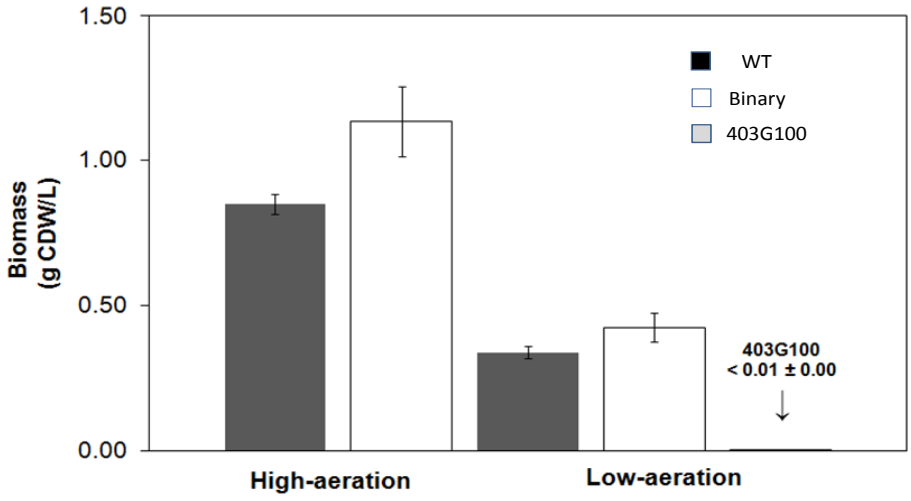

Figure 4. 4. Binary consortium and monoculture biomass concentrations during glucose-limited chemostat cultivation. Cultures were grown continuously in glucose-limited chemostats (D= 0.1/hr) under two different aeration regimes (high-aeration = 1 L/min, low-aeration = 0.15 L/min air sparge). Strain 403G100 monocultures had negligible steady-state biomass concentrations (below detection limit of 0.01 g CDW/L) for both aeration regimes. All error bars represent ± 1 standard deviations from three independent chemostat experiments.

During low-aeration growth, both the binary and wild-type cultures secreted significant amounts of acetate. The binary consortia demonstrated a decreased specific acetate production rate (Fig. 4.4). During high aeration growth, the binary consortium did not produce measurable amounts of acetate while the wild-type monocultures secreted detectable, albeit small, amounts of acetate. Acetate specialist monocultures produced negligible biomass (below detection limit of 0.01 g CDW/L) and consumed negligible glucose during glucose only chemostat experiments (Fig. 4.4).

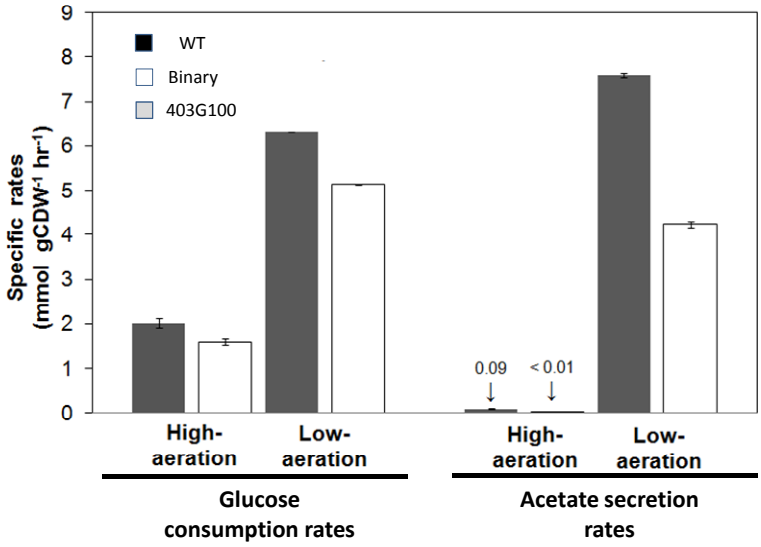

Figure 4. 5. Binary consortium and monoculture chemostat specific glucose uptake and acetate secretion rates. Cultures were grown continuously in glucose-limited chemostats (D= 0.1/hr) under two different aeration regimes (high-aeration = 1L/min, low-aeration = 0.3 L/min). High-aeration data error bars represent ± one standard deviation from three independent chemostat experiments. Low-aeration data error bars represent ± 1 standard deviation from three technical measurements of a representative data set. The low-aeration cultures were highly sensitive to small differences in the rotameter controlled sparge rate. All three low-aeration chemostat experiments exhibited the presented trends.

4.4.4. Binary Consortium Colony
Biofilm Characterization

Binary consortium (403G100 + wild-type) and appropriate monocultures were also grown as biofilms to compare culture productivity under non-planktonic conditions. Biofilms represent a common, naturally occurring physiological growth state for microbes and a promising bioprocess platform with high cell densities, high volumetric productivities and increased stress tolerance (Gross et al. 2007; Rosche et al. 2009).

When grown for 72 hours, the binary consortium exhibited higher culture productivities ($P_{biofilm} = \Delta CFU/\Delta t$) than either monoculture individually. The binary system produced approximately 50% more CFUs per biofilm than the sum of the wild-type and 403G100 monocultures (Fig. 4.6). The large improvement in productivity is likely due to the close spatial proximity of the two strains which facilitates and rewards syntrophic exchanges.

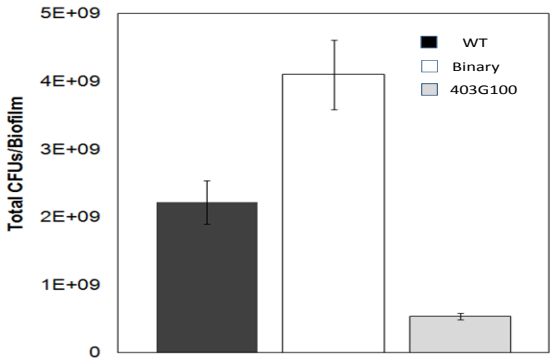

Figure 4. 6. Colony forming units per biofilm (CFUs/biofilm) for the binary consortium (403G100 + WT) and monoculture controls. All biofilms were cultured on M9 agar containing 1% (w/v) glucose as the sole reduced carbon source. CFUs were enumerated on non-selective (LB) agar. The binary consortium produced more CFUs/ biofilm than the sum of both monocultures. Error bars represent ± 1 standard deviation from at least three independently cultured biofilms.

4.4.5. Dual Engineered Binary Consortium

The primary producer/secondary consumer template was further developed with a dual engineered binary consortium. An engineered primary producer strain (*E. coli* MG1655*ΔaceAΔldhAΔfrdA*) was designed and constructed to emphasize metabolite exchange thought to be important to the observed syntrophic division of labor. The strain was engineered to prevent acetate from serving as the sole reduced carbon source via an *aceA* deletion (glyoxylate shunt) and to increase flux toward acetate via removal of lactate and fumarate fermentative pathways (*ΔldhA* and *ΔfrdA* respectively). The original gene deletion mutant was adapted to growth on glucose minimal medium over 100 generations of carbon-limited chemostat growth (M9 + 4g/L glucose, D=0.3 hr^{-1}). Recovered isolates were screened for increases in specific growth rate relative to original deletion mutant. The selected isolate designated strain 307G100 demonstrated a μ_{max} of 0.49 ± 0.02 hr^{-1} compared to 0.43 ± 0.02 hr^{-1} for the original deletion mutant. Specific growth rates were averaged from three individual experiments, ± one standard deviation. As designed, strain 307G100 did not grow on acetate as the sole reduced carbon source (data not shown).

Functionality of the dual engineered consortium was tested using batch shake flask and colony biofilm cultures. During batch growth, the dual engineered consortium (strains 307G100 + 403G100) and the control monoculture (strain 307G100) exhibited nearly identical volumetric glucose consumption rates (Fig. 4.7A). The consortium demonstrated a ~10% increase in biomass productivity after the 24 hour exponential growth phase relative to the monoculture control (Fig. 4.7A). As expected, the

consortium accumulated less acetate than the monoculture. Acetate concentrations, measured during stationary phase, were 2.83 ± 0.18 and 2.41 ± 0.01 for the 307G100 monoculture and dual engineered consortium respectively. The dual engineered consortium exhibited a ~50% increase in biomass productivity relative to the monoculture controls when cultured as a biofilm (Fig. 4.7B).

The dual engineered biofilm cultures demonstrated an additional emergent property; the strains self-organized into a laminated biofilm (Fig. 4.8A). The two strains were tagged with different fluorescent proteins (pRSET-mcitrine and pRSET-td-tomato, Tsien, San Diego) to permit visual identification. Control biofilms, comprised of two 307G100 strains expressing different fluorescent proteins, did not exhibit the same lamination nor did they grow to the same thickness as the engineered consortium (Fig. 4.8C). Quantitative image analysis of the average fluorescent intensity supported the visual observation of consortium based lamination (Fig. 8B and 8D). The spatial assembly of the acetate consumer strain (403G100 pRSET-td-tomato) at the biofilm air interface is expected since this is where oxygen and acetate concentrations are believed to be highest. Hence, the spatial pattern formation observed in the current study is the result of engineered reaction, spatial substrate availability and diffusion phenomena (Kondo and Miura 2010). Self-assembly of strain specific biofilm spatial structures have previously been observed in synthetic microbial consortia built upon very different culturing techniques and genetic platforms (Brenner and Arnold 2011).

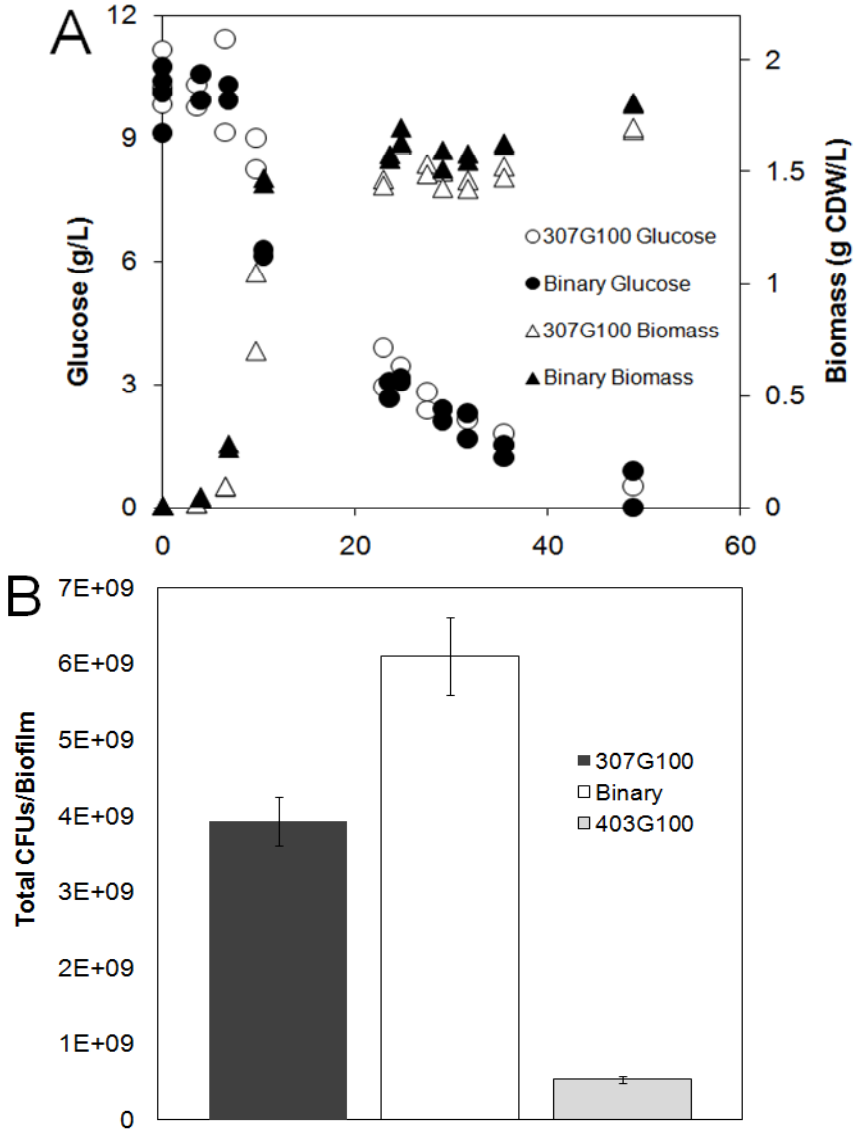

Figure 4. 7. Culturing properties of a dual engineered binary consortium comprised of glucose positive strain 307G100 (ΔaceAΔldhAΔfrdA) and glucose negative strain 403G100. A) Biomass and glucose concentration time profiles (x-axis in units of hrs) for dual engineered binary consortium and monoculture control during batch shake flask cultivation. Data collected from four independent shake flask experiments with different sampling intervals. B) Colony biofilm cultivation data for the dual engineered binary consortium and appropriate monoculture controls grown on M9 medium with glucose as the sole reduced carbon source. Error bars represent ± 1 standard deviation from three independently cultured biofilms.

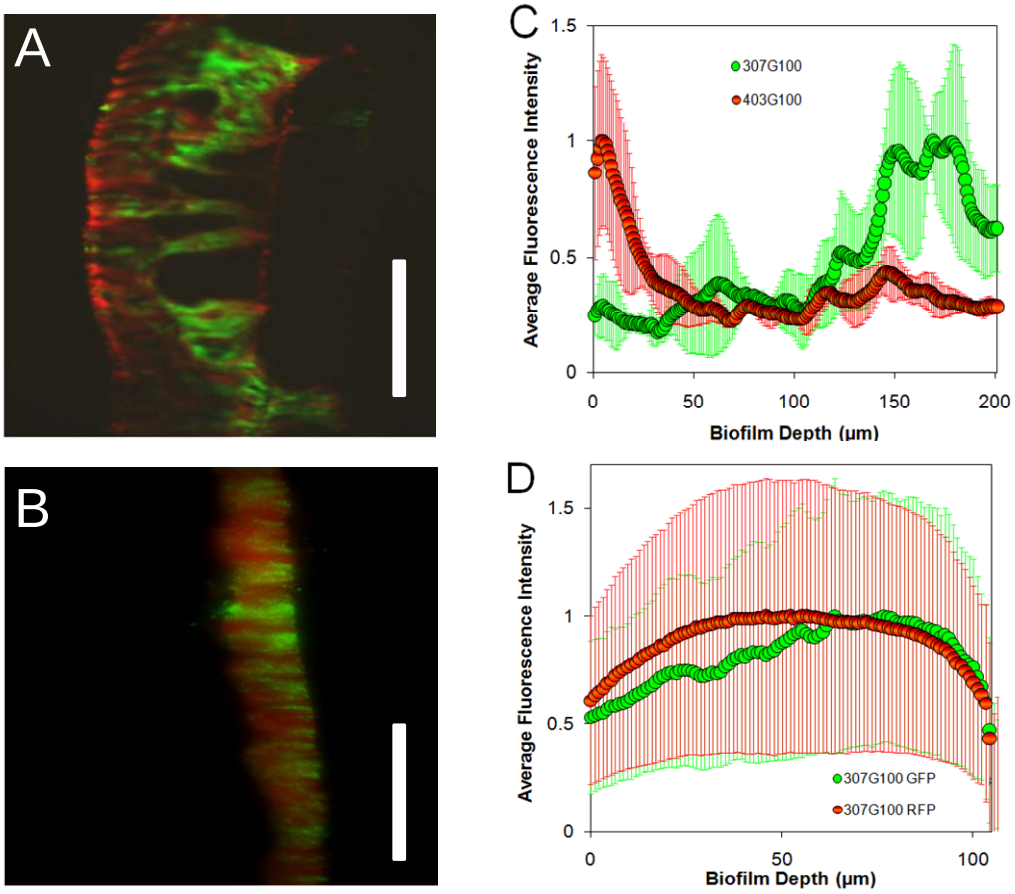

Figure 4. 8. Epi-fluorescent micrographs and quantitative image analysis of dual engineered binary consortium and strain 307G100 monoculture colony biofilms. A) Dual engineered binary consortium biofilm micrograph with glucose negative strain 403G100 expressing reporter protein td-tomato (red) and glucose positive strain 307G100 expressing reporter protein m-citrine (green). Biofilm image oriented with air-interface on left. Glucose negative strain 403G100 localized primarily at the air interface; red cells at the membrane interface are a result of daily aerobic biofilm plate transfers. Dark regions within biofilm are an artifact of cryosectioning thick biofilms. B) Micrograph of control biofilm comprised of two 307G100 strains each expressing a different fluorescent protein (td-tomato, m-citrine). C) Average fluorescence intensity of red and green reporter proteins as a function of position within biofilm for the dual engineered consortium. Depth is measured from the air interface into the biofilm. D) Average fluorescence intensity as a function of position within the biofilm for strain 307G100 expressing either a red or green fluorescence reporter protein. Fluorescence intensity versus position data is the mean of four line segments chosen at random biofilm positions. Error bars represent ± 1 standard deviation.

4.5. Discussion

Synthetic binary consortia engineered for syntrophy demonstrated increased biomass productivity under three distinct culturing conditions. This emergent property, based on consortial interactions, improved batch and chemostat culture biomass productivities by approximately 15% and 30% respectively and improved biofilm productivities by approximately 50%. The presented strategy is in strong contrast with traditional metabolic engineering optimization approaches. These approaches frequently aim to optimize glucose-based productivity by deleting genes associated with inefficient metabolic routes or futile cycles (Calhoun et al. 1993; Hua et al. 2003; Trinh et al. 2006). The current work optimizes glucose yields by removing one consortium member's ability to utilize glucose. When the glucose negative strain is cultured with a glucose consuming strain, the resulting binary consortia can simultaneously optimize both glucose and byproduct catabolism, enhancing overall system productivity.

The deletion-mutant, 403G100, was specifically engineered and adapted for secondary heterotrophy because acetate is often a major byproduct during *E. coli* growth. Improvements in maximum specific growth rate after adaptation were consistent with previously reported adaptive evolution studies (Conrad et al. 2009; Fong and Palsson 2004; Ibarra et al. 2002). Acetate was the predominant organic acid measured during the experiments; however trace amounts of other fermentation products were also detected (*e.g.,* lactate, succinate, fumarate, formate) and potentially served as exchange compounds. While acetate served as the representative byproduct for metabolite exchange, other byproduct exchanges are possible as are the incorporation of additional

byproduct metabolizing specialist strains. The engineered ecological role of the current study's glucose negative strain is quite different than other recent uses of glucose negative strains in artificial consortia (Eiteman and Altman 2006; Eiteman et al. 2008). In these studies, the glucose negative strain was utilized to co-metabolize a glucose and xlyose sugar mixture, the strain was not designed to metabolize inhibitory byproducts. The presented system is also distinct from a range of synthetic consortia that are built on auxotrophic complementation (Wintermute and Silver 2010b). These systems are comprised of mutants typically unable to grow in minimal medium without a complementing strain and are arguably not designed for direct incorporation into bioprocess applications. The presented primary producer strains are not dependent on the consumer to grow.

The engineered consortium's partitioning of metabolic functionality is analogous to cascading trophic levels observed in naturally occurring microbial communities as well as in highly adapted, long term *E. coli* chemostat cultures (Egland et al. 2004; Kinnersley et al. 2009; Rosenzweig et al. 1994). For instance, the primary producer/consumer relationship spontaneously establishes itself from monocultures during long term cultivation. The presented study demonstrates that it is possible to engineer these naturally occurring ecological patterns into *E. coli* cultures further establishing the possibility of metabolically and genetically defined model systems for testing microbial ecology phenomena. The consortia are also designed to remove complications associated with multisubstrate growth. The scavenging strain in Rosenzweig *et al.*(1994) utilizes a

combination of both glucose and acetate while the current specialist strain cannot catabolize glucose.

While the engineered binary consortia members are designed to not compete for the same reduced carbon source, they may compete for the same electron acceptor (*e.g.,* oxygen). The acetate specialist requires an external terminal electron acceptor to oxidize organic acids while the primary producer strains are facultative. Competition for terminal electron acceptor is a potential limitation of current binary systems. However, building a consortium with community members engineered for partitioned electron donor and electron acceptor (*e.g*. oxygen and nitrate) functionality would free the strains from resource competition. Again, this is a common theme in naturally occurring systems (Taffs et al., 2009).

The largest emergent increase in culture productivity was observed in biofilms. The culturing environment of the colony biofilm, with the microbes' close physical proximity, differs considerably from the planktonic batch and chemostat cultures. Biofilms contain inherent chemical gradients including oxygen gradients which produce localized byproduct secretion and accumulation (Stewart and Franklin 2008a; Xu et al. 1998). Colony biofilms serve as an excellent test system for the current engineered binary consortia due to the immobile nature and proximity of cells. The presence of a dedicated acetate-consuming population increases overall population productivity likely by moderating position specific organic acid concentrations and pH while concurrently capturing byproduct carbon. The close physical localization and specialization of metabolism can be compared to interactions between subcellular compartments in

eukaryotes. Eukaryotic cellular organization is analogous to microbial communities and the increased productivity observed in the current study could support competitive advantages associated with the eukaryote cellular organization and metabolic regulation.

This study establishes the design, construction and characterization of synthetic *E. coli* consortia based on productivity enhancing syntrophic metabolic exchange. The metabolic engineering blueprint was demonstrated using three distinct culturing systems including batch, chemostat and biofilms. The study presents proof of concept for a novel bioprocess strategy which mimics an ecological phenomenon found in most natural microbial communities; primary productivity enhancement through interactions with specialized, secondary heterotrophs. Integrating this global ecological theme with synthetic biology represents a powerful tool for optimizing bioprocesses and can be incorporated easily with most existing microbial bioprocess systems.

4.6. Acknowledgements

The authors would like to acknowledge the helpful discussions and assistance of Betsey Pitts and Trevor Zuroff. The authors would also like to thank an anonymous reviewer for insightful comments and suggestions. This work was funded by the National Institutes of Health (NIH) grants (EB006532 and P20 RR16455) and by the National Science Foundation IGERT program in Geobiological Systems (DGE 0654336).

4.7. Citation

Bernstein, Hans C., Steven D. Paulson, and Ross P. Carlson. “Synthetic Escherichia coli consortia engineered for syntrophy demonstrate enhanced biomass productivity.” *Journal of Biotechnology* (2011). Doi/10.1016/j.jbiotec.2011.10.001

5. DIRECT MEASUREMENT AND CHARACTERIZATION OF ACTIVE PHOTOSYNTHESIS ZONES INSIDE BIOFUEL PRODUCING AND WASTE-WATER REMEDIATING ALGAL BIOFILMS

Contribution of Authors and Co-Authors

Manuscript in Chapter 5

Author: Hans C. Bernstein

Contributions: Conception and critical analysis of research, data collection and analysis, manuscript drafting and editing.

Co-Author: Maureen Kessano

Contributions: Data collection and analysis.

Co-Author: Karen Moll

Contributions: Data collection and analysis, manuscript drafting and editing

Co-Author: Terence Smith

Contributions: Data collection

Co-Author: Robin Gerlach

Contributions: Conception and critical analysis of research.

Co-Author: Ross P. Carlson

Contributions: Conception and critical analysis of research

Co-Author: Brent M. Peyton

Contributions: Conception and critical analysis of research.

Co-Author: Robert D. Gardner

Contributions: Conception and critical analysis of research, data collection and analysis, manuscript drafting and editing.

Contribution of Authors and Co-Authors…Continued

Co-Author: Ronald C. Sims

Contributions: Conception and critical analysis of research.

Manuscript Information Page

Hans C. Bernstein, Maureen Kessano, Karen Moll, Terence Smith, Robin Gerlach, Ross P. Carlson, Brent M. Peyton, Robert D. Gardner* and Ronald C. Sims**
Journal Name: Biotechnology and Bioengineering
Status of Manuscript:
_X_ Prepared for submission to a peer-reviewed journal
__ Officially submitted to a peer-reviewed journal
__ Accepted by a peer-reviewed journal
__ Published in a peer-reviewed journal

Wiley
Expected submission: May 2013

*Department of Chemical and Biological Engineering, and Center for Biofilm Engineering, Montana State University, Bozeman, MT 59717.
Rob.Gardner@biofilm.montana.edu

**Department of Biological Engineering, Utah State University, Logan UT 84322-4105
Ron.Sims@usu.edu

5.1. Abstract

Algal biofilm based technologies are of keen interest for engineering processes due to their ability to utilize renewable resources light and carbon dioxide. Two relevant applications are considered in this study: biofuel production and waste-water remediation. Although photoautotrophic biofilms have long been used for waste-water remediation applications, concurrent or strict biofuel production represents a relatively new and under-represented focus. This study employed a novel rotating algal biofilm reactor (RABR) in a pilot scale and laboratory setting for waste-water remediation and biofuel production, respectively. The specific aims of this study were to (i) characterize and compare two different RABR biofilms in the context of active photo-synthesis zones (ii) directly measure spatial gradients in steady-state oxygen and photosynthesis microprofiles, (iii) determine rates of photosynthesis and respiration processes and (iv) characterize and compare the biofuel potential and (neutral lipid) precursor biomolecule composition in these biofilms. Clear differences in photosynthesis, respiration and biofuel-precursor capacities were observed between the two RABR systems and also between different conditions based on biofilm growth orientation in the field and nitrogen availability in the laboratory. Nitrogen depletion was not found to have the same effect on lipid accumulation in the laboratory algal biofilm cultures as compared to traditional planktonic studies. Physiological characterization of these algal biofilms identify potential areas for future process optimization.

5.2. Introduction

Photoautotrophic microorganisms are used as biotechnology platforms for many relevant applications including biofuel production, waste-water remediation, carbon sequestration, and agriculture (Christenson and Sims 2011; Ordog et al. 2004; Pokoo-Aikins et al. 2010). Of these, algal biofuel production has been identified as a promising field due to its potential for sustainable supplementation or replacement of fossil fuels (Chisti 2007; Hu et al. 2008). To date, microalgae biotechnologies have typically focused on traditional suspended culturing methodologies designed to facilitate photo-production; the capture and conversion of energy from photons into chemical energy stored in extractable biomolecules (*e.g.,* lipids). This study focuses on characterization of oxygenic photosynthesis and respiration in photo-biofilm reactors, an alternative and often under-represented growth system.

Biofilms are matrix-enclosed microbial cells attached to biological or non-biological surfaces (Characklis and Cooksey 1983; Hall-Stoodley et al. 2004). Photoautotrophic biofilms, composed of microalgae and/or cyanobacteria, are ubiquitous to nearly all photic aquatic environments. An important attribute of biofilms is that they both create and are functionally controlled by gradients in substrates, products and energy sources (de Beer et al. 1994; Stewart and Franklin 2008). Spatial gradients in light have been shown to directly control rates of oxygenic photosynthesis and corresponding oxygen concentrations inside biofilms (Kuhl et al. 1996). Oxygen distributions in biofilms are directly influenced by diffusion limitations and can result in localized supersaturated concentrations during active oxygenic photosynthesis. The resulting high

oxygen concentrations can inhibit CO_2 incorporation and subsequent photo-production of carbon storage compounds by competing as a substrate for ribulose 1,5-bisphosphate carboxylase-oxygenase (rubisco) activity (Beardall and Raven 1981; Glud et al. 1992; Ogren 1984). Thus, the characterization of spatial gradients in oxygenic photosynthesis and respiration activities is a key consideration for algal biofilm based technologies.

This study employed a recently developed rotating algal biofilm reactor (RABR) that was designed, built and tested at both the laboratory scale (lab-RABR) and pilot field scale (field-RABR) (Christenson and Sims 2012) (Fig. 5.1). The advantage of the RABR is the ability to simultaneously facilitate algal-growth, biomass concentration and dewatering. Biofilm reactors can also reduce the water and energy requirements for biomass and photo-production compared to traditional suspended culturing strategies (Ozkan et al. 2012).The RABR and other algal-based biofilm technologies have been investigated for their potential to concurrently remediate waste-water and produce biofuel precursor molecules (Boelee et al. 2012; Farooq et al. 2013). The RABR can facilitate efficient biomass harvesting via the reported spool harvesting technique (Christenson and Sims 2012). However, optimal biomass harvesting practices need to be determined in the context of biofilm specific physiology, such as optimal biomass areal density and biofilm thickness as it relates to active photo-production and photosynthesis zones.

The current study focuses on spatial physiological characterization of algal biofilms cultured through the RABR method. The specific aims of this study were to (i) characterize and compare two different RABR biofilms (biofuel-producing and waste-water remediating) in the context of active photo-synthesis zones (ii) directly measure

spatial gradients in steady-state oxygen and photosynthesis microprofiles, (iii) determine rates of photosynthesis and respiration processes and (iv) characterize and compare the biofuel potential and (neutral lipid) precursor biomolecule composition in these biofilms.

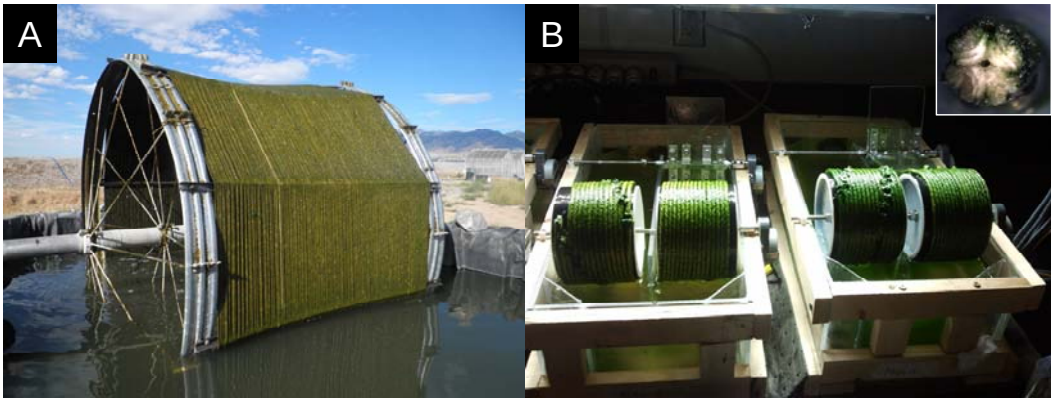

Figure 5. 1. Representative photographs for the field-RABR (A) and lab-RABR (B) culturing systems designed for algal biofilm culturing (insert shows cross-sectioned excised cotton cord substratum with biofilm growth). Note the 'top' and 'bottom' biofilm orientation corresponding to the inner and outer sections of the field-RABR, respectively.

5.3. Materials and Methods

5.3.1. Laboratory Strains, Culturing Conditions, and Biomass Sampling

The Chlorophyte isolate Botryococcus sp. strain WC-2B (WC-2B) was cultured with the 8 L lab-RABR operated in batch mode. WC-2B was isolated from an alkaline stream in Yellowstone National Park (USA), confirmed unialgal using SSU 18S rDNA and revealed 99% alignment (1,676 bp) with Botryococcus sedeticus UTEX 2629, which has previously been described (Senousy et al. 2004; Vazquez-Duhalt and Greppin 1987). Reactors were operated in triplicate and grown at 25ºC in Bold's basal medium buffered

at 25 mM with 2-[N-cyclohexylamino]-ethane-sulfonic acid (CHES, pKa 9.3) and rotated at 15.3 RPM. All RABR experiments were loaded with untreated cotton cord as the biofilm-substratum (0.64 cm diameter) (Christenson and Sims 2012b). The lab-RABRs consisted of cords coiled onto plastic cylindrical-spools (10 cm in diameter) submerged ~5 cm in the liquid medium. The lab-RABRs were cultured under custom light emitting diode (LED) banks (Box Elder Innovations, LLC and T&L Design, Box Elder UT) programed with LabVIEW (National Instruments Corp.) to simulate a cyclic diurnal cycle with photosyntheticly active radiation (PAR) values ranging from 0-900 µmol photons·m-2·sec-1 on a 14:10 L/D diel cycle following Equation 5.1.

$$I = cos\left(\frac{\pi}{t_L} * (t - t_M)\right)^2 \qquad \text{Eq. 5.1}$$

Where I is the light intensity, t_L is the total light time in minutes, t is the current time, and t_M is the midpoint time corresponding to the maximum light intensity.

Medium nitrate concentrations were monitored using NitraVer 5 pillow packets (HACH). 10x concentrated medium and supplemental diH_2O (distilled) were added, as needed, to maintain nutrient replete conditions and offset evaporation. Culturing and sampling was performed under non-aseptic conditions (*i.e.,* open-air). Nitrate depletion was induced (after 28 day replete culturing) by removing all liquid media from the reactors followed by immediate replacement of Bold's basal medium without nitrate. Nitrate deplete analysis and sampling was performed 60 h post depletion.

Biomass cell dry weights (CDW, $g_{CDW} \cdot cm^{-2}$) were obtained throughout culturing by excising a known length cotton cord and its attached biofilm, followed by biofilm removal into preweighed aluminum weigh boats. The biomass was dried at 70°C for 18 h until the biomass weight was constant. Biomass CDWs were calculated by subtracting the dry weight of the preweighed aluminum boat from the oven dried boat with biomass and normalizing by the cylindrical surface area for a known length of cotton cord substratum.

5.3.2. Outdoor Culturing Conditions

Field scale biofilms were cultured outdoors (August 4th –October 17th 2012) with a pilot scale RABR (field-RABR) in accordance with previously described methods and procedures (Christenson and Sims 2012b). Briefly, biofilms were grown on cotton cord (identical to lab-RABR experiments) coiled onto aluminum wheels (193 cm in diameter) which rotated (1.25 RPM) partially submerged in ~4080 L tanks (~1700 L liquid volume). An important difference from the lab-RABR was that the cord-substratum of the field-RABR was exposed on top and bottom (discussed further below). The field-RABR was placed in a continuous flow channel of waste water (~6 ºC and pH~7.4) fed at ~1.25 LPM located at an outdoor waste-water lagoon facility (Logan, Utah, USA).

5.3.3. Oxygen Microsensor Analysis

Microsensor measurements were performed using Clark-type oxygen micro-electrodes with outside tip diameters of 25 μm, response time < 5 s and < 5% stirring sensitivity (Unisense, A/S) (Revsbech 1989a; Revsbech and Jorgensen 1986a).

Amplification and sensor positioning were controlled with a microsensor multi-meter coupled with an ADC216 USB converter and a motor controlled micromanipulator. Data collection was aided by software packages, SensorTrace Pro ver.3.0.1 and Sloper ver. 3.0.3 (Unisense, A/S). Two point calibrations were performed in air saturated diH2O ($[O_2] \approx 260$ μM) and in a 1 M NaOH, 0.1 M ascorbic acid solution (anoxic standard). Calibrations were repeatedly checked in the anoxic standard and in air saturated diH2O throughout the experiments. Microsensor measurements were performed between 21 and 25 ºC under both dark and light conditions (PAR = 700 μmol photons$\cdot m^{-2} \cdot sec^{-1}$). Spatial O_2 measurements were performed in one-dimension (depth-wise) from the biofilm-air interface down towards the cotton cord substratum in 25-100 μm steps. The effective diffusion coefficient (D_e) for O_2 in the algal biofilms was estimated to be 1.2·10-5 $cm^2 \cdot sec^{-1}$, by assuming it to be 50% of the aqueous value corresponding to fresh water at 25 ºC (Stewart 1998). The oxygen micro-profile and light:dark shift techniques used here have been previously described in detail (Bernstein et al. 2013; Glud et al. 1992; Kuhl et al. 1996; Lassen et al. 1998; Revsbech and Jorgensen 1986; Revsbech et al. 1983). Briefly, Fick's law was used to calculate the total oxygen flux exported from the surface of the biofilm (net areal rate of biofilm photosynthesis or P_n) and from the photic zone inside the biofilm (net areal rate of photosynthesis of the photic zone or $P_{n,phot}$). Additionally, the light:dark shift measurements were used to estimate gross photosynthesis profiles and areal rates (P_g) which represent the total amount of oxygenic photosynthesis under the assumptions that: (i) there is an initial steady-state O_2 distribution prior to darkening (ii) the O_2 consumption rate is identical between the light

and dark time periods (iii) the O_2 diffusion coefficient remains constant during the measurement time at each position. Detailed calculations for oxygen transport, photosynthesis, photosynthesis-coupled respiration and respiration processes are included in the supplemental material for this manuscript.

5.3.4. Microscopy and Imagining

Biofilm structure and lipid accumulation were examined using confocal microscopy. Three components of these biofilms were visually analyzed: (i) chlorophyll autofluorescence, (ii) neutral lipids via Bodipy 505/515 staining, and (iii) biofilm substratum via Calcofluor white M2R staining (cellulose containing cotton-cord strands) (Cooper et al. 2010). Each component/stain was visualized with distinct excitation/emission spectra. Images were acquired using a Leica TCS SP5 with Leica Advanced Suite-Advanced (LAS-AF) software (version 2.5.1.6757). Clean cross-sections of intact RABR biofilms samples were embedded in O.C.T. Compound (Tissue-Tek) on dry ice and cut using a clean razor blade. Each cut sample was immersed in 5 mL of filter sterilized diH2O, and stained with Bodipy 505/515 (5 mM) (final concentration of 10 μM) for approximately 20 minutes. Bodipy and chlorophyll autofluorescence were excited by 488 nm and 633 nm lasers, and captured with emission ranges 499-547 and 647-761 nm, respectively. To visualize the biofilm substratum (cellulose containing cotton-cord strands), samples were stained for an additional 20 minutes with 10 μL Calcofluor white M2R per mL of diH2O. Calcofluor white M2R was excited by a 405 laser and captured with an emission range of 419-474 nm. Samples were rinsed once with filter-sterilized diH2O prior to imaging. To minimize movement, each sample was

partially embedded in 2% Agarose (Fisher). Composite images were obtained with combined z-stacks up to the maximum depth at which autofluorescence by chlorophyll was detected (~200 μm) using a 63x water immersion objective. Planar images were captured every 0.6 μm. z-stacks were compiled into Maximum Intensity Projection (MIP) images using Imaris x64 (version 7.5.2, Bitplane Scientific Software).

5.3.5. Lipid Analysis

At the time of oxygen microsensor analysis, bulk biomass was harvested from the RABRs and washed, by centrifugation and diH2O resuspension, four times to remove media salts. After which, the biomass was pelleted and frozen for lyophilization and lipid analysis. Extractable precursor analysis of free fatty acid, mono-, di-, tri-acyl glycerol (FFA, MAG, DAG, and TAG, respectively) was done in accordance to the reported bead beating extraction method and coupled with gas chromatography – flame ionization detection (Lohman et al. in-press). Additionally, biofuel potential, defined as total fatty acid methyl esters (FAME) produced directly from the biomass (Eustance et al. 2013; Gardner et al. 2013), along with fatty acid profiles were analyzed by direct in situ biomass transesterification and quantified with gas chromatography – mass spectroscopy following the protocols developed by Lohman, et al. 2013 (Lohman et al. in-press). A brief description of these protocols is included in the supplementary methods section.

5.4. Results and Discussion

5.4.1. Biofilm Cultivation

Biofilms were successfully cultured on the cotton cord substratum during field and laboratory scale RABR experiments (Fig. 5.1). Samples from the lab-RABR were analyzed based on nitrate replete or deplete conditions. Additionally, samples from the field-RABR were separated according to growth orientation on the substratum. The field-RABR 'top' and 'bottom' samples correspond to biofilms formed on the outer and inner section of the rotating wheel respectively. Field-RABR top samples were cultured in an orientation directly exposed to ambient sun light (average daily maximum PAR = 2000 μmol photons$\cdot m^{-2}\cdot sec^{-1}$) compared to the more shaded bottom (average daily maximum PAR = 80 μmol photons$\cdot m^{-2}\cdot sec^{-1}$). Hence, there were four chosen biofilm sample-types analyzed and compared in this study; (i) lab-RABR nitrate replete, (ii) lab-RABR nitrate deplete, (iii) field-RABR top, and (iv) field-RABR bottom. It is important to emphasize that the laboratory and field-RABR systems are not identical and represent two different process objectives. However, a future goal for the RABR technology is to better integrate the waste-water remediating and biofuel producing processes; hence comparisons between the two systems are considered in this study.

The maximum specific growth rates, measured during early exponential phase, were 0.09 and 0.17 day^{-1} for the laboratory and field cultured biofilms, respectively. The maximum measured biomass areal density (observed at stationary phase) were 0.36 and 0.65 $g_{CDW}\cdot cm^{-2}$ for the laboratory and field-RABRs, respectively. The final biomass areal density decreased 0.01 $g_{CDW}\cdot cm^{-2}$ post nitrate depletion in the lab-RABR replicates. The

measured biofilm thickness (distance from substratum to biofilm surface at stationary phase) was approximately 1 mm for each lab-RABR condition and approximately 2 mm for each field-RABR biofilm type (top and bottom).

5.4.2. Steady-state Oxygen Microprofiles

The laboratory and field-RABR samples exhibited clear differences in the illuminated steady-state oxygen profiles. The upper part of all biofilm samples became supersaturated with O_2, reaching 3 times air saturation (Fig. 5.2). The air saturated dissolved O_2 concentrations (25 ºC) were experimentally measured to be 266.7 ± 0.7 and 240 ± 1.9 μM (mean ± 1 standard deviation, n = 8) for liquid media supplied to the lab and field scale RABRs, respectively. The depth of the oxic zone (oxygen penetration depth) was measured to extinction in the field-RABR biofilms under illumination (~1800 μm). In the illuminated lab-RABR biofilms, the oxic zone extended to depths greater than 2675 μm below the biofilm surface (~1675 μm into the substratum) where the flux of oxygen became very low or approached zero. The lab-RABR biofilms showed active transport driven by oxygen consumption in portions of the substratum indicating that some biofilm is formed inside the cotton cord pore volume, which was also observed by confocal microscopy (Supplemental Fig. S2). The lab-RABRs showed a higher degree of heterogeneity with respect to replicate oxygen profile positions compared to the field-RABR biofilms.

Steady-state oxygen profiles were also obtained after 15 min of dark conditioning (Fig. 5.3). The oxic zone in the absence of light ranged from 850-1150 μm and 450-700 μm for the laboratory and field-RABR samples, respectively. The field-RABR biofilms

exhibited less oxygen penetration (both illuminated and dark conditions) compared to the lab-RABR samples indicating that there was higher degree of oxygen consumption (discussed further below). This was expected since the field-RABR was inoculated with the native waste-water microbial flora and was likely composed of a more adapted complex community of environmental biofilm-forming microorganisms compared to the WC-2B inoculated lab-RABR.

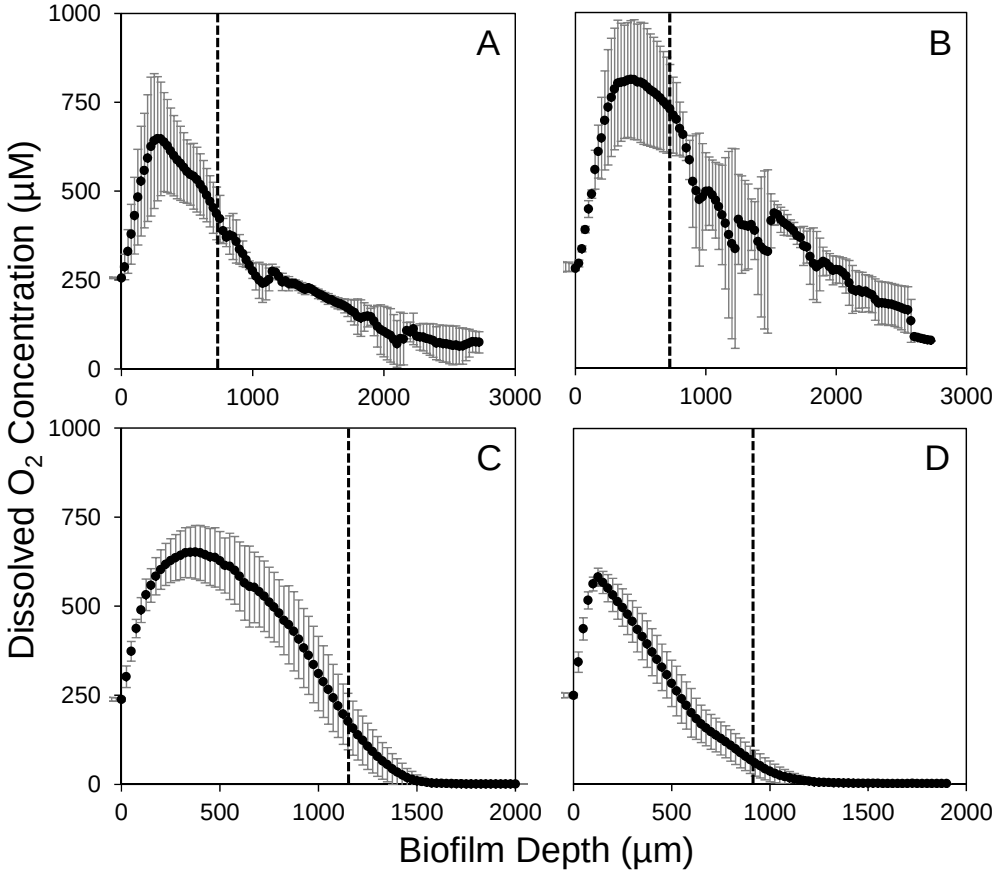

Figure 5. 2. Dissolved oxygen microprofiles measured in the light extending from the surface of the biofilms (x = 0): (A) Lab-RABR cultured under nitrate replete conditions, (B) Lab-RABR cultured under nitrate deplete conditions, (C) Field-RABR top side biofilm, and (D) Field-RABR bottom side biofilm. Note that the biofilm surface position (depth = 0) is approximated by the position at which oxygen responses were measureable (subject to ± 25 µm error). Individual data points represent the mean values from 3-4 replicate measurements. Error bars represent plus or minus one standard deviation. Dotted lines indicate the photic-zone termination depth. Note the scale change on the x-axis.

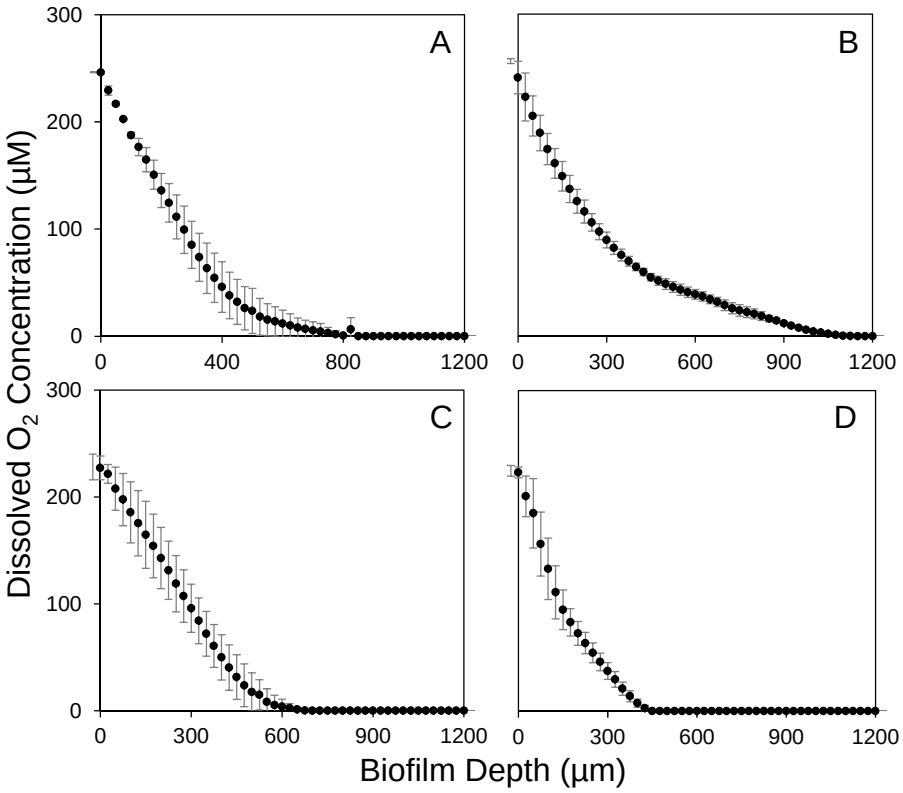

Figure 5. 3. Dissolved oxygen microprofiles measured in the dark extending from the surface of the biofilms (x = 0): (A) Lab-RABR cultured under nitrate replete conditions, (B) Lab-RABR cultured under nitrate deplete conditions, (C) Field-RABR top side biofilm, and (D) Field-RABR bottom side biofilm. Note that the biofilm surface position (depth = 0) is approximated by the position at which oxygen responses were measureable (subject to ± 25 µm error). Individual data points represent the mean values from 3 replicate measurements. Error bars represent plus or minus one standard deviation.

The oxygen distributions measured for this study are only representative of steady-state reaction and diffusion processes. However, the rotating mechanism employed by the RABR alternates the biofilms between different light and fluid regimes in a periodic fashion corresponding to the submerged-liquid and ambient air surroundings. Diffusive oxygen flux was measured inside the biofilms. The steady-state microprofiles were obtained on biofilms exposed to the ambient air did not provide

enough resolution to identify or determine the thicknesses of the diffusive boundary layer (DBL) at the surface of the biofilms. However, DBLs almost certainly were present and are not ruled out as an important regulating factor in the oxygen transport processes, especially while being exposed to the liquid media during rotation. It has been previously established that DBL thickness is a function of velocity differentials between the biofilm and bulk fluid (Jorgensen and Marais 1990; Jorgensen and Revsbech 1985; Kuhl et al. 1996). This is an important consideration for RABR operation since the rotational speed can be optimized to reduce the effects of mass transfer limitations external to the biofilm matrix.

5.4.3. Photosynthesis and Respiration

The laboratory and field-RABR samples also exhibited measureable differences in the steady-state profiles in rates of photosynthesis (Fig. 5.4). The measured areal rates of gross photosynthesis (P_g) were higher in the field-RABR compared to the lab-RABR (Table. 1). The active zones of photosynthesis were also greater (up to 40 % deeper) in the field-RABR biofilms. The active zone of photosynthesis is defined here as the position in the biofilm where the volumetric gross photosynthesis rate [$P_g(z)$] is greater than zero and its depth assumed to be equal to the biofilm photic zone (L_{phot}). This assumption is validated by the observation that L_{phot} occurs within the oxic zones of the biofilms and is likely not dictated by a strong heterotrophic respiration component (Fig. 5.2). The difference in L_{phot} values between the laboratory and field biofilms confirms expected differences in biofilm physical structures and/or light attenuation. Differences in physical structure likely translate into differences in the effective diffusion coefficients;

however, these differences are expected to be very small based on previously reported measurements (Stewart 1998) and were not considered in detail.

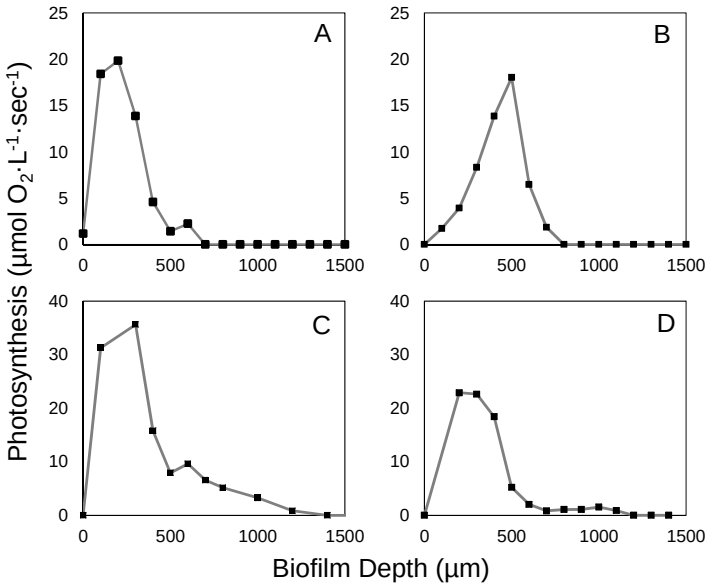

Figure 5. 4. Photosynthesis profiles extending from the surface of the biofilms (depth = 0): (A) Lab-RABR cultured under nitrate replete conditions, (B) Lab-RABR cultured under nitrate deplete conditions, (C) Field-RABR top side biofilm, and (D) Field-RABR bottom side biofilm. Note that the biofilm surface position (depth = 0) is approximated by the position at which oxygen responses were measureable (subject to ± 100 µm error). Each data point is a representative gross volumetric photosynthesis rate from 2-3 replicates.

The measured net areal rates of photosynthesis for the biofilm and photic zone (P_n and $P_{n,phot}$) were higher in the field-RABR (Table 5.1). This result indicates that the waste-water remediating biofilms have the potential to supply a greater flux of oxygen to their environment as compared to the WC-2B inoculated lab-RABRs. However, this implication is based only on the measurements of the steady-state oxygen profiles which were not directly obtainable on biofilms during rotating operation. The higher $P_{n,phot}$

values for the field-RABR can be partially attributed to the larger L_{phot} depths corresponding to larger areas of active photosynthesis.

Table 5. 1. Measurements of areal photosynthesis rates, areal respiration rates and relevant depth scales for the laboratory- and field-RABR cultured biofilms.

Areal rates (μmol $O_2 \cdot cm^{-2} \cdot sec^{-1}$)	Laboratory RABR Nitrate Replete	Laboratory RABR Nitrate Deplete	Field RABR Top Biofilm	Field RABR Bottom Biofilm
Photosynthesis, P_g	[a] $7.51 \cdot 10^{-4}$	[a] $5.70 \cdot 10^{-4}$	[a] $11.84 \cdot 10^{-4}$	[a] $5.23 \cdot 10^{-4}$
Net areal rate of biofilm photosynthesis, P_n, ($\%P_g$)	$2.31 \cdot 10^{-4}$ (30.8%)	$2.41 \cdot 10^{-4}$ (42.3%)	$3.01 \cdot 10^{-4}$ (25.4%)	$3.55 \cdot 10^{-4}$ (67.9%)
Net areal rate of photic zone photosynthesis, $P_{n,phot}$, ($\%P_g$)	$3.10 \cdot 10^{-4}$ (41.3%)	$2.91 \cdot 10^{-4}$ (51.1%)	$3.64 \cdot 10^{-4}$ (30.7%)	$3.96 \cdot 10^{-4}$ (75.7%)
Areal respiration of the biofilm, R_{light} ($\%P_g$)	$5.20 \cdot 10^{-4}$ (69.2%)	$3.29 \cdot 10^{-4}$ (57.7%)	$8.83 \cdot 10^{-4}$ (74.6%)	$1.68 \cdot 10^{-4}$ (32.1%)
Areal respiration of the photic zone, R_{phot} ($\%P_g$)	$4.41 \cdot 10^{-4}$ (58.7%)	$2.79 \cdot 10^{-4}$ (48.9%)	$8.20 \cdot 10^{-4}$ (69.3%)	$1.27 \cdot 10^{-4}$ (24.3%)
Respiration in the dark, R_{dark}	$0.65 \cdot 10^{-4}$	$0.74 \cdot 10^{-4}$	$0.54 \cdot 10^{-4}$	$1.11 \cdot 10^{-4}$
Depth of photic zone, L_{phot} (μm)	[b] 675 ± 25	[b] 650 ± 25	[b] 1100 ± 200	[b] 900 ± 200
Depth of oxic zone in light (μm)	> 2675	> 2675	[b] 1750 ± 25	[b] 1800 ± 25
Depth of oxic zone in dark (μm)	[b] 850 ± 25	[b] 1150 ± 25	[b] 700 ± 25	[b] 450 ± 25

[a] Mean of 2-3 independent measurements plus or minus average 25% range from the mean.
[b] Plus or minus measurement step-size, n = 2-3

The difference between the gross and net areal rates of photosynthesis provided measurements for the rates of oxygen consumption under illuminated conditions. The observed areal rate of respiration for the biofilm and photic zones (R_{light} and R_{phot}) between lab-RABR samples were higher for nitrate-replete measurements and consumed

~10 % more of the total oxygen evolved compared to the nitrate-deplete conditions (Table 5.1). Overall, there were only modest differences observed in rates of photosynthesis and respiration between the two lab-RABR nitrate availability conditions. This result implies that nitrate depletion in the media may not have a strong effect on the physiology of the biofilm (in the context of photosynthesis and respiration). This is an important observation since nitrogen stressing is a common strategy for triggering lipid accumulation in planktonic algae cultures (Converti et al. 2009; Mus et al. 2013; Stephenson et al. 2010).

Areal respiration rates, in this study, (R_{light} and R_{phot}) were highest and lowest for the field-RABR top and bottom samples, respectively (Table 1). These comparative differences between respiration and photosynthesis rates observed in the biofilms grown on different sides of one substratum must be due to intrinsic biofilm properties (*i.e.,* physical structure, photo-pigment amount and composition and/or community composition) since all steady-state profiles were obtained under the same illumination and experimental conditions. There is a clear difference between the field-RABR biofilm's capacity to produce and consume oxygen based only on the position/orientation in which the biofilm was grown.

The field-RABR top biofilm samples showed the highest rates of photosynthesis and respiration. These two processes are tightly coupled inside biofilms and likely not independent from each other. In fact, it has been shown previously that photosynthesis and respiration increase concurrently with increasing irradiance in tightly controlled algal biofilms (Jensen and Revsbech 1989). However, the results from the current study imply

that the biofilm's capacity for photosynthesis and simultaneous respiration change based on the amount of irradiance delivered during the culturing process (field-RABR top biofilms were exposed to 96 % more PAR based on the average daily maximum).

The measured oxygen consumption during illumination is attributed to heterotrophic and photosynthesis-coupled respiration processes. The combined steady-state profile measurements, from illuminated and dark conditions, imply that the field-RABR (particularly the bottom biofilm) had a higher degree of heterotrophic respiration compared to the WC-2B inoculated lab-RABR. This result was expected since the field-RABR biofilms form via colonization from the native waste-water microbial flora. Of the biofilms observed in this study, the field-RABR bottom samples showed both the highest and lowest rates of areal respiration in the dark and light, respectively. This indicates that these biofilms are more strongly influenced by heterotrophic respiration when compared to the field-RABR top samples. Increased rates of photosynthesis-coupled respiration can be advantageous to overall photo-production by lowering the localized O_2/CO_2 ratios inside the biofilm and resulting in higher affinities for CO_2 fixation at the rubisco complex (Beardall and Raven 1981; Glud et al. 1992; Ogren 1984). Hence, the encouragement and control of localized respiration processes may be an important design feature for RABR operation and needs to be considered for future optimization of photo-production.

5.4.4.Biofuel Analysis

Extractable lipid fractions were recovered from the biofilms and analyzed by gas chromatography for assessment of biofuel properties (Table 5.2). In addition, direct

transesterification was performed on the lyophilized biomass to identify fatty acids and to determine total biofuel potential (extractable and non-extractable) for each biofilm-type (Table 5.3). Modest increases of extractable precursor concentrations were measured in the nitrate deplete biofilms, as compared to the nitrate replete. This observation was also confirmed in confocal images (compare Fig. 5.5A and 5.5B); where Bodipy 505/515 was used to visualize the neutral lipid precursors. The total potential FAME-weight %, which is representative of the total biofuel potential of the biofilm, was also modestly higher for the nitrate deplete lab-RABR biofilms.

The most notable observations regarding lipid analysis of the lab-RABR, was the differences in total extractable weight % (sum of the FFA, MAG, DAG, and TAGs) between the nitrate replete and deplete biofilms (Table 5.2). The largest differences were observed in the DAG and TAG weight % and the respective areal concentrations. Although the WC-2B inoculated, biofuel producing biofilms exhibited reasonable biofuel potentials; the lab-RABR production-system is not considered optimized. This is evident in the fact that the extractable precursors only accumulated to 7.3 % of the biomass, which is much smaller than previously reported planktonic systems of WC-2B-like algae, accumulating ~23 % neutral lipids after 18 weeks of culturing (Vazquez-Duhalt and Greppin 1987). Additionally, planktonic cultures of WC-2B can accumulate up to 13.9 % of biomass as extractable precursors (7.7 % of which is TAG) under high pH and nitrate deplete conditions (Gardner, unpublished data). This evinces that media nitrate depletion alone may not be an effective condition for inducing neutral lipid accumulation in algal biofilms, likely due to heterogeneous distributions of nitrate caused by mass transfer

limitations. It should be noted that comparisons of these preliminary biofilm oil-production systems to well-mixed planktonic systems does not account for culturing times, biomass production rates or differences associated with required resource investments (*e.g.,* energy required for mixing or biomass harvesting or water input requirements). Future culturing optimization is needed to evaluate the effects of known parameters associated with lipid accumulation, such as nitrate and/or pH stress or chemical addition (Gardner et al. 2011; Gardner et al. 2012; Guckert and Cooksey 1990; Mus et al. 2013; Valenzuela et al. 2012).

Table 5. 2. Mean extractable biofuel precursor weight % and areal concentrations for the laboratory- and field-RABR cultured biofilms (n=3 with one standard deviation error, or n=2 with range reported as error).

	Condition	FFA	MAG	DAG	TAG	Total Extractable
eight % (w/w)	Replete	2.24 ± 0.39	1.17 ± 0.21	0.76 ± 0.35	0.11 ± 0.09	4.27 | 0.37
	Deplete	2.91 ± 0.46	1.48 ± 0.21	1.98 ± 0.32	0.94 ± 0.31	7.32 | 0.70
	RABR	1.49 ± 0.50	0.91 ± 0.48	0.34 ± 0.12	0.13 ± 0.01	2.86 | 1.09
real Conc. ($g \cdot m^{-2}$)	Replete	0.78 ± 0.19	0.41 ± 0.10	0.26 ± 0.10	0.04 ± 0.03	1.48 | 0.24
	Deplete	0.97 ± 0.22	0.50 ± 0.10	0.66 ± 0.14	0.31 ± 0.08	2.44 | 0.38
	RABR	0.98 ± 0.33	0.60 ± 0.31	0.22 ± 0.08	0.09 ± 0.01	1.89 | 0.72

[a] Mean and range for n=2

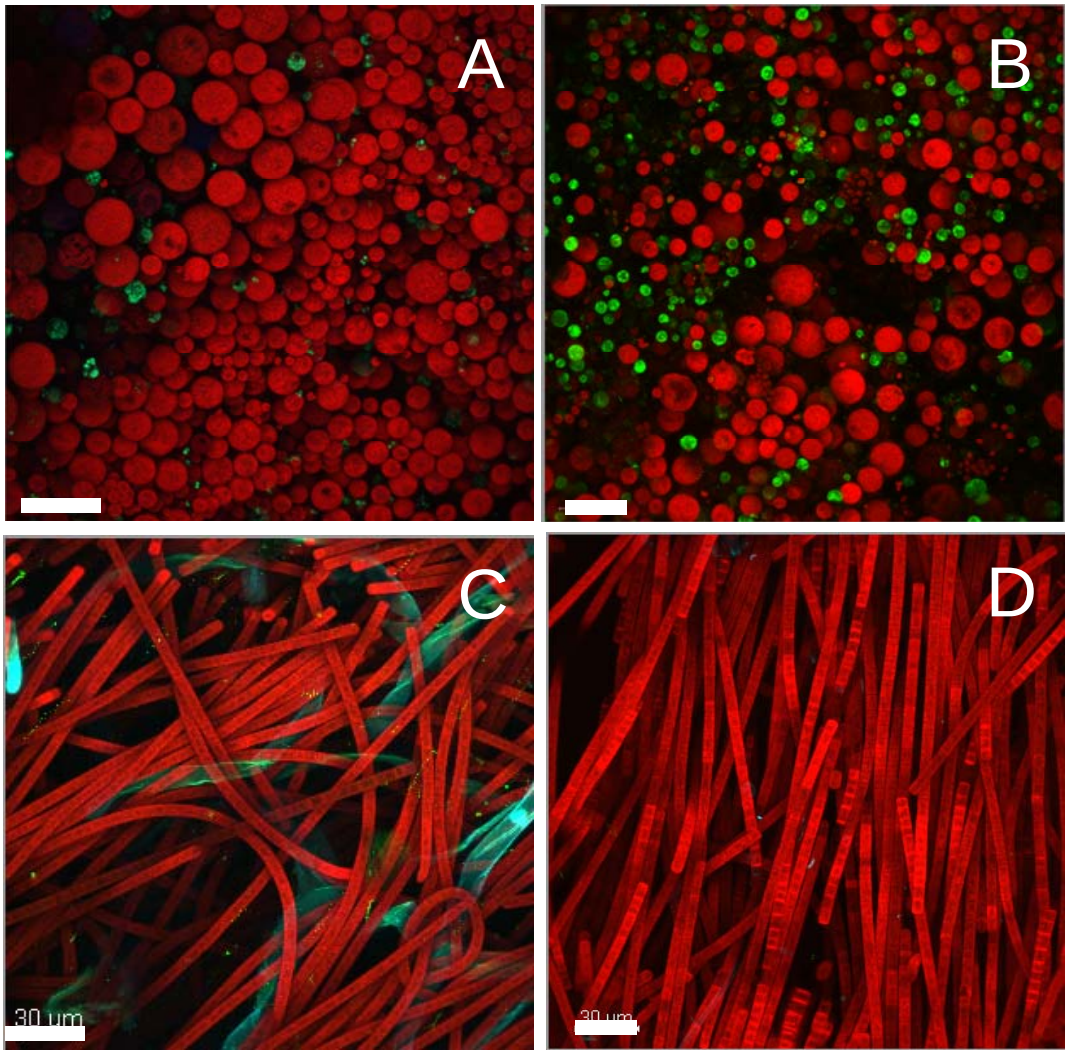

Figure 5. 5. Confocal Microscopy images of intact RABR biofilms. Samples are represented by the following: red (chlorophyll autofluorescence), green (neutral lipids, and light blue (cotton-cord strands -evident in panel C only). The top Panels indicate lipid accumulation in the lab RABR before (A) and after (B) nutrient stress showing higher neutral lipid content. Lower panels represent field RABR biofilm samples top (C) and bottom (D). Scale bars represent 30 µm.

Table 5. 3. Mean FAME %, weight %, and areal concentration from the laboratory- and field-RABR cultured biofilms. Biomass was directly transesterified to determine total biofuel potential from all fatty acid precursor molecules (extractable and non-extractable) (n=3 with one standard deviation error, or n=2 with range reported as error).

	FAME %			Weight % (w/w)			Areal Concentration ($g \cdot m^{-2}$)		
Fatty Acids	LRR	LRD	FR[a]	LRR	LRD	FR[a]	LRR	LRD	FR[a]
C12:0	N/D	0.24 ± 0.06	0.54 | 0.04	N/D	0.03 ± 0.01	0.03 | 0.01	N/D	0.01 ± 0.002	0.02 | 0.005
C14:0	0.39 ± 0.01	0.39 ± 0.06	1.65 | 0.69	0.03 ± 0.003	0.04 ± 0.01	0.08 | 0.02	0.01 ± 0.002	0.01 ± 0.003	0.05 | 0.01
C15:0	0.40 ± 0.02	0.43 ± 0.09	0.60 | 0.04	0.03 ± 0.003	0.05 ± 0.01	0.03 | 0.01	0.01 ± 0.002	0.02 ± 0.004	0.02 | 0.01
C16:1-3	19.85 ± 1.34	19.50 ± 0.41	22.97 | 2.64	1.67 ± 0.02	2.05 ± 0.03	1.17 | 0.36	0.58 ± 0.05	0.68 ± 0.05	0.77 | 0.24
C16:0	16.68 ± 1.61	18.68 ± 1.14	15.58 | 0.93	1.41 ± 0.23	1.96 ± 0.06	0.79 | 0.11	0.49 ± 0.11	0.65 ± 0.06	0.52 | 0.07
C18:1-3	50.15 ± 2.60	50.42 ± 1.76	42.28 | 2.02	4.24 ± 0.47	5.30 ± 0.34	2.15 | 0.52	1.47 ± 0.27	1.76 ± 0.16	1.42 | 0.34
C18:0	0.88 ± 0.08	0.95 ± 0.07	2.90 | 3.21	0.07 ± 0.01	0.10 ± 0.01	0.14 | 0.13	0.03 ± 0.01	0.03 ± 0.004	0.09 | 0.09
C20:4-5	3.35 ± 1.12	2.51 ± 0.65	5.67 | 0.83	0.28 ± 0.10	0.26 ± 0.06	0.29 | 0.10	0.10 ± 0.04	0.09 ± 0.03	0.19 | 0.06
C20:1-3	0.71 ± 0.13	0.64 ± 0.19	N/D	0.06 ± 0.01	0.07 ± 0.02	N/D	0.02 ± 0.01	0.02 ± 0.01	N/D
C20:0	N/D	N/D	0.18 | 0.37	N/D	N/D	0.01 | 0.02	N/D	N/D	0.01 | 0.01
C22:0	0.48 ± 0.08	0.51 ± 0.13	0.63 | 0.07	0.04 ± 0.01	0.05 ± 0.01	0.03 | 0.01	0.01 ± 0.004	0.02 ± 0.01	0.02 | 0.01
C24:0	0.28 ± 0.04	0.29 ± 0.01	0.63 | 0.03	0.02 ± 0.002	0.03 ± 0.000	0.03 | 0.005	0.01 ± 0.000	0.01 ± 0.001	0.02 | 0.003
C26:0	0.37 ± 0.03	0.42 ± 0.04	0.56 | 0.07	0.03 ± 0.003	0.04 ± 0.004	0.03 | 0.002	0.01 ± 0.002	0.01 ± 0.003	0.02 | 0.001
C28:0	N/D	0.35 ± 0.31	0.90 | 0.41	N/D	0.04 ± 0.03	0.04 | 0.01	N/D	0.01 ± 0.01	0.03 | 0.01
Other	6.46 ± 2.45	4.68 ± 1.30	4.90 | 0.05	0.54 ± 0.18	0.49 ± 0.14	0.25 | 0.05	0.18 ± 0.05	0.16 ± 0.04	0.16 | 0.03
Total	100	100	100	8.45 ± 0.61	10.51 ± 0.33	5.07 | 0.99	2.92 ± 0.42	3.49 ± 0.28	3.34 | 0.65

LRR: Laboratory RABR nitrate replete
LRD: Laboratory RABR nitrate deplete
FR: Field RABR
[a] Mean and range for n=2
N/D: not detected

5.4.5. Summary

This manuscript explores algal biofilms in the context of applied biotechnologies associated with biofuel production and waste-water remediation though the described laboratory and field-RABR culturing systems. The current study focuses on spatial photosynthetic and respiration physiologies as well as biofuel capacities for these under-

represented and potentially advantageous production platforms. The RABR systems are ideal for concurrent algal culturing, biomass concentration and dewatering by forming active photosynthetic biofilms on and in a cotton cord substratum. The field-RABR biofilms were composed of native waste-water microbial communities that were likely better adapted for the culturing conditions compared to the artificially inoculated lab-system. Environmentally adapted biofilm consortia were likely responsible for the higher biomass productivities, photosynthetic rates and respiration rates measured in the field-RABR. Interestingly, the field-RABR biofilms showed measurable differences in their capacities for photosynthesis and respiration based on the position/orientation in which the biofilm was cultured. However, the current field-RABR biofilms are not well suited for biofuel production and exhibited a relatively low biofuel potential. In fact, even the known biofuel producing WC-2B isolate also exhibited a relatively low biofuel potential compared to planktonic cultures. Hence, more research and development is necessary to optimize RABR systems for viable biofuel production.

Of the physiological parameters measured in the current study, photosynthesis-coupled respiration is of key importance and should be promoted/optimized as a design feature for locally optimizing O_2/CO_2 ratios to promote carbon fixation and subsequent photo-productivity. One potential strategy for maximizing gross photosynthesis while minimizing localized oxygen concentration would be to promote heterotrophic activity via mixed culturing techniques. A hybridization of the two processes described here (biofuel production and waste-water remediation) may be better achieved via mixed species inoculation or ‘seeding’ with known lipid accumulating photoautotrophic

community members combined with heterotrophic oxygen scavengers. Consortial cooperation in microbial biofilm technology has previously been demonstrated in a number of different cell factory systems (Bernstein and Carlson 2012b). Nitrogen stress (through nitrate depletion) as implemented here, was not identified to be as viable of a strategy for triggering lipid accumulation when compared to previously reported planktonic studies (Gardner et al. 2011; Mus et al. 2013), highlighting another avenue for future optimization studies.

5.5. Supplementary Text and Figures

5.5.1. Definition of Terms

J: Diffusive flux of oxygen (μmol $O_2 \cdot cm^{-2} \cdot sec^{-1}$)
C_{O2}: Concentration of oxygen (μmol$\cdot L^{-1}$)
D_e: Effective diffusion coefficient of oxygen ($cm^2 \cdot sec^{-1}$)
z: Spatial coordinate extending from surface (*z=0*) down towards the substratum
L_{phot}: Depth of the photic zone (μm)
t: Time coordinate (sec)
P_n: Areal rate of photosynthesis for the biofilm (μmol $O_2 \cdot cm^{-2} \cdot sec^{-1}$)
$P_{n,phot}$: Areal rate of photosynthesis for the photic zone (μmol $O_2 \cdot cm^{-2} \cdot sec^{-1}$)
R_{dark}: Areal respiration rate in the dark (μmol $O_2 \cdot cm^{-2} \cdot sec^{-1}$)
P_g(z): Gross volumetric rate of photosynthesis (μmol $O_2 \cdot L^{-1} \cdot sec^{-1}$)
R_{light}(z): Gross volumetric rate of respiration in the light (μmol $O_2 \cdot L^{-1} \cdot sec^{-1}$)
P_g: Gross areal rate of photosynthesis (μmol $O_2 \cdot cm^{-2} \cdot sec^{-1}$)

5.5.2. Oxygen Flux and Net Areal Rates of Photosynthesis

The one-dimensional diffusive flux of oxygen (*J*) inside the biofilm matrix was calculated with respect to the biofilm depth (z-axis) using Fick's law (Eq. 5.S1).

$$J = -D_e \frac{dC_{O_2}}{dz} \qquad \text{Eq. 5.S1}$$

A previously described analysis can be used to equate the diffusive flux of oxygen from various biofilm specific positions to the net areal rates of oxygenic photosynthesis or respiration (Glud et al. 1992; Kuhl et al. 1996). For example, under illuminated conditions and active photosynthesis, the flux of oxygen being expelled from the surface of the biofilm was equated to the net areal rate of photosynthesis of the biofilm (P_n, Eq. 5.S2). In this study, P_n was calculated at the surface positions of the biofilm; however, it may also be calculated in the diffusive boundary layer (DBL) at the biofilm fluid interface if there is sufficient the resolution of the DBL from the microprofile data. Note that the diffusive flux through the DBL would be calculated with the aqueous diffusion coefficient. Additionally, if the photic zone termination position (L_{phot}) is known, the flux of oxygen moving through that positional plane can be used in conjunction with P_n to calculate the net areal rate of photosynthesis of the photic zone ($P_{n,phot}$, Eq. 5.S3).

$$P_n = J_{z=0}^{biofilm} = J_{z\leq 0}^{DBL} \quad \text{Eq. 5.S2}$$

$$P_{n,phot} = |P_n| + \left|J_{z=L_{phot}}\right| \quad \text{Eq. 5.S3}$$

The areal rate of biofilm respiration in the dark (R_{dark}) was calculated from the steady-state oxygen profiles in the dark in an identical fashion as P_n was calculated under illuminated conditions.

5.5.3. Gross Photosynthesis, Photosynthesis-coupled Respiration and Photic-zone Identification.

The total amount of oxygenic photosynthesis or gross photosynthesis (P_g) was calculated by the previously described light:dark shift method (Glud et al. 1992; Kuhl et al. 1996). During these measurements the tip of the oxygen microsensor was placed at some position (z) inside the illuminated biofilm. Time dependent oxygen concentration measurements were obtained through a period spanning the illuminated steady-state and initial darkening (see supplementary Figure. S1). The time dependent and steady-state oxygen mass balances are described by Equations.5. S4 and 5. S5, respectively.

$$\frac{dC_{O_2}}{dt} = D_e \frac{d^2C_{O_2}}{dz^2} + P_g(z) - R_{light}(z) \quad \text{Eq. 5.S4}$$

$$P_g(z) = R_{light}(z) - D_e \frac{d^2C_{O_2}}{dz^2} \quad \text{Eq. 5.S5}$$

The light:dark shift measurements are based on non-steady-state measurements directly following the darkening procedure when the photosynthesis term is equal to zero (Eq. 5.S6). The initial-slope of time dependent oxygen response to darkening can be equated to the $P_g(z)$ by summing equations 5.S5 and 5.S6 (resulting in Eq. 5.S7). The initial-slopes were measured between 0 and 3 seconds for this study.

$$\frac{dC_{O_2}}{dt} = -R_{light}(z) + D_e \frac{d^2C_{O_2}}{dz^2} \quad \text{Eq. 5.S6}$$

$$\frac{dC_{O_2}}{dt} = -P_g(z) \quad \text{Eq. 5.S7}$$

Steady-state photosynthesis profiles were generated by taking $P_g(z)$ measurements through the depth positions-z in the biofilm. The active-photic zone was defined here as the depth of the biofilm from the surface to L_{phot}. The position L_{phot} was assumed to be equal to the position-z where $P_g(z)$=0. This assumption is validated in the current study by the observation that L_{phot} occurs within the oxic zones of the biofilms and is not dictated by a strong heterotrophic respiration component. The gross areal rate of photosynthesis (P_g) of the biofilm was calculated by integrating the function $P_g(z)$ from z=0 to z= L_{phot}. Integration was performed by the Simpson's five point quadrature rule. The areal rates of biofilm and photic zone respiration in the light were calculated by subtracting the respective net areal rates of photosynthesis (P_n and $P_{n,phot}$) from P_g.

5.5.4. Bead Beating Extraction of Lipids from Dry Biomass

Dried biomass (approximately 30 mg) was combined with 1 mL of chloroform in a 1.5 mL stainless steel bead beating microvial with silicone cap (BioSpec Products, Bartlesville, OK). Three types of beads (0.6 g of 0.1 mm zirconium/silica beads, 0.4 g of 1.0 mm glass beads, two 2.7 mm glass beads) were added to each vial before capping. A FastPrep bead beater (Bio101/Thermo Savant, Carlsbad, CA) was used to agitate the vials for six 20 s pulses at power level 6.5 followed by a 1 min cool down period between pulses. Total bead beating exposure time was 2 min. The mixture of solvent, residual biomass and beads was then transferred to a disposable 15 mL boro-silicate test tube, and the steel microvial was rinsed twice with 1 mL of chloroform, which was also added to the test tube, bringing the total solvent volume to 3 mL. Samples were then centrifuged at

1,200x g for 2 min to pellet the residual biomass. One mL of the organic phase was removed from the bottom of the test tube using a glass syringe and transferred to a 2 mL GC vial for GC-FID analysis.

5.5.5. Direct Transesterification for FAME Analysis

FAME composition was analyzed using gas chromatography – mass spectroscopy detection (GC-MS). Approximately 30 mg of dried biomass was transferred into a screw-cap glass tube for subsequent transesterification. One mL of toluene and 2 mL sodium methoxide (Fisher Scientific, Pittsburgh PA) were added to each test tube along with 10 µL of a 10 mg/mL standard mix (C11:0 and C17:0 TAG to monitor transesterification efficiency of the TAG into FAME). Samples were heated in an oven for 30 min at 90°C and vortexed every 10 min. Samples were allowed to cool to room temperature before 2 mL of 14% boron tri-fluoride in methanol (Sigma-Aldrich, St. Louis, MO) were added and samples were heated again for an additional 30 min. Samples were again allowed to cool before 10 µL of a 10 mg/mL of C23:0 FAME was added to assess the completeness of partitioning FAME into the organic phase. Additionally, 0.8 mL of hexane and 0.8 mL of a saturated salt water solution (NaCl in diH2O) were added. Samples were heated for 10 min to facilitate FAME partitioning into the organic phase, vortexed for 10 s, and centrifuged at 1,200x g for 2 min to enhance phase separation. One mL of the organic phase was removed from the top layer using a glass syringe and transferred to a 2 mL GC vial for GC-MS analysis.

5.5.6. GC-FID Analysis

GC-FID (Agilent 6890N, Santa Clara CA) analysis was conducted using 1 μL splitless injections onto a 15 m (fused silica) RTX biodiesel column (Restek, Bellefonte PA). The initial column temperature was held at 100°C for 1 min, before being increased to 370°C at a rate of 10°C min^{-1}. The injector temperature was held constant at 320°C. Helium was used as the carrier gas and column flow was held at 1.3 mL min^{-1} for 22 min, increased to 1.5 mL min^{-1}, held for 2 min, increased to 1.7 mL min^{-1} and held for 12 min. All flow rate increases were set to 0.2 mL min^{-2}. Calibration curves were constructed for each of the following standards: C10:0, C12:0, C14:0, C16:0, C18:0, C20:0 FFAs; C12:0, C14:0, C16:0, C18:0 MAGs; C12:0, C14:0, C16:0, C18:0 DAGs; and C11:0, C12:0, C14:0, C16:0, C17:0, C18:0, C20:0, C22:0 TAGs (Sigma-Aldrich, St. Louis MO) for quantification ($r^2 > 0.99$). This GC method allows for an estimate of the amounts of FFA, MAGs, DAGs and TAGs in a single analysis.

5.5.7. GC-MS Analysis

GC-MS (Agilent 6890N and 5973 Network MS) analysis was done according to a previously published protocol (Bigelow et al. 2011).

5.5.8. Supplementary Figures

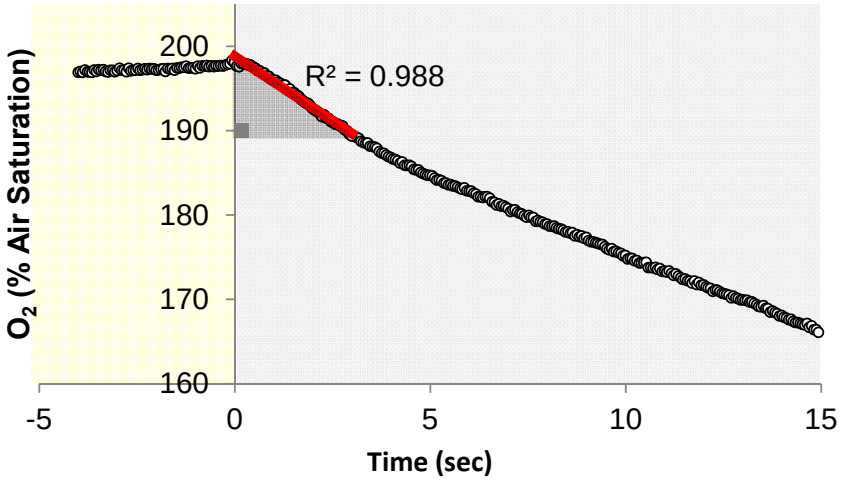

Figure 5.S 1. A representative light:dark measurement showing the transition from steady-state localized oxygen concentration (proportional to % air saturation) to time dependent oxygen depletion initiated by darkening. The slope of the initial oxygen decrease over time (red line) can be equated to –Pg(z).

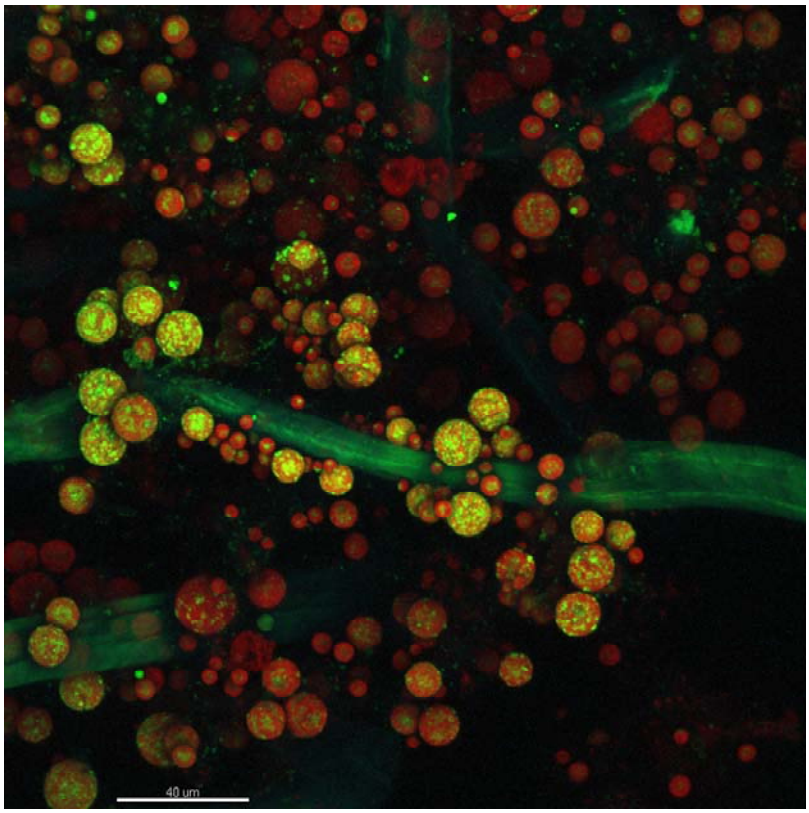

Figure 5.S 2. Cross-sectional image of a lab-RABR biofilm with WC-2B cell-material attached to the cotton cord substratum. This sample was stained with Bodipy 505/515, Calcofluor white and DAPI where: red (cholorophyll autofluorescence), green-intracellular (neutral lipids), blue-green (cotton cord fibers). DAPI (20 µg/mL) was found to be an enhancer of samples stained with Calcofluor white without staining intracellular nucleic acid. The scale bar represents 40 µm.

6. IN SITU ANALYSIS OF OXYGEN CONSUMPTION AND DIFFUSIVE TRANSPORT IN HIGH-TEMPERATURE ACIDIC IRON-OXIDE MICROBIAL MATS

Contribution of Authors and Co-Authors

Manuscript in Chapter 6

Author: Hans C. Bernstein

Contributions: Conception and critical analysis of research, data collection and analysis, manuscript drafting and editing.

Co-Author: Jacob P. Beam

Contributions: Conception and critical analysis of research, data collection and analysis, manuscript drafting and editing.

Co-Author: Mark A. Kozubal

Contributions: Data analysis

Co-Author: Dr. Ross P. Carlson

Contributions: Conception and critical analysis of research

Co-Author: Dr. William P. Inskeep

Contributions: Conception and critical analysis of research, manuscript drafting and editing.

Manuscript Information Page

Hans C. Bernstein, Jacob P. Beam, Mark A. Kozubal, Ross P. Carlson and William P. Inskeep*
Journal Name: Environmental Microbiology
Status of Manuscript
__Prepared for submission to a peer-reviewed journal
__Officially submitted to a peer-reviewed journal
__Accepted by a peer-reviewed journal
_X_Published in a peer-reviewed journal

Wiley
Article first published online: 2-20-2013

*Department of Land Resources and Environmental Sciences, and Thermal Biology Institute Montana State University, Bozeman, MT.
binskeep@montana.edu

6.1. Summary

The role of dissolved oxygen as a principal electron acceptor for microbial metabolism was investigated within Fe(III)-oxide microbial mats that form in acidic geothermal springs of Yellowstone National Park (USA). Specific goals of the study were to measure and model dissolved oxygen profiles within high-temperature (65-75 °C) acidic Fe(III)-oxide microbial mats, and correlate the abundance of aerobic, iron-oxidizing *Metallosphaera yellowstonensis* organisms and mRNA gene expression levels to Fe(II)-oxidizing habitats shown to consume oxygen. *In situ* oxygen microprofiles were obtained perpendicular to the direction of convective flow across the aqueous phase/Fe(III)-oxide microbial mat interface using oxygen microsensors. Dissolved oxygen concentrations dropped from ~50-60 μM in the bulk-fluid/mat surface to below detection (<0.3 μM) at a depth of ~700 μm (~10 % of the total mat depth). Net areal oxygen fluxes into the microbial mats were estimated to range from $1.4\text{-}1.6 \cdot 10^{-4}$ μmol cm^{-2} sec^{-1}. Dimensionless parameters were used to model dissolved oxygen profiles and establish that mass transfer rates limit the oxygen consumption. A zone of higher dissolved oxygen at the mat surface promotes Fe(III)-oxide biomineralization, which was supported using molecular analysis of *Metallosphaera yellowstonensis* 16S rRNA gene copy numbers and mRNA expression of heme Cu oxidases (FoxA) associated with Fe(II)-oxidation.

6.2. Introduction

Yellowstone National Park (YNP), Wyoming, USA contains a diverse collection of pristine high-temperature environments containing stable thermophilic microbial communities. Acidic (pH ~3), amorphous Fe(III)-oxyhydroxide microbial mats located in Norris Geyser Basin (NGB) are of particular interest due to the interplay between geochemical cycling, nutrient transport, and unique microbial metabolic capabilities associated with dominant community members of the domain *Archaea* (Inskeep et al. 2005; Inskeep et al. 2004; Inskeep and McDermott 2005; Inskeep et al. 2010; Jackson et al. 2001; Kozubal et al. 2008; Kozubal et al. 2011; Macur et al. 2004). Both autotrophic and heterotrophic Fe-metabolizing community members have been isolated and observed in metagenomes from Fe(III)-oxide mats in NGB (Inskeep et al. 2010; Kozubal et al. 2008; Kozubal et al. 2012b). Of these, Fe-oxidizing *Metallosphaera yellowstonensis*-like organisms have been shown to comprise near 20% of the total archaeal community in numerous Fe(III)-oxide microbial mats (Kozubal et al. 2008). *M. yellowstonensis* is known to utilize dissolved O_2 as the principal terminal electron acceptor *via* a heme Cu oxidase (FoxA) associated with the Fox terminal oxidase complex (Kozubal et al. 2008; Kozubal et al. 2011). An additional Fe-metabolizing community member (Sulfolobales strain MK5) has been characterized and found to be a heterotrophic Fe(II)-oxidizer and Fe(III)-reducer under aerobic and anaerobic conditions, respectively (Kozubal et al. 2012b). Other dominant organisms in Fe-oxide mat communities include a deeply-rooted archaeal lineage also thought to utilize O_2 based on analysis of respiratory pathways (Kozubal et al. 2012a). The growth and development of Fe(III)-oxide microbial mats is

likely influenced by the availability of electron donors and acceptors (and/or key nutrients) present within the mat microenvironments. The mass transfer of dissolved O_2 to and within the Fe(III)-oxide microbial mat is of specific interest due to the O_2 requirement of microbially mediated Fe(II)-oxidation as well as aerobic oxidation of organic carbon (heterotrophy) and arsenite (Hamamura et al. 2009).

Iron-oxidizing microorganisms are also important in deep sea hydrothermal vents, acid mine drainages, seeps, and other geothermal springs (Baker and Banfield 2003; Emerson and Moyer 2002; Emerson and Revsbech 1994a; Inskeep et al. 2004). Several neutrophilic Fe(II)-oxidizing microbial mat communities and structures have been characterized *in situ* using microsensors to evaluate gradients in oxygen (Druschel et al. 2008; Emerson and Revsbech 1994a; Emerson and Revsbech 1994b; Sobolev and Roden 2001). Typically, these studies have reported O_2 gradients extending from the oxic bulk-fluid interface towards anoxic regions. Microsensors (or microelectrodes) represent a reasonably noninvasive approach for measuring concentration profiles of dissolved O_2 and other chemical gradients *in situ* (Revsbech and Jorgensen 1986b).

Amorphous Fe(III)-As(V) oxyhydroxide microbial mats from NGB have been shown to form as a result of microbial activity (Inskeep et al. 2004). The rate of abiotic Fe(II)-oxidation is very slow at low pH (<4.5) (Konhauser 1998; Singer and Stumm 1970). Moreover, *M. yellowstonensis* strain MK1 has been shown to be highly relevant in these habitats and oxidizes Fe(II) in pure culture (Kozubal et al. 2008). Rapid microbial oxidation of As(III) to As(V) has also been observed in the outflow channels of acidic hot springs which has been linked with the expression of arsenite oxidase genes (Langner et

al. 2001; Macur et al. 2004). These microbial mats are comprised of fairly porous Fe(III)-oxides that form on rhyolitic parent material and are essentially equivalent to biofilm structures (Hall-Stoodley et al. 2004b). In other aerobic biofilms, it has been established that the transport of dissolved O_2 from the bulk fluid is influenced by the physical and structural properties of the biofilm matrix (de Beer et al. 1994a). Similarly, the consumption of dissolved O_2 and subsequent Fe(III)-oxide biomineralization rates in acidic geothermal systems are controlled by a combination of reaction kinetics (principally associated with microbial growth) and mass transport processes originating from the overlying gaseous oxygen ($p_{O2} \approx 0.16$ atm at this elevation). Few studies have coupled *in situ* O_2 microprofiles with the depth-wise distribution and transcriptional activity of a microbial community, especially in geothermal microbial mats.

M. yellowstonensis is an Fe(II)-oxidizing Sulfolobales abundant in acidic, high-temperature Fe(III)-oxide microbial mats in YNP, however, little is known regarding the distribution of these organisms with depth into the mat. It was previously shown that *M. yellowstonensis* is an obligate aerobe and actively transcribes its *foxA* gene within NGB geothermal springs (Kozubal et al. 2008; Kozubal et al. 2011). The *foxA* gene encodes for subunit 1 (heme Cu oxidase, HCO) of a terminal oxidase complex that is specific for the oxidation of ferrous Fe (Bathe and Norris 2007). Thus, this gene is essential as the final step of oxygen reduction in the electron transport chain of Fe(II) oxidation in *M. yellowstonensis* (Kozubal et al. 2011). The *foxA* gene has also been identified in other iron-oxidizing Sulfolobales (Auernik and Kelly 2008; Bathe and Norris 2007).

The current study focuses on *in situ* O_2 analysis as a function of depth in high-temperature Fe(III)-oxide mats to evaluate the extent and possible mechanisms of microbial O_2 consumption in archaeal-dominated communities. The specific aims of this study were to (i) measure *in situ* dissolved oxygen profiles within high-temperature acidic Fe(III)-oxide microbial mats, (ii) quantitatively compare O_2 mass transfer and consumption rates with rates of Fe(III)-oxide biomineralization, and (iii) link population abundance and mRNA gene expression levels of *Metallosphaera yellowstonensis* to Fe(II)-oxidizing habitats shown to consume O_2.

6.3. Results

6.3.1. Oxygen Microprofiles

The concentration of dissolved O_2 declined significantly as a function of depth in high-temperature Fe(III)-oxide mats (Fig. 6.1) from approximately 40-70 μM in the stream water to below detection (<0.3 μM) at depths ranging from 400 to 750 μm (Fig. 6.2, Table 6.1). Oxygen was detected to depths of 250-1300 μm in *Beowulf* (BE_D) iron mats. An average depth of 730 ± 500 μm was obtained from three oxygen profiles located within a 2 cm radius. Depths of O_2 penetration were more similar among replicates measured at *One Hundred Springs Plain* (OSP_B), and averaged 800 ± 88 μm. Based on a measured total mat thickness (L_f) of ~7 mm, these results show that detectable levels of oxygen were observed in the top ~10% of the Fe(III)-oxide microbial mat.

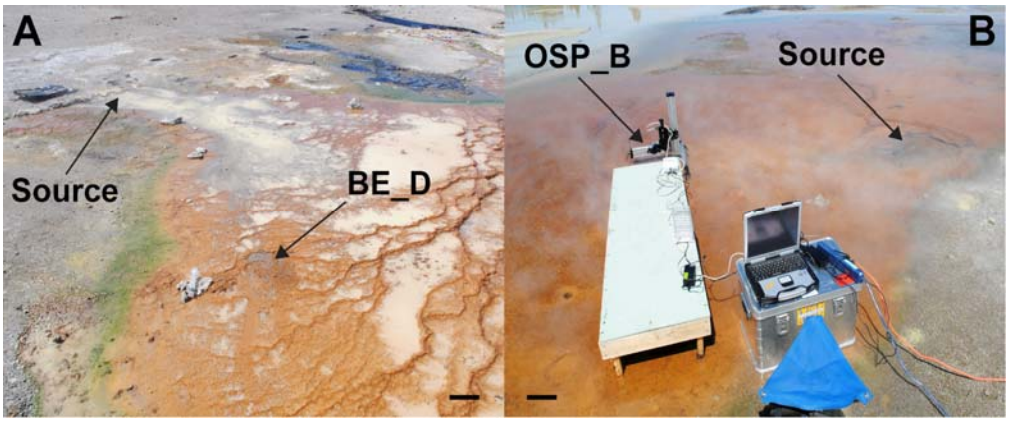

Figure 6. 1. Photographs of sampling sites at (A) Beowulf Spring (BE) and (B) One-Hundred Springs Plain (OSP). Arrows represent approximate positions where aqueous geochemical and solid phases were sampled for molecular analysis and where oxygen microelectrode measurements were obtained (scale bar = 20 cm).

Dissolved O_2 profiles from both sites (*Beowulf* and *One-Hundred Springs Plain*) show the zones of most rapid concentration change near the surface of the mat (Fig. 6.2). The predominant concave curvature of all O_2 profiles implies that there was no and/or negligible amounts of O_2 being produced and evolved from the mat. Although some O_2 profiles exhibited minor inflections in curvature, these are likely due to flow-oriented laminations (*i.e.*, thin layers exhibiting variable O_2 consumption rates) and structural heterogeneity (*i.e.*, channels and voids) observed as a function of mat depth (Fig. 6.3). Dissolved O_2 measurements made at different water column depths above the Fe-oxide mat surface were fairly constant (60 ± 15 μM) indicating that the stream water above the mat is well-mixed and below the measured O_2 saturation (100 μM; see methods). Moreover, these measurements did not have the resolution to identify a diffusive boundary layer (DBL). The DBL thickness is primarily a function of velocity. Measured surface velocities over the Fe mats are high (5-20 $cm \cdot sec^{-1}$), and mass transfer limitations

external to the Fe mat were assumed negligible. The observed transition from a well-mixed bulk liquid to a depth-dependent O_2 concentration profile suggest that diffusion is the primary mechanism of mass transport within the Fe(III)-oxide mat.

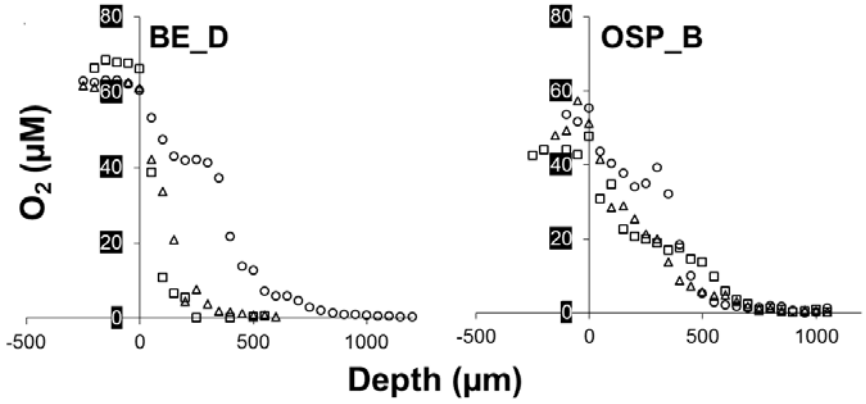

Figure 6. 2. Dissolved O2 microprofiles measured at sampling locations (BE_D and OSP_B) within Beowulf and OSP geothermal springs. Each plot contains 3 individual profiles taken at different positions within a ~2 cm radius [individual data points were measured in 50 µm step sizes; x = 0 corresponds with the mat surface].

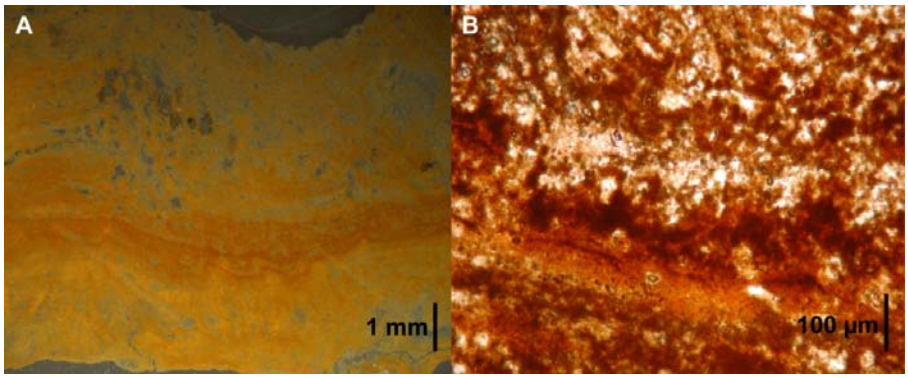

Figure 6. 3. Stereo-micrographs of epoxy thin sections of BE_D iron-oxide microbial mat cut perpendicular to the bulk stream flow. Orientated visual structural variations (e.g., laminations and voids) represent heterogeneity in the Fe(III)-oxide mat structure. A) Full-scaled image of an excised bulk-mat sample. B) Fine-scaled image of laminated portion of a second excised bulk-mat sample.

Fick's law was used to calculate the net flux of dissolved O_2 into the near surface of the Fe(III)-oxide mat using measured oxygen concentration profiles and the linear portions of the profile that span the aqueous-mat interface. Diffusion coefficients for dissolved O_2 in water were estimated to be $6.1 \cdot 10^{-5}$ and $6.2 \cdot 10^{-5}$ $cm^2 \cdot sec^{-1}$ at 68 °C and 75 ºC (BE_D and OSP_B, respectively) using the Wilke-Chang correlation (Wilke and Chang 1955). The calculated O_2 flux values were $1.64 \cdot 10^{-4}$ and $1.41 \cdot 10^{-4}$ µmol $O_2 \cdot cm^{-2} \cdot sec^{-1}$ for BE_D and OSP_B, respectively. Assuming steady-state, these values represent a net areal rate of O_2 consumption by the Fe-oxide microbial mats.

Table 6. 1. Select aqueous geochemistry at sampling positions (BE_D and OSP_B) within Beowulf and OSP Springs, Norris Geyser Basin (YNP). Values represent multiple sampling times corresponding to the study period over two summer seasons (2010-2011).

Site	pH	pH (Mat)	Temp (˚C)	DS	O_2 (aq)	CO_2 (aq)	Fe (TS)
				----------µM----------			
BE_D	3.0(0.1)	2.7	68(2)	6 (4)	60(20)	800 (322)	39 (5)
OSP_B	3.4(0.1)	3.75	75(2)	4(2)	51(12)	340 (221)	32 (8)

[1] DS=dissolved sulfide; Fe(TS)=total soluble Fe (essentially 98% ferrous-Fe)
[2] Standard deviations are in parentheses (n=4).

6.3.2. Reaction-Diffusion Analysis

Oxygen profiles were used to fit steady-state reaction-diffusion models assuming either first or zero-order kinetics (Eq. 6.1 and 6.2) using profile data scaled to the unitless parameters u (dimensionless concentration) and ζ (dimensionless mat depth) (see methods). A concentration-dependent (first-order) model fit the data from both sites (R^2

values ≥ 0.96) compared to poor fits using a zero-order model ($R^2 < 0.5$, data not shown). Consequently, the O_2 consumption rates are best described with concentration-dependent kinetics (Fig. 6.4). The first-order Thiele modulus ϕ_1 (see methods and supplementary text) is defined as a ratio of the reaction to diffusion time scales and was used as the single fitting parameter for modeling experimental dissolved O_2 profiles. Values of the fitted first-order Thiele moduli ranged from ~30 to 60 (OSP_B and BE_D profiles, respectively), suggesting that under these conditions, the reaction time-scale is an order of magnitude greater than the diffusion time-scale. Consequently, the rate of microbial oxygen consumption is likely controlled by the diffusion rate of dissolved oxygen in the mat.

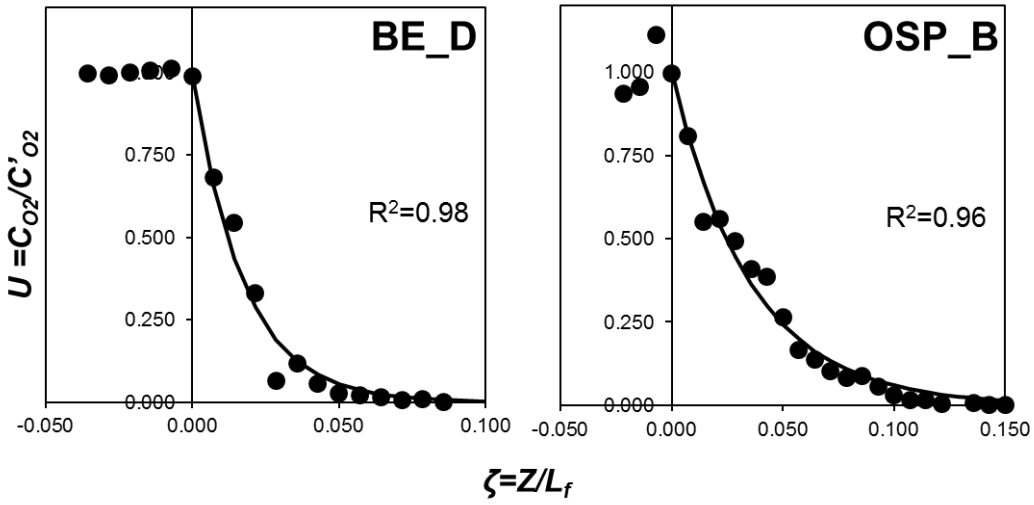

Figure 6. 4. Representative dissolved O2 micro-profiles expressed in terms of dimensionless parameters u and ζ (also see methods). Solid lines represent the fitted reaction diffusion models assuming a first-order rate equation (Eq. 6.1) and optimized values of the Thiele modulus (ϕ_1) to maximize R^2 values. The models are limited to spatial regions defined by $\zeta > 0$, corresponding to positions inside the Fe(III)-oxide mat matrix.

6.3.3. Fe(III)-Oxide Accretion Rates

The rate of Fe(III)-oxide deposition was determined *in situ* using glass slides (75 x 25 x 1 mm) (Fig. 6.S 1) introduced and analyzed during the study period corresponding to O_2 profile measurements. The amount of Fe(III)-oxide accumulated on the slide surface increased linearly over 133 days (Fig. 6.5), resulting in measured Fe(III)-oxide accumulation rates of $0.4 \cdot 10^{-5}$ and $3.0 \cdot 10^{-5}$ μmol $Fe \cdot cm^{-2} \cdot sec^{-1}$ for BE_D and OSP_B, respectively. Aqueous Fe(III) was also produced as a direct result of Fe(II) oxidation at these spring positions and was as much as 5-10% of the total aqueous Fe (Table 1) (Inskeep et al. 2004; Kozubal et al. 2012b; Macur et al. 2004).

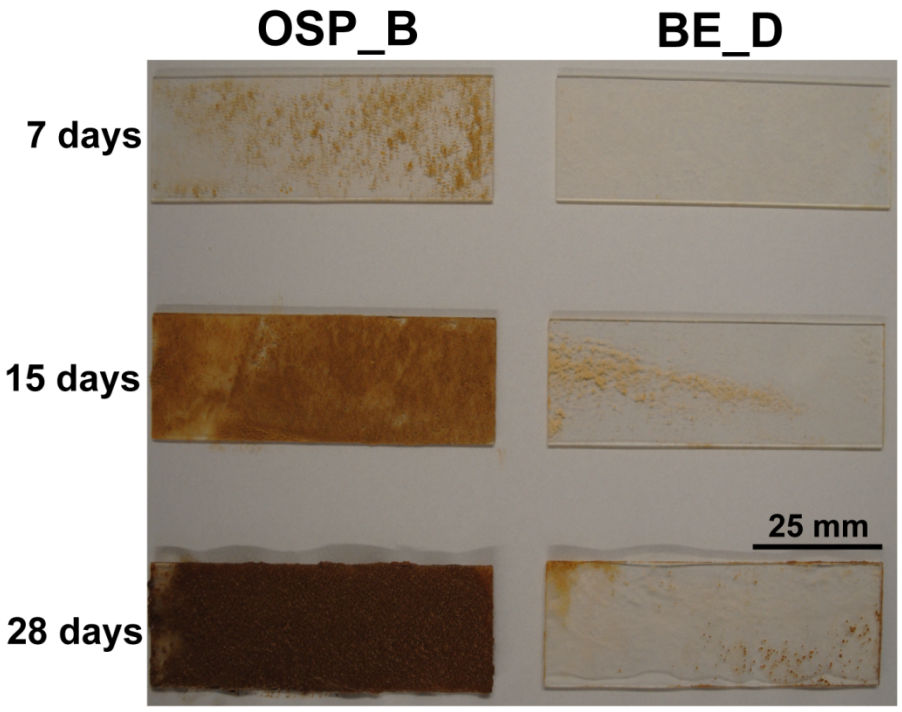

Figure 6.S 1. Photograph of in situ incubated glass microscope slides over 28 total days of biomineralization from OSP_B and BE_D. Scale bar = 2.5 cm. Supplementary figure from original manuscript (Bernstein et al. 2013)

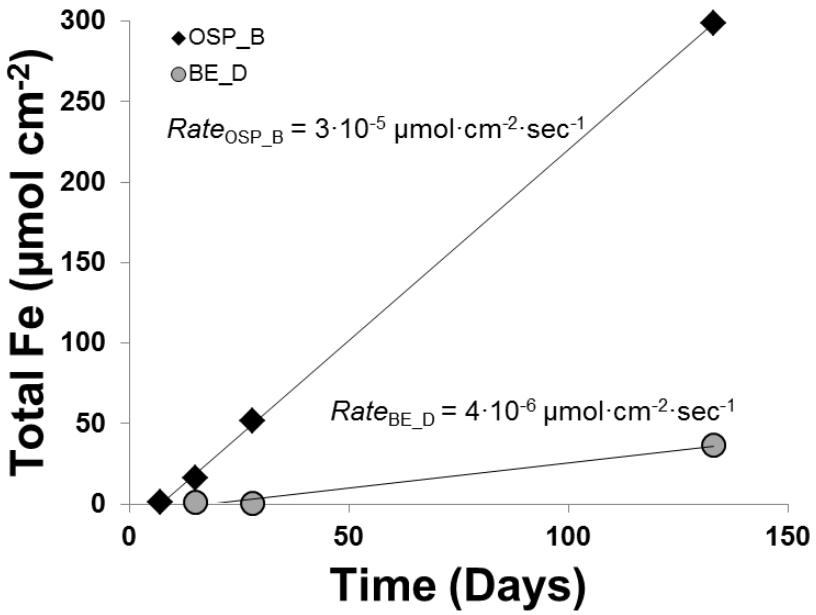

Figure 6. 5. Total iron accumulation on glass microscope slides incubated in situ for 133 days. Slopes of the linear accretion curves represent the net iron accumulation rates ($Rate_{BE\_D}$ and $Rate_{OSP\_B}$).

Electron micrographs of material accumulated in OSP_B show cell attachment within 7 days of incubation, formation of amorphous Fe(III)-oxide within 14 days and complete slide coverage within 30-45 days depending on site (Beam 2011; Macur et al. 2004). The heterogeneous Fe(III)-oxide surfaces forming at the aqueous/mat interface are replete with Fe-encrusted cells resulting from the oxidation of Fe(II) (Fig. 6.6), and reveal the type of surface in which oxygen microelectrodes were introduced. Previous analysis of the Fe(III)-oxide mats in NGB have shown that the predominant Fe phases formed in these systems are amorphous Fe(III)-oxyhydroxides containing significant levels of sorbed arsenate (As^{V}:Fe^{III} mole ratios~0.65) (Inskeep et al. 2004). Measured rates of Fe(III)-oxide accumulation represent the total rate of Fe(III) produced minus any aqueous

Fe(III) and Fe(III)-oxides that are reduced or transported away in the stream channel (discussed further below). Accumulation of Fe(III)-oxide on the slides due to erosion from upstream sources is negligible, in part because there is a direct linkage between cell surfaces and Fe(III)-oxide mineralization. The measured net vertical growth (L_f = mat depth) of the Fe(III)-oxide microbial mat was ~7 mm (after 133 days of *in situ* incubation at the OSP_B site). Similarly, the measured L_f at BE_D ranges from ~5-10 mm determined by direct measurement of the native mat and epoxy embedded thin sections (Fig. 6.3). Although the absolute mat depth varies across cm scales, localized electrode (50 μm diameter) measurements were made in mats with average thicknesses of ~ 7 mm at both sites.

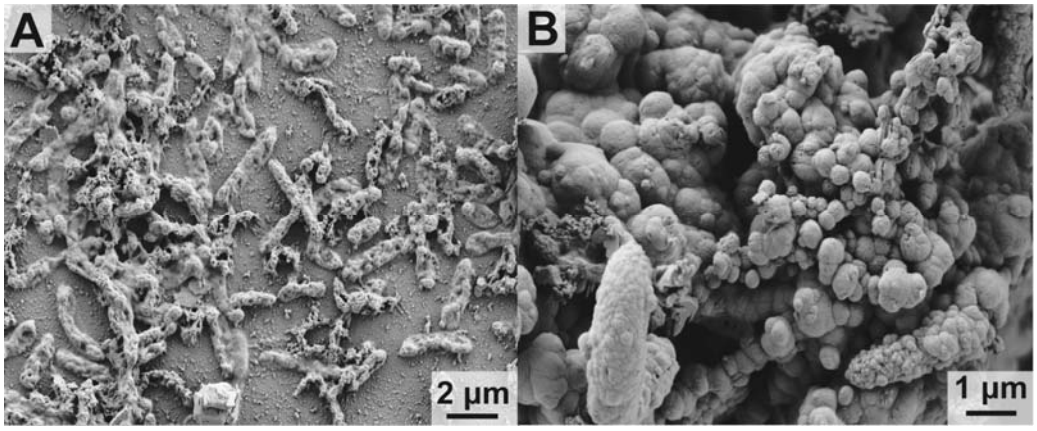

Figure 6. 6. SEM micrographs of glass slides incubated in the OSP_B site. A) Attached cells observed after 1 week. B) Mature amorphous Fe(III)-oxyhydroxide mat showing encrusted cells and ubiquity of biomineralized Fe(III)-oxides after 2 weeks.

6.3.4. Vertical Distribution and Activity of *M. yellowstonensis*

M. yellowstonensis has been well established as an active and abundant Fe(II)-oxidizing Sulfolobales in acidic, geothermal Fe(III)-oxide microbial mats in NGB (Kozubal et al. 2008; Kozubal et al. 2011). Microbial mats subjected to O_2 profile measurements were sampled and dissected to remove top and bottom samples (see methods), and to establish a direct linkage between the presence of this population and measured Fe(III)-oxide deposition. Significant numbers of *M. yellowstonensis* were observed in all Fe-mat samples, and quantitative estimates of 16S rRNA gene copy number were higher in the top 1 mm of mat (bulk-liquid/mat interface) at both sampling sites. This result was more evident at OSP_B where 16S rRNA gene copy numbers ranged from 2.3±0.1 to $0.7\pm0.1\cdot10^5$ per gram in top and bottom mat samples, respectively. At BE_D, gene copy numbers for *M. yellowstonensis* ranged from $5.5\pm1.2\cdot10^5$ to $4.9\pm0.6\cdot10^5$ per gram in top and bottom mat samples, respectively (Fig. 6.7A).

Corresponding Fe(III)-oxide mat samples were also used to obtain semi-quantitative estimates of *M. yellowstonensis*-like *foxA* mRNA transcripts using reverse transcriptase-PCR. *foxA* gene transcripts (mRNA) were observed in Fe(III)-oxide mats from both sites (semi-quantitative estimates are normalized to 16S rRNA gene copy number, Figure 6.7B), and trends among the two sites and mat depths were similar to those observed using estimates of *M. yellowstonensis* 16S gene copy number. Specifically, *foxA* gene transcripts (mRNA) were also higher in top versus bottom mat samples from OSP_B (Fig. 7B). Normalized *foxA* transcript levels in BE_D were similar

between top ($1.00 \pm 0.00 \cdot 10^{-2}$) and bottom ($0.94 \pm 0.05 \cdot 10^{-2}$) mat samples, suggesting that *M. yellowstonensis*-like organisms were still active in lower mat regions. These expression values agree with those found for *M. sedula* and *M. yellowstonensis* in pure culture grown on Fe(II) as the sole electron donor (Kappler et al. 2005; Kozubal et al. 2011). Among all Fe(III)-oxide samples evaluated, the top 1 mm of the OSP_B mat showed the highest localized O_2 concentrations (~ 50-70 μM), greater *M. yellowstonensis* 16S rRNA gene copy numbers, and higher amounts of *M. yellowstonensis foxA* mRNA.

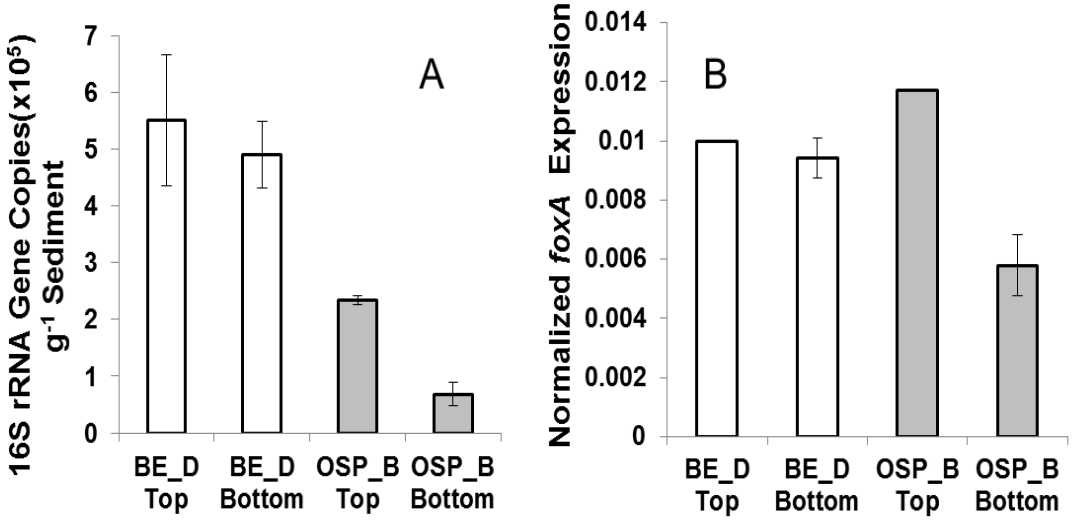

Figure 6. 7. A) Spatial distribution of M. yellowstonensis 16S rRNA gene copies and B) relative expression of foxA mRNA to 16S rRNA gene copies in BE_D and OSP_B. The designations "Top" refers to the first 1mm of mat material at the mat/bulk-liquid interface; 'bottom mat' refers to the remainder of the mat. P-values: A) = 0.46 and $9.6 \cdot 10^{-5}$ for BE_D and OSP_B, respectively and B) = 0.13 and 0.005 for BE_D and OSP_B, respectively. Error bars represent ± 1 standard deviation from three technical replicates.

6.4. Discussion

6.4.1. Contributions to Biological Oxygen Consumption

High-temperature acidic Fe(III)-oxide microbial mats are reactive O_2 sinks. The net areal oxygen consumption rates estimated from the measured microprofiles encompass the sum of all oxygen-consuming reactions occurring *in situ*. The microbial populations present in high-temperature acidic Fe(III)-oxide mats from Norris Geyser Basin have been studied in considerable detail (*e.g.,* Inskeep et al., 2010; Kozubal et al., 2012ab) and results from these efforts form a basis for interpreting O_2 consumption observed in the current study. The microbial processes that contribute to O_2 consumption in these systems include the aerobic oxidation of electron donors such as reduced-C, Fe(II), As(III), hydrogen and reduced sulfur (e.g., sulfide and or elemental S). Of these possible electron donors, those likely to be responsible for the majority of O_2 consumption include reduced-C, Fe(II), and As(III), based on the concentrations measured *in situ*. Organic carbon utilized by aerobic chemoorganotrophs (Table 6.2) likely originates from three sources: decaying biomass of autotrophic microorganisms (*e.g., M. yellowstonensis*), dissolved organic carbon from source waters (~ 50 μM C), and exogenous inputs from the local landscape (*e.g.,* atmosphere, plant, animal, soil). Although highly exergonic, the concentrations of other electron donors (hydrogen, reduced S, methane) are too low to support significant O_2 consumption (Inskeep et al. 2005). The rates of Fe(III)-oxide deposition (*e.g.,* $3 \cdot 10^{-5}$ μmol $Fe \cdot cm^{-2} \cdot sec^{-1}$ at OSP_B)

were used to estimate the O_2 flux required to account for this fraction of total Fe(II) oxidation.

The rates of Fe(III)-oxide deposition (*e.g.,* $3 \cdot 10^{-5}$ μmol Fe·cm^{-2}·sec^{-1} at OSP_B) were used to estimate the O_2 flux required to account for this fraction of total Fe(II) oxidation. It is understood that the actual oxygen flux attributable to the total Fe(II) oxidation rate in these systems will be higher, because some Fe(II) oxidized is lost as aqueous Fe(III), eroded as Fe(III)-oxides in the stream channel, and/or lost due to reductive-dissolution. For OSP_B, the amount of oxygen consumed by Fe(II) oxidation, specifically resulting in Fe(III)-oxide solids accumulated, was estimated at 5.3% of the total measured O_2 flux (one mole Fe(III) requires 0.25 mole O_2). The estimates are an order of magnitude lower at BE_D (only 0.61% of the measured O_2 flux can be attributed to Fe(III)-oxide deposition). The lower values at BE_D are due in part to higher stream channel velocities in *Beowulf Spring* (~14-20 cm sec^{-1}), which results in greater erosion of Fe(III)-oxide particles. The *OSP* site discharges on a lower slope than *Beowulf Spring* resulting in a shallower water column with lower channel velocities (~6-10 cm·sec^{-1}). Shear forces from bulk liquid flow coupled with photo-reduction and dissolution are both potential mechanisms for Fe(III)-oxide material loss, but the lower velocities in *OSP Spring* suggest that Fe(III)-oxide deposition rates measured at OSP_B are closer to an upper value of the contribution of Fe(II)-oxidation to O_2 flux (~ 5 %). These estimates are reasonably consistent with the abundance of *M. yellowstonensis* like organisms in BE and OSP determined from prior studies (Inskeep et al. 2010; Kozubal et al. 2008; Kozubal et al. 2012b) to range from ~12-23% of the community using different molecular

approaches (summarized in Table 2). Another aerobic Fe(II)-oxidizing organism from the BE site Fe(III)-oxide mat is the Sulfolobales strain MK5 confirmed to be an Fe(II)-oxidizing organism in culture and by the presence of a Fox terminal oxidase complex (Kozubal et al. 2012b).

Correlation of oxygen consumption and Fe(III)-oxide deposition rates coupled with expression of Fe(II)-oxidizing heme Cu oxidases (*foxA*) from *M. yellowstonensis*-like organisms provides direct evidence for the linkage between the activity of this population and measured O_2 profiles across a mat depth of approximately 700 µm. However, a significant percentage of the total O_2 consumption is due to other aerobic members present in these communities. For example, microbially mediated As(III) oxidation by *Hydrogenobaculum* sp. (order Aquificales) represents another O_2 consuming process (Table 6.2) that has been reported in other studies (Hamamura et al. 2009; Langner et al. 2001; Macur et al. 2004). Estimated arsenite oxidation rates in these same Fe(III)-oxide mat systems are $0.26 \cdot 10^{-5}$ and $1.95 \cdot 10^{-5}$ µmol As(III)$\cdot cm^{-2} \cdot sec^{-1}$ for BE_D and OSP_B, respectively (Fe(III) accretion rates scaled by As^{V}:Fe^{III} mole ratios ~0.65) (Inskeep et al. 2004). Stoichiometrically, this corresponds to oxygen consumption rates of $0.13 \cdot 10^{-5}$ and $0.98 \cdot 10^{-5}$ µmol $O_2 \cdot cm^{-2} \cdot sec^{-1}$ for BE_D and OSP_B, which represents approximately 0.8 and 6.9% of the net areal O_2 consumption directly measured in BE_D and OSP_B, respectively.

Table 6. 2. Estimates of abundance of predominant taxa determined in iron oxide mat samples (BE_D and OSP_B) taken at similar locations to those used for oxygen microelectrode profiles. The presence or absence of heme copper oxidases (HCO) used for the reduction of oxygen in aerobic respiration is summarized.

Site/Population	Estimated Abundance[1]	HCO[2]	Reference
OSP_B (T=75 C,			
• Novel Archaea Group 1	50-	Y	Kozubal et al.
• *M. yellowstonensis*	15-	Y	Kozubal et al.
• *Vulcanisaeta* spp.	13-	N	Jay et al. 2011
• *Acidilobus* spp.	5-10	N	Jay et al. 2011
• *Hydrogenobaculum* spp.	~1-2	Y	Kozubal et al.
• Other	<2		
BE_D (T=68 C,			
• Novel Archaea Group 2	35-	Y	Kozubal et al.
• *M. yellowstonensis*	20-	Y	Kozubal et al.
• Sulfolobales_MK5	5-10	Y	Kozubal et al.,
• Thermoplasmatales-like	5-10	Y	Inskeep et al.
• Thaumarchaeota	5-10	Y	Beam et al.
• Novel Archaea Group 1	3-5	Y	Kozubal et al.,
• *Acidilobus* spp.	3-5	N	Inskeep et al.
• *Hydrogenobaculum* spp.	3-5	Y	Inskeep et al.
Other	<2		

[1] Estimated abundance based on phylogenetic classification of contigs (> 4,000 bp) from assembled metagenome sequence (see references cited)
[2] Yes/No is based on the presence or absence of a terminal oxidase complex containing a subunit-1 heme Cu oxidase (HCO)
[3] Contains a Fox terminal oxidase complex specific for Fe(II)-oxidation in the Sulfolobales (Kozubal et al., 2011; 2012a)

The dominant members of the OSP_B and BE_D Fe(III)-oxide microbial mats also include representatives from two novel lineages in the *Archaea* (Kozubal et al. 2012a; Kozubal et al. 2012b) (Table 6.2). The 'novel archaeal group 1' (NAG1) population is in higher abundance at OSP_B, while the 'novel archaeal group 2' lineages are more abundant in BE_D. However, all of these community members appear to be aerobic chemoorganotrophs based on the presence of terminal oxidase complexes including the subunit I HCO (Inskeep et al. 2010; Kozubal et al. 2012a; Kozubal et al.

2012b). Although *de novo* sequence assemblies of NAG1 show no evidence of Fe(II)-oxidation genes, the population appears capable of aerobic oxidation of complex carbon and CO as potential energy sources (Kozubal et al. 2012a). The Desulfurococcales and Thermoproteales-like populations present in OSP_B and BE_D do not likely respire O_2, based on the absence of heme Cu oxidases in *de novo* assemblies from these sites (Jay et al. 2011) as well as the fact that most cultured organisms from these orders are strict anaerobes that often require reduced forms of sulfur (Jay et al. 2011; Meyer-Dombard et al. 2005).

6.4.2. Oxygen Mass-Transfer Limitations

The rapid biotic consumption of O_2 in these Fe(II)-oxidizing biofilms is ultimately limited by the diffusive mass transfer rates through the Fe(III)-oxide matrix. Estimates of the first-order Thiele modulus (used as a single data fitting parameter) allowed quantification of time scales for oxygen consumption rates relative to mass transfer (diffusion) rates, and suggested that the system is *mass transfer limited* with regards to dissolved O_2. The rapid rates of O_2 consumption are consistent with the importance of terminal oxidase complexes found in the organisms inhabiting these Fe mats (Inskeep et al. 2010; Kozubal et al. 2012a; Kozubal et al. 2012b). However, the biomineralization and evolution of an Fe(III)-oxide biofilm (matrix) results in a *diffusion-limited* system that exhibits a pronounced gradient in dissolved O_2 from bulk-aqueous levels of ~50-60 μM to below detection (<0.3 uM), all within approximately 700 μm. Given that the top of these mineralized structures contain the most oxygen, it is expected that Fe(II)-oxidation rates are greater near the aqueous-mat interface. Evidence for this

hypothesis was obtained for OSP_B, however, *foxA* transcripts were nearly equally abundant throughout the entire depth of BE_D Fe(III)-oxide mats. Certainly, the Fe-oxide mats studied here also exhibit heterogeneity that could contribute to differential O_2 diffusion rates to lower mat depths (e.g., preferential versus restricted convective or diffusive transport, Fig. 6.3).

6.4.3. Biological Iron-cycling

Acidic geothermal springs in NGB are anoxic at the source and Fe(II)-oxidizing microbial communities do not occur until the springs have sufficient dissolved O_2 from atmospheric mixing, after dissolved sulfide has degassed. Abiotic Fe(II)-oxidation in the springs is negligible in contrast to the microbially mediated process at these pH values (Singer and Stumm 1970). Anaerobic Fe(II)-oxidation has not been observed *in situ.* In fact, the ΔG_{rxn} for the reduction of nitrate ($8Fe(II) + NO_3^- + 21\ H_2O = 8Fe(OH)_3(s) + 14H^+ + NH_4^+$) has been shown to be endergonic and would not be expected to be a dominant metabolism in these systems (Inskeep et al. 2005). Therefore, Fe(II)-oxidation is a direct result of aerobic members of the orders Sulfolobales (*e.g., M. yellowstonensis* and Sulfolobales MK5-like organisms).

The reduction of Fe(III)-oxides has not been measured directly in these iron mats, however, this process cannot be ruled out. Prior work on these systems shows other community members that may contribute to the reduction of Fe(III)-oxides including Sulfolobales strain MK5 (Kozubal et al. 2012b). The predominant geochemical process in these environments is Fe(II)-oxidation as evinced from several important observations that have preceded this work. First, depth-wise mineralogical characterization of these

amorphous iron oxides revealed no transformation to other Fe oxide phases (*e.g.,* magnetite) (Inskeep et al. 2004; Kozubal et al. 2012b), which is a likely indicator that Fe(III)-reduction does not contribute significantly to losses of Fe(III). Second, these mats contain very few bacteria and prior 16S rRNA gene surveys show no evidence of known Fe(III)-reducing populations (Inskeep et al. 2004; Kozubal et al. 2012b). Additionally, no outer membrane cytochromes known to catalyze Fe(III)-reduction have been found in metagenomes from these sites (Inskeep et al. 2010).

6.4.3. Conclusion

Results from this study highlight the importance of a potentially limiting substrate (dissolved oxygen) for microbial metabolism at high temperatures and the subsequent aerobic biomineralization of Fe(III)-oxide phases in acidic springs of YNP. These biotic oxygen-sinks are ultimately limited by the mass transfer of O_2 through the Fe(III)-oxide matrix. The consumption of O_2 is a multi-scale process spanning molecular, cellular and macroscopic (pore-scale) regimes. Measured O_2 depth-profiles in two acidic springs of Norris Geyser Basin reveal a defined spatial zone where the majority of oxygen-consuming reactions are occurring. The spatial abundance of an established Fe(II)-oxidizing community member (*M. yellowstonensis*) was shown to correlate with the presence of dissolved oxygen and we expect the same will be true for other aerobic heterotrophs containing terminal oxidase complexes that require oxygen as a terminal electron acceptor (Table 2). The formation of microbial structures (*e.g.,* mats, biofilms) containing Fe(III)-oxides *via* biomineralization is inextricably linked to the diffusive

transport of oxygen, which also defines a pronounced gradient of dissolved oxygen in the top ~ 700 μm of Fe(III)-oxide microbial mat.

6.5. Experimental Procedures

6.5.1. Site Description and Geochemistry

Two iron-oxide microbial mats from NGB were chosen for this study: *Beowulf Spring*, east discharge, position D (BE_D) and One Hundred Springs Plains, position B (OSP_B) (Fig. 6.1, Table 6.1). These sites were prime candidates for this study due to prior detailed geochemical, physical, and microbiological characterization (Inskeep et al. 2004; Inskeep and McDermott 2005; Inskeep et al. 2010; Kozubal et al. 2008; Kozubal et al. 2011). *Beowulf Spring* is a heavily terraced iron-oxide mat system flowing north on a relatively steep-grade, whereas *OSP Spring* is a slower (pulse-type) stream channel flowing southwest on a lower grade that yields a shallower, lower-velocity system. The coordinates of the study sites are: BE_D (44°43’53.224” N, 110°42’40.727” W) and OSP_B (44° 43' 58.8" N, 110° 42' 32.1" W). Temperature was measured with a digital thermometer equipped with a T-type thermocouple (Omega Engineering, Inc) with an error of ± 1°C. A portable Accumet® AP71 pH/mV/°C meter (Fisher Scientific) was used to measure pH and was calibrated in the field using pH standards of 4.01 and 7.0. Dissolved oxygen, aqueous CO_2, total sulfide, and ferrous-ferric iron were measured from duplicate samples in the field as previously described using colorimetric methods (Loeppert and Inskeep 1996).

6.5.2. Oxygen Profiles

Dissolved O_2 profiles were obtained in the direction normal to the bulk flow and surface of the mat (i.e., the aqueous-mat interface). All profiles were taken with high-temperature tolerant 50 μm (tip diameter) Clark-type microsensors (custom equipment provided by Unisense A/S, Aarhus DK). The O_2 consumption rate by the microsensors was estimated at $8 \cdot 10^{-3}$ $\mu mol \cdot year^{-1}$, which was considered negligible. Sensor positioning was controlled with a micromanipulator coupled to a motor controller. The micromanipulator was housed on a custom, adjustable tripod stand that was used in the field to perform profile measurements. Data collection and positioning controls were performed with Sensor TracePro software (Unisense). Sensors were individually calibrated in the field, using the anoxic calibration point from either 100 mM Na_2S (pH=10) or by positioning the sensor inside the iron-oxide mat where the oxygen signal was less than 5% of the bulk liquid value (e.g., near detection). The oxic calibration point was obtained by positioning the sensor in the bulk liquid directly above the Fe-oxide mat; this value was also confirmed using independent measurements obtained by the Winkler method. The O_2 saturation values were also directly measured by the Winkler method by aerating 100 ml spring water at ~1 LPM inside a beaker (incubated at 75 ºC inside the spring) connected to an air pump and air stone. All profiles were performed in triplicate (three positions within a ~2 cm radius of each other) for each sample site. Triplicate technical replicates were done for profiles taken in the OSP_B site, however the brittle nature of the mat at BE_D only allowed for a single accurate profile per position.

Locations corresponding to the surface of the mat were confirmed both visually and by initial changes in the profile slope.

6.5.3. Calculations and Modeling

Classical reaction and diffusion theory was used to quantitatively analyze coupled reaction and mass transfer rates. Reaction and diffusion of substrates in microbial mats, biofilms, and catalyst materials has been studied extensively (Karel and Robertson 1987; Stewart 2003; Stewart and Raquepas 1995; Thiele 1939; Williamson and Mccarty 1976). Briefly, by assuming a steady-state mass balance and one-dimensional slab geometry, Fick's law was used as a basis for modeling the experimental data and the empirical analysis of the bulk O_2 flux. The model was simplified by assuming constant effective diffusion constants and a singular reaction term which represents the sum of all O_2 consuming processes. The volumetric reaction rate was assumed to be bounded by either a first-order ($R=k_1 C_{O2}$) or zero-order rate expression ($R=k_0$). Dimensionless parameters were defined as:

$$u=C_{O2}/C_{O2}', \quad \zeta=z/L_f, \quad \phi_o^2=k_o \cdot L_f/(C_{O2}' \cdot D_e), \quad \phi_1^2=k_1 \cdot L_f^2/D_e$$

where u is the ratio of the observed dissolved O_2 concentrations in the mat relative to the bulk liquid, ζ is the dimensionless depth parameter, z is the mat depth, L_f is the total depth of the Fe(III)-oxide mat, ϕ is the Thiele modulus, a dimensionless rate constant defined using a ratio of the reaction rate coefficient to the effective diffusion coefficient (D_e) scaled to a characteristic area (L_f^2) (Thiele 1939). Actual L_f values were obtained either by microscopy of excised mat sections (site BE_D) and by direct

measurement of iron oxide mat accretion samples under steady-state conditions (site OSP_B) (see results and discussion sections). The effective diffusion coefficient of O_2 in the iron oxide microbial mat matrix is not known nor easily measured; consequently, the Thiele modulus is a useful parameter, which is inversely proportional to D_e.

Dimensionless analytical solutions (equations 6.1 and 6.2) to differential mass balances were obtained by imposing a zero-flux boundary condition at the bottom of the mat ($z=L_f$) and setting the observed concentration of dissolved O_2 to the constant bulk liquid concentration at the top of the mat (z=0).

$$u=\cosh(\phi_1\cdot\zeta)-\tanh(\phi_1)\cdot\sinh(\phi_1\cdot\zeta) \quad \text{Eq. 6.1}$$

$$u=(\phi_o^2\cdot\zeta^2)/2-\phi_o^2\cdot\zeta+1 \quad \text{Eq. 6.2}$$

Equations 6.1 and 6.2 are the analytical solutions for the first and zero-order reaction models, respectivly. The analytical solutions were used to fit O_2 profile data (non-linear least squares regression) resulting in estimates of the Thiele moduli. Detailed and step-wise interpretations of the reaction-diffusion models and dimensionless number interpretations are contained in the supplementary text of this manuscript.

6.5.4. Iron-oxide Accretion Rates

Glass microscope slides (75 x 25 x 1 mm) were cleaned in a 2% hydrochloric acid bath for ~2 hours to remove organic carbon, rinsed in 18 MΩ H_2O (free of organic carbon), and autoclaved for 15 minutes. The cleaned slides were placed in the primary outflow channel of OSP_B (73 ˚C) and BE_D (68 ˚C) such that the 75 x 25 mm surface was exposed to flow and visually flush with the mat surface (see supplementary Fig. S1).

Slides were carefully removed at 7, 15, 28, and 133 days, rinsed in bulk stream water to remove non-adhered material and placed in 0.175 M ammonium oxalate buffer (pH=3) to dissolve Fe-oxides (Loeppert and Inskeep 1996). Temperatures at these spring conditions remained relatively constant (±2˚ C) over the timescale of the experiment. Ferrous and total soluble iron were measured using the Ferrozine method at an absorbance of 562 nm (Stookey 1970).

6.5.5. Microscopy

Images of thin sections from excised Fe(III)-oxide mat were taken with a stereo microscope (Nikon SMZ1500). Excised mat samples from BE_D were embedded with epoxy under a vacuum and thin sectioned. Stereoscope images were calibrated by direct measurement with a 1 mm stage micrometer. Scanning electron micrographs were obtained of slides sampled from field incubations with a field emission-scanning electron microscope set at low voltage (1 kV) after sputter-coating with Ir to minimize charging.

6.5.6. Quantitative-PCR and Spatial mRNA Analysis

The relative spatial abundance of *Metallosphaera yellowstonensis* strain MK1 16S rRNA gene (1 copy per chromosome) was determined by slicing 1 mm from the top of an excised portion of mat. The remainder of the mat, known to contain lower levels of oxygen, was termed ‘bottom-mat’. Community DNA was extracted from both top and bottom samples using the FastDNA SPIN Kit for Soil (MP Biomedicals, LLC, OH). Quantitative PCR (qPCR) was performed using *M. yellowstonensis* specific 16S rRNA gene primer and the Sso Fast EvaGreen qPCR Kit and protocol in 50 µL reactions

(BioRad) on a RotorGene 3000 qPCR machine (Corbett Research). The specific primer and reaction conditions were as previously described (Kozubal et al. 2008). Statistical analysis was performed using an independent, two-tailed Student's T-Test.

Iron-oxide microbial mat squares (approximately 2 x 2 cm) were excised at the position where microsensor measurements were made for each sampling position. The mat sections were placed in sterile Petri dishes and sliced into "tops" and "bottoms" in same fashion as described in the qPCR section. All mat samples were stored in RNA Later in RNase free tubes. Total RNA was extracted (in triplicate) from approximately 500 mg of cut microbial mat using the FastRNA® Pro Soil Direct Kit (Qbiogene, Inc., CA) and FastPrep® Instrument (Qbiogene, Inc., CA), for 40 seconds at a speed setting of 6.0. Total RNA was then treated with RNase free DNase I (New England Biolabs, Inc., MA) for 15 minutes and 37˚ C. The DNase I reaction was terminated by precipitation of total RNA with nuclease free lithium chloride (final concentration 1.6 M) and absolute ethanol overnight (Sambrook and Russell 2001). RNA was resuspended in nuclease free water after centrifugation at 4˚ C for 15 minutes and washing once in ice cold 70 % ethanol. The terminal heme copper oxidase subunit I (*foxA*) specific to the iron oxidation pathway of *M. yellowstonensis* was reverse transcribed using the AccessQuick RT-PCR System and protocol (Promega) with *M. yellowstonensis* specific *foxA* primers (Kozubal et al., 2011). The cDNA *foxA* amplicons were purified with the GenElute™ PCR CleanUp Kit (Sigma-Aldrich). The qPCR reaction was the same as for the 16S rRNA gene from *M. yellowstonensis* as described in the above section. Relative expression was determined by comparing the observed C_T values of *foxA* and *M. yellowstonensis* 16S

rRNA gene (Kozubal et al. 2011). Statistical analysis was performed as described in the above section.

6.6. Supplementary Text and Calculations

6.6.1. Definition of Terms

C_i: Concentration of solute i ($\mu mol \cdot L^{-1}$)
D_e: Effective diffusion coefficient (typically reported in units $cm^2 \cdot sec^{-1}$)
L_f: Characteristic length scale defined (by convention) as thickness of mat (μm)
z: Spatial coordinate extending from surface $(z=0)$ towards bottom of mat $(z=L_f)$
t: Time coordinate
R: Reaction rate ($\mu mol \cdot L^{-1} \cdot sec^{-1}$)
X_b: Biomass concentration constant (typically reported in units of g-dry mass$\cdot L^{-1}$)
μ_{max}: Maximum specific growth rate constant of biomass (X_b) (hr^{-1})
$Y_{x/C}$: Biomass to solute yield (ratio X_b/C_i)
k_s: Half-saturation constant ($\mu mol \cdot L^{-1}$)
k_0: Zero-order rate constant ($\mu mol \cdot L^{-1} \cdot sec$)
k_1: First-order rate constant (sec^{-1})
u: Dimensionless concentration coordinate (defined below)
ζ: Dimensionless length coordinate (defined below)
ϕ_0: Zero-order Thiele modulus (dimensionless)
ϕ_1: First-order Thiele modulus (dimensionless)
$\eta_{0,i}$: Zero-order internal effectiveness factor (dimensionless)
$\eta_{1,i}$: First-order internal effectiveness factor (dimensionless)

6.6.2. Mass Balance for One-Dimensional Solute Transport (O2) Into Biofilm/Fe(III)-mat

Mass balance accounting for only a diffusive transport term and a reaction term

$$\frac{dC_{O_2}}{dt} = D_e \frac{d^2 C_{O_2}}{dz^2} - R \qquad \text{Eq. 6.S1}$$

Mass Balance with the steady-state assumption/simplification

$$R = D_e \frac{d^2 C_{O_2}}{dz^2} \qquad \text{Eq. 6.S2}$$

Set boundary conditions (BC) defining L_f as the length from surface of the biofilm to the bottom

$$BC\#1: \frac{dC}{dz} = 0 \; when \; L_f \quad \text{Eq. 6.S3}$$

$$BC\#2: C_{O_2} = C_o \; when \; z = 0 \quad \text{Eq. 6.S4}$$

6.6.3. Dimensionless Mass Balance
Assuming Zero-order Reaction Kinetics

Zero-order reaction term

$$R = \frac{\mu_{max} \cdot X_b}{\frac{Y_X}{C}} = k_o \quad \text{Eq. 6.S5}$$

Dimensionless parameter assignments

$$u = \frac{C_{O_2}}{C_o} \quad \text{Eq. 6.S6}$$

$$\zeta = \frac{z}{L_f} \quad \text{Eq. 6.S7}$$

Definition of the zero-order Thiele modulus *(ϕ_0)*

$$\frac{d^2u}{d\zeta^2} = \frac{\mu_{max} \cdot X_b \cdot {L_f}^2}{\frac{Y_X}{C} \cdot C_o \cdot D_e} = {\phi_o}^2 \quad \text{Eq. 6.S8}$$

$$\frac{d^2u}{d\zeta^2} = {\phi_o}^2 \quad \text{Eq. 6.S9}$$

Evaluations of set boundary conditions with the dimensionless parameter assignments

$$BC\#1: \frac{du}{d\zeta} = 0 \; when \; \zeta = 1 \quad \text{Eq. 6.S10}$$

$$BC\#2: u = 1 \; when \; \zeta = 0 \quad \text{Eq. 6.S11}$$

Solution to steady-state mass balance differential equation assuming zero-order reaction kinetics

$$u = \frac{{\phi_o}^2 \cdot \zeta^2}{2} - {\phi_o}^2 \cdot \zeta + 1 \qquad \text{Eq. 6.S12}$$

6.6.4. Dimensionless Mass Balance

Assuming first-order reaction kinetics fromfrom Monod expression when $k_s >> C_{O2}$

$$R = \frac{\mu_{max} \cdot X_b}{k_s \cdot Y_{\frac{X}{C}}} \cdot C_{O_2} = k_1 \cdot C_{O_2} \qquad \text{Eq. 6.S13}$$

The dimensionless mass balance equation uses the same dimensionless parameter assignments previously given and defines a different form of the Thiele modulus specific for first-order reaction *(ϕ_1)*

$$\frac{d^2u}{d\zeta^2} = \frac{k_1 \cdot {L_f}^2}{D_e} \cdot u = {\phi_1}^2 \cdot u \qquad \text{Eq. 6.S14}$$

The first-order mass balance equation can be solved explicitly

$$u = A \cdot sinh(\phi_1 \cdot \zeta) + B \cdot cosh(\phi_1 \cdot \zeta) \qquad \text{Eq. 6.S15}$$

Boundary conditions remain the same as specified in the zero-order form

$$u = cosh(\phi_1 \cdot \zeta) - tanh(\phi_1) \cdot sinh(\phi_1 \cdot \zeta) \qquad \text{Eq. 6.S16}$$

or

$$u = \frac{cosh(\phi_1 \cdot (1-\zeta))}{cosh(\phi_1)} \qquad \text{Eq. 6.S17}$$

6.6.5. Effectiveness Factor for
First and Zero Order Kinetics

Another way to extract meaningful information about the system from fitting the first-order reaction-diffusion models is by evaluating the internal effectiveness factor ($\eta_{1,i}$). This parameter is a function of ϕ_1 and is defined as the ratio of the observed rate of reaction to the rate that would occur if the concentration of dissolved O_2 was equal to the bulk phase concentration (C_o) everywhere in the mat.

First-order rate law

$$R = k_1 \cdot C_{O_2} \qquad \text{Eq. 6.S18}$$

Zero order rate law

$$R = k_o \qquad \text{Eq. 6.S19}$$

Definition of the internal effectiveness factor as the ratio of the observed rate of reaction to the rate of reaction that would otherwise be in the absence of mass transfer effects

$$\eta_{1,i} = \frac{\int_0^{L_f} R(z)dz}{L_f \cdot R} \qquad \text{Eq. 6.S20}$$

Internal effectiveness factor as a function of the first order Thiele modulus

$$\eta_{1,i} = \frac{\tanh(\phi_1)}{\phi_1} \qquad \text{Eq. 6.S21}$$

Internal effectiveness factor as a function of the zero order Thiele modulus

$$\eta_{0,i} = \begin{cases} \frac{1}{\phi_0}, & \phi_0 > 1 \\ 1, & 0 < \phi_0 \leq 1 \end{cases} \qquad \text{Eq. 6.S22}$$

The calculated quantities of $\eta_{1,i}$ are 0.017 and 0.035 for BE_D and OSP_B, respectively. These values are much less than 1 demonstrating that the observed rate of reaction (concentration dependent) in the Fe(III)-oxide mats are much less than the rate when the concentration of dissolved O_2 is equal to that of the bulk liquid. The zero order effectiveness factors were derived but not considered relevant to this system based on the poor agreement between the zero-order kinetic rate law and experimental data. This analysis supports the understanding that the behavior of O_2 consumption in the Fe (III)-oxide microbial mats is very different from that of the well mixed system corresponding to the oxic bulk liquid phase in the springs.

6.7. Acknowledgements

The authors acknowledge funding from the National Science Foundation-Integrative Graduate and Education Training (IGERT) Program (DGE 0654336) for support to H.C.B and J.P.B and the Department of Energy-Genome Science Program, Microbial Interactions Foundational Science Focus Area (Pacific Northwest National Laboratory subcontract 112443 to MSU). Additional support was provided by Unisense A/S (Aarhus,DK), the DOE-Joint Genome Institute Community Sequencing Program (CSP 787081), E. Booth for building customized field equipment, C. Hendrix and S. Gunther (YNP Center for Resources) for research permit administration, and Drs. P. Stewart, M. Kühl and Mr. S. Davis for helpful discussions and field assistance.

7. CONCLUSIONS AND FUTURE DIRECTIONS

7.1. Thesis Synopsis

This dissertation focuses on interactions and observable phenomena within microbial consortia. Interacting microbial communities are ubiquitous in nature and are also employed as important engineering platforms. The technical research presented in this dissertation explores microbial consortia on three main fronts: (i) metabolically engineered heterotrophic systems, (ii) photoautotrophic-heterotrophic biofilm systems and (iii) naturally occurring thermo-acidophilic microbial mat systems. Fundamental microbial ecology is a re-occurring foundation throughout all aspects of this work. Additionally, primary-productivity and biologically mediated oxygen reactions are used as interconnecting, cross-cutting themes.

7.2. Metabolically Engineered Heterotrophic Microbial Consortia

Synthetic and semi-synthetic microbial consortia are most commonly engineered into heterotrophic organisms (Bernstein and Carlson 2012a). This dissertation highlights some synthetic microbial consortia composed of *Escherichia coli*, which is a genetically tractable and industrially relevant heterotrophic microorganism. The *E. coli* consortia described here (Chapter 4 and Bernstein et al. 2012) demonstrated enhanced biomass productivity based on syntrophic metabolite exchange and partitioning of reduced carbon sources. This specific project has already been expanded upon in a published follow-up study that employed laser desorption postionization mass spectrometry (LDPI-MS)

imaging for analysis of small molecules within intact biofilm cocultures (Bhardwaj et al. In-Prep; Bhardwaj et al. 2012).

Another expansion of the *E. coli* consortia project characterizes the rate laws and reaction kinetics associated with substrate and product inhibition of acetic acid. The goal of this project continuation is to provide an enhanced mechanistic understanding of acetic acid inhibition, which is important to fundamental biology and for designing efficient industrial fermentation bioprocesses. This project employs the previously described *E. coli* MG1655 deletion mutants, 403G100 (glucose(-) acetate consumer; Δglk, ΔptsG, ΔptsM, Δgcd) and 307G100 (acetate(-) glucose consumer; ΔaceA, ΔfrdA, ΔldhA), which effectively uncouple the glucose and acetate catabolic strategies contained in the native wild-type strain (Bernstein et al. 2012b). Batch reactor experiments are used to measure culture specific growth rates as a function of acetic acid concentration and pH in the presence of excess glucose. For cultures consuming and producing acetate, small changes in pH results in substantial changes in growth inhibition measured in the context of maximum obtainable specific growth rates. These data are being used to parameterize modified-Monod kinetic expressions and for generating novel kinetic expressions via symbolic regression methods.

Preliminary work on the existing synthetic *E. coli* consortia has also been performed to create anaerobic systems capable of partitioning reduced carbon sources and terminal electron acceptors (TEA). This work capitalizes on the native ability for *E. coli* to reduce nitrate as a viable TEA under anaerobic conditions (Unden and Bongaerts 1997). Additional deletions have been made to the 307G100 strain (via P1 phage

transduction methods described in Chapter 3 and 4) to generate the new 604 strain (ΔaceA, ΔfrdA, ΔldhA, ΔnarG, ΔnarY, ΔnapA). The 604 deletion mutant was subjected to the 100-generation chemostat adaptation experiment to yield the 604G100 strain (methods described in Chapter 4) which was found to have a 20 % increase in the maximum specific growth rate compared to the un-adapted 604 strain. Preliminary experiments also confirmed that the 604G100 strain does not grow under micro-aerobic/anoxic conditions when supplied glycerol (a non-fermentable reduced carbon source) and nitrate as the sole TEA. Preliminary data and details on the anaerobic consortium are supplied in Appendix C. This anaerobic system could substantially improve the dynamics of the previously reported, acetate-exchanging consortia (Bernstein et al. 2012b) by eliminating competition scenarios for oxygen as a TEA and permitting anaerobic oxidation of inhibitory acetate.

7.3. Photoautotrophic-Heterotrophic Microbial Consortia

Photoautotrophic microbial consortia are of keen interest to chemical and biological engineers as promising catalytic systems capable of utilizing renewable resources light and carbon dioxide. Naturally occurring phototrophic organisms often couple with heterotrophic counterparts and engage in mutualistic interactions such as syntrophic exchanges of mass and chemical free energy originally derived from the environment. Industrial photoautotrophic catalytic systems, often employed for waste-water remediation and biofuel production, typically exist as undefined multispecies communities capable of photosynthesis and heterotrophy (Bender and Phillips 2004;

Christenson and Sims 2012a). Even axenic monocultures of phototrophic organisms often have the innate ability to perform both photoautotrophic and photoheterotrophic metabolic strategies (Joset-Espardellier et al. 2006; Vu et al. 2012).

This dissertation reports a study (Chapter 5) which directly measures and characterizes active photosynthesis and respiration processes in biofuel-precursor producing and waste-water remediating algal biofilms. Steady-state oxygen and oxygenic-photosynthesis profiles were measured inside phototrophic biofilms cultured from two different rotating algal biofilm reactors (RABR). The RABR culturing system has the advantage of being able to simultaneously facilitate algal-growth, biomass concentration and dewatering (Christenson and Sims 2012). The two experimental systems characterized, for this study, were: (i) a field scale RABR capable of concurrent remediation of waste-water and algal biomass production and (ii) a laboratory scale RABR inoculated with a known lipid accumulating *Chlorophyte* WC-2B isolated from an alkaline stream in Yellowstone National Park (USA). This study characterized the respective biofilm's capacity for biofuel production, photosynthesis and respiration. It also identified active zones of photosynthesis which is an important consideration towards optimizing biomass loads (*i.e.,* biofilm thickness) in the RABR systems. Another aspect of this project was determining the rates of photosynthesis-coupled respiration which should be encouraged as an important design feature for photoautotrophic biofilm catalysis since localized O_2/CO_2 ratios can affect CO_2 fixation rates and influence the overall productivity of the system.

Another study based on photoautotrophic-heterotrophic consortia represents a future direction in this important research arena. This study focused on a biofilm consortium composed of photoautotrophic *Synechococcus* PCC 7002 and heterotrophic *Escherichia coli* MG1655. Both *Synechococcus* and *E. coli* are industrially relevant microbial catalyst strains often engineered for potentially commercial products such as biofuels, bioplastics, amino acids and organic acids (Atsumi et al. 2008; Atsumi et al. 2009; Carlson et al. 2005; Ducat et al. 2011; Takahashi et al. 1998; Trinh et al. 2008). Coculturing permits a mutually beneficial metabolite exchange between the strains: *Synechococcus* photosynthates support *E. coli* growth while *E. coli* consumption of potentially inhibitory organic acids and photosynthetically derived O_2 increases *Synechococcus* biomass productivity. Cocultured *Synechococcus* biomass productivity was 50% higher than monocultures during early exponential growth. A detailed micron-scale spatial analysis of oxygen gradients within the binary biofilms provided a basis for estimating photosynthetic rates in monocultures and cocultures. Details on the current progress of this study are contained in Appendix A. This artificial binary biofilm culture represents a novel and adaptable microbial catalyst platform which exploits renewable carbon and energy inputs.

7.4. Natural Microbial Consortia

Many successful engineered microbial consortia designs mimic fundamental ecological principles observed from natural communities (Bernstein and Carlson 2012a). Microbial ecology has been adopted as an important tool for chemical and biological

engineers and offers a plethora of unexplored scientific territory that can be adapted towards biotechnologies (McMahon et al. 2007; Momeni et al. 2011). Extreme natural environments, such as the acidic geothermal iron-oxide mats described here (Chapter 6), are of particular interest due to unique interactions between novel microorganisms and their environment. The *in situ* iron-oxide mat study fundamentally examined oxygen as an important terminal electron acceptor and potentially limiting substrate inside a complex thermo-acidophilic microbial consortia dominated by the domain *Archaea* (Bernstein et al. 2013b). Steady-state oxygen microprofiles were measured within the high temperature (65-75°C) acidic (pH = 2.7-3.7) microbial mats and correlated to abundances of aerobic, iron-oxidizing *Metallosphaera yellowstonensis* organisms and mRNA gene expression levels. This study employed classical chemical engineering reaction and diffusion modeling to establish that oxygen is consumed through concentration depended reaction kinetics and is mass transfer limited within the microbial mats. An identified zone of higher dissolved oxygen near the mat surface promotes microbially mediated iron-oxidation and results in an active spatial region of Fe(III)-oxide biomineralization.

In situ experimentation is often challenging due to the remote location and dynamic factors associated with field research sites. An expansion, or future direction for this study involves designing and constructing flow-cell bioreactors capable of mimicking the extreme biological conditions found within sites such as the acidic geothermal springs located in Yellowstone National Park (USA). Tightly controllable bioreactors can be beneficial for circumventing the complications of field

experimentation but also for examining physical phenomena not obtainable *in situ*. For example, a natural microbial mat from a hot spring environment is likely adapted to a defined range of environmental constraints such as temperature, pH and/or flow and perturbations to these constraints can be more reliably examined via *ex situ* experimentation. Appendix B contains a detailed report for the design, construction and operation of a flow-cell biofilm reactor capable of mimicking and controlling some key environmental parameters associated with geothermal hot spring systems. This work will be further expanded upon to incorporate photic-environmental parameters for studying phototrophic microbial mat systems from extreme environments.

7.5. Final Statement

The technical research presented in this dissertation explores microbial consortia on three main fronts: (i) metabolically engineered heterotrophic systems, (ii) photoautotrophic-heterotrophic biofilm systems and (iii) naturally occurring thermo-acidophilic microbial mat systems. The overarching goal for this work was to observe and quantitatively characterize the interactions and physical phenomena occurring in these microbial community systems. Both primary-productivity and biologically mediated oxygen reactions were used as cross-cutting themes for this work. This scientific research has been performed through interdisciplinary chemical and biological engineering approaches that utilize fundamental microbial ecology as a foundation.

APPENDICES

APPENDIX A

CHARACTERIZATION OF AN ARTIFICIAL PHOTOAUTOTROPHIC-HETEROTROPHIC BIOFILM CONSORTIUM COMPOSED OF *SYNECHOCOCCUS* PCC 7002 AND *ESCHERICHIA COLI* MG1655

Front Matter Details

Manuscript in Preparation: Incomplete rough-draft

Current Contributing Authors: Hans C. Bernstein, Alissa Bleem, Steven Davis and Ross P. Carlson

Contributions of Current Authors: HCB: Conception and critical analysis of research, data collection and analysis, manuscript drafting and editing. AB: Data collection and analysis. SD: Data collection. RPC: Conception and critical analysis of research.

Abstract

Microbial consortia can be engineered to optimize multiple functions simultaneously providing a robust platform for bioprocesses. Photoautotrophic consortia have the added benefit of using renewable sunlight and CO_2 as energy and carbon sources. Naturally occurring phototrophic organisms often couple with heterotrophic counterparts in an ancient and globally distributed ecological partnership based on syntrophic exchange of mass and energy via chemical species. This naturally occurring ecological template has been reconstructed using an artificial binary community comprised of photoautotrophic *Synechococcus* PCC 7002 and heterotrophic *Escherichia coli* K-12 MG1655. Both *Synechococcus* and *E. coli* are industrially relevant microbial catalyst strains often engineered for commercial products such as biofuels, bioplastics, amino acids and organic acids. Coculturing permits a mutually beneficial metabolite exchange between the strains: *Synechococcus* photosynthates support *E. coli* growth, while *E. coli* consumption of potentially inhibitory organic acids and photosynthetically derived O_2 increases *Synechococcus* biomass productivity. Cocultured *Synechococcus*

cell productivity was 50% higher than monocultures. A detailed micron-scale spatial analysis of oxygen gradients within the binary biofilms provided a basis for estimating photosynthetic rates in monocultures and cocultures. The binary system exhibited decreased local oxygen concentration with respect to position. This result corresponds with increased rates of respiration and reduced product inhibition of *Synechococcus* with respects to O_2 production and accumulation of photorespiration byproducts. This artificial binary biofilm culture represents a novel and adaptable microbial catalyst platform which exploits renewable carbon and energy inputs.

Introduction

The coexistence of photoautotrophic cyanobacteria coupled with symbiotic, heterotrophic counterparts represents an ancient and global ecological partnership. Both biofilms and planktonic cultures engaged in this fundamental exchange and conversion of carbon and electrons are ubiquitous. This ecological template has been integrated into an artificial binary community comprised of industrially relevant microorganisms, primary producer *Synechococcus* strain PCC 7002 and consumer strain *Escherichia coli* MG1655. Both *Synechococcus* and *E. coli* are industrially relevant microbial catalyst strains for production of commercial products such as biofuels, bioplastics, amino acids and organic acids (Atsumi et al. 2008; Atsumi et al. 2009; Carlson et al. 2005; Ducat et al. 2011; Takahashi et al. 1998; Trinh et al. 2008). Coculturing these strains demonstrates a novel consortial platform based on symbiotic metabolite cross feeding or syntrophy.

The overarching goal of this study was to characterize beneficial emergent properties associated with the artificial binary cultures in colony biofilm systems which utilize CO_2 and light as the sole carbon energy inputs. It was hypothesized that aerobic heterotrophy associated with *E. coli* growth and activity would be sustainable under culturing conditions which utilize *Synechococcus* PCC 7002 as the primary producer. An additional and complementary hypothesis was that the overall cyanobacterial productivity would increase when cultured in a biofilm with *E. coli* as a result of increased respiration and subsequent lowering of local O_2 concentrations which can be inhibitory to photosynthesis (Paerl and Pinckney 1996).

Microbial consortia driven by photoautotrophic primary productivity have the advantage of being able to utilize CO_2 and sunlight as the sole carbon and energy inputs. Aerobic heterotrophs coupled in close physical proximity with oxygenic phototrophs may be less affected by mass transfer limitations associated with oxygen and required reduced carbon sources. Syntrophic cross-feeding of reduced carbon and terminal electron acceptors between producer and consumer members within biofilms is a naturally robust and competitive environmental strategy. This fundamental ecological motif has been observed and reported on extensively in many natural environments (Bateson and Ward 1988; Canfield and Marais 1993; Nold and Ward 1996; Paerl and Pinckney 1996; Taffs et al. 2009). Artificial and synthetic systems which mimic this proven exchange strategy are desirable in the context of bioprocess catalyst technology (Bernstein et al. 2012; Ducat et al. 2012; Niederholtmeyer et al. 2010).

Biofilms are used in microbial bioprocesses as immobilized catalyst systems (Rosche et al. 2009). Diffusion is the primary transport mechanism in biofilms and mass transfer rates are often limiting to microbial processes (Stewart 2003). Syntrophic consortial biofilms have the advantage of close physical proximity between cells which can help overcome rate limiting steps associated with nutrient transport. When accumulation of a byproduct is inhibitory to one community member, such as O_2 to *Synechococcus*, the closeness of a complementary scavenger strain can reduce the effects of product inhibition (Bernstein et al. 2012; Paerl and Pinckney 1996; Taffs et al. 2009).

Materials and Methods

Bacterial Strains, Culturing and Media. Cynaobacteria species *Synechococcus* PCC 7002 and *Escherichia coli* MG1655 K-12 were the two bacterial strains used for this study (Van Baalen 1962). Microscopy work utilized an *E. coli* MG1655 containing a reporter plasmid (pAKN84) expressing an IPTG inducible cyan-fluorescent-protein. Biofilms were cultured on a previously described A+ cyanobacteria agar medium which does not contain a viable carbon source (Stevens et al. 1973). The A+ media was enriched with 4 mg/L vitamin B12 unless otherwise stated. *Synechococcus* and *E. coli* liquid cultures (used as biofilm inocula) were cultured in A+ and M9 minimal media + 10g/L glucose media respectively (Miller 1972). Inoculum for each species consisted of exponentially growing cultures diluted to an optical density (600 nm) value of 0.05. *E. coli* inoculum was cultured in a shaker at 37ºC. *E. coli* cells were separated from the M9 media by centrifugation (1800 g for 10 min) and resuspended in A+ liquid media to

minimize transfer of external carbon source. Colony biofilms were cultured according to a previously established method (Bernstein et al. 2012; Hamilton 2003; Zuroff et al. 2010). Briefly, colony biofilms were cultured on 0.22 μm filters placed on A+ agar media and incubated at 37ºC under 14:10 hour light:dark cycle (PAR = 275 μmol photon·m^{-2}·sec^{-1}). Controls included monocultures of both cyanobacteria and *E. coli*. Time dependent species abundance was measured by enumeration; a previously described drop plate method utilizing both A+ and Luria-Bertani agar plates as the enumeration media specific for *Synechococcus* and *E .coli* strains respectively (Herigstad et al. 2001).

Microsensor Experimental Analysis. Microsensor measurements were performed with clark-type oxygen micro-electrodes with outside tip diameters of 25 μm, a response time < 5 sec and a < 5% stirring sensitivity (Revsbech 1989; Revsbech and Jorgensen 1986). Amplification and sensor positioning was controlled with a microsensor multi-meter coupled with an ADC216 USB converter and a motor controlled micromanipulator. Data collection was aided by software packages, SensorTrace Pro ver.3.0.1 and Sloper ver. 3.0.3(Unisense). Two point calibrations were performed in air saturated DI water ($[O_2]$≈270 mM) conditions and in a 1 M NaOH, 0.1 M ascorbic acid solution (anoxic standard). Calibrations were repeatedly checked in the anoxic standard and in air saturated DI water throughout the experiments. Microsensor measurements were performed at 35ºC (biofilm temperature only, air-biofilm interface temperature gradients were not accounted for) under both dark and light conditions (PAR = 43 μmol photon·m^{-2}·sec^{-1}). Spatial O_2 measurements were done in one-dimension (depth-wise) from the biofilm-air interface down. The step size between measurements was 25 μm. The micro-

profile and light:dark shift techniques have been previously described in detail (Glud et al. 1992; Kuhl et al. 1996; Lassen et al. 1998; Revsbech and Jorgensen 1986; Revsbech et al. 1983). Briefly, the light:dark shift measurements were used to measure the gross oxygenic-photosynthesis volumetric rates ($P_g(z)$) at specific depth wise positions and are valid under the assumptions that (i) there is an initial steady-state O_2 distribution prior to darkening (ii) the O_2 consumption rate is identical between the light and dark time periods (iii) the O_2 diffusion coefficient remains constant during the measurement time at each position.

Profile Analysis. Net diffusive O_2 fluxes in and from the biofilm matrix (J_{ox}) were estimated in the biofilms using a form of Fick's first law ($J_{ox} = -D_e \cdot dO_2/dz$) applied to linear portions of the steady-state oxygen profiles. The effective diffusion coefficient of O_2 in the biofilm matrix (D_e) was estimated to be $1 \cdot 10^{-5}$ $cm^2 \cdot sec^{-1}$ by assuming it to be ~30% of the aqueous value corresponding to sea water at 37ºC ($D_{aq} = 3.4\ 10^{-5}$ $cm^2 \cdot sec^{-1}$). This estimate is also consistent with previously reported value specific for cyanobacterial mats and ratios of effective diffusion coefficients to aqueous values (Jorgensen et al. 1979; Stewart 1998). The sum of J_{ox} terms calculated from the surface and bottom of the biofilms are defined here as the areal net biofilm photosynthesis ($P_{n,BF}$). The areal gross photosynthesis rate (P_g) was estimated by integrating the photosynthesis profiles [$P(z)$ spatial curves)] over the photic zone/biofilm depth. The respiration rate in the light (R_{light}) was calculated by taking the difference between P_g and P_n. Again, detailed descriptions of biofilm oxygenic photosynthesis profile theory have previously been described (Glud et al. 1992; Kuhl et al. 1996).

Confocal Laser Scanning Microscopy (CSLM). Samples were viewed using a Leica TCS SP5 II inverted confocal laser scanning microscope with 488, 561 and 633 nm lasers. Images were taken of biofilms in their native state and in cross sectional slices. Sections were cut from mature biofilms covered with TissueTek O.T.C. tissue embedding medium and frozen on dry ice. Embedded biofilms were cut into 5 um thick sections using a Leica CM 1850 cryostat operated at -20°C. Images were analyzed with Imaris software (ver.7.4.2).

Results

Biofilm Physical Structure. The microstructures of the biofilms were found to be heterogeneous. Confocal scanning laser microscopy experiments of the binary cultures revealed that *Synechococcus* and *E .coli* aggregated with their own respective cell type and that these aggregates were in close physical proximity to each other (Figure. A.1). Individual community member cell clusters were readily identifiable in biofilms imaged within the initial 25 hr growth cycle (14:10 light:dark).

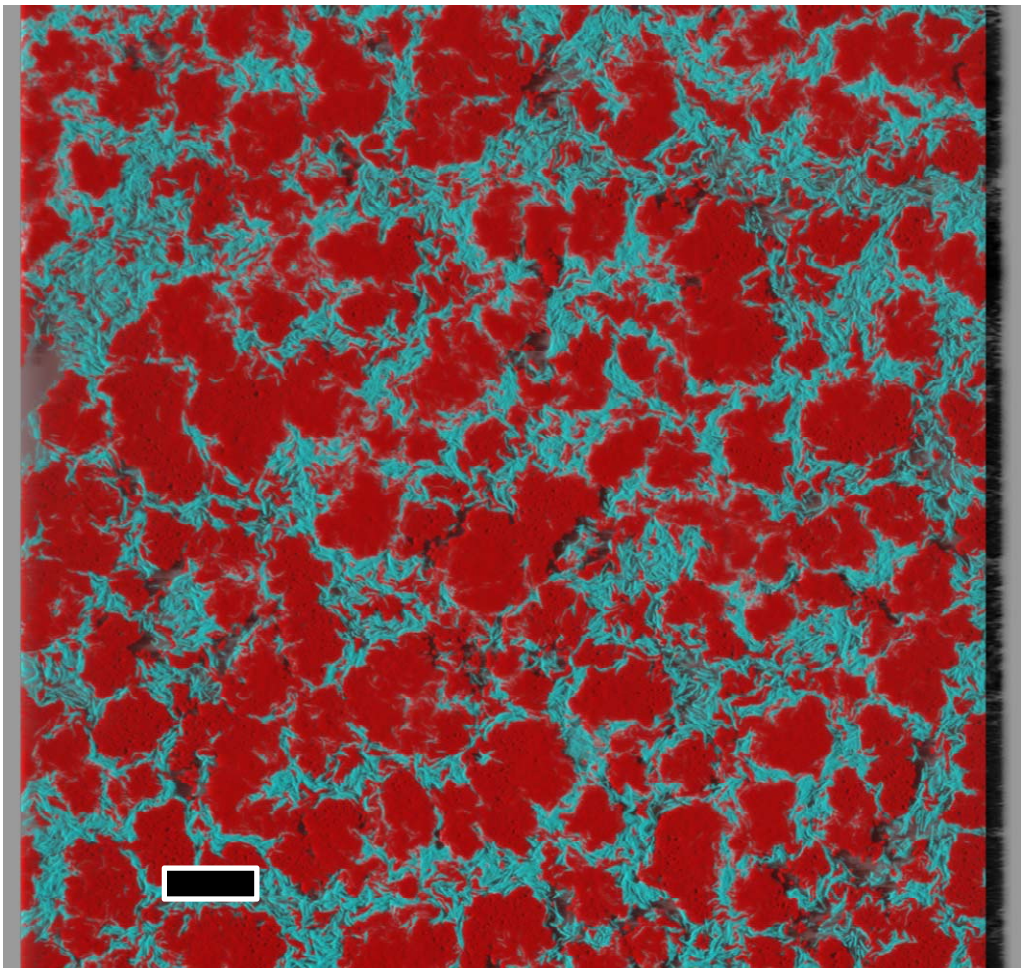

Figure A. 1. Confocal micrograph of a representative binary culture colony biofilm. Synechococcus PCC 7002 auto-fluorescence is shown in red and E. coli MG1655 pAKN84 is seen in blue via the induced cyan fluorescent protein. The scale bar represents 50 μm.

Biomass Productivity. The binary culture colony biofilms exhibit increased biomass productivity over the respective monoculture controls (Figures. A.2-4). Biomass productivity is defined here as the log change in enumerated colony forming units (CFU) over time. The binary culture biomass productivity, calculated during exponential biofilm growth, was 100% higher than the *Synechococcus* monoculture during early exponential phase (Figure. A.3). Additionally, the binary culture *Synechococcus*-specific biomass

productivity was 50% higher than the monoculture (measured during early exponential phase). Enumeration of cultures on cyanobacteria specific A+ agar showed that the binary culture and *Synechococcus* monocultures achieved the same stationary phase values after one 25 hr growth cycle. The *Synechococcus*-specific counts achieved this stationary phase after 15 and 20 hrs for the binary culture and monoculture respectively. However, extended growth (10 light-dark cycles) showed *Synechococcus* monoculture biomass sustaining slightly higher CFU values (Figure. A.4). *E. coli* monoculture counts began to decrease more rapidly after 4 light-dark cycles compared to *E. coli* binary culture counts.

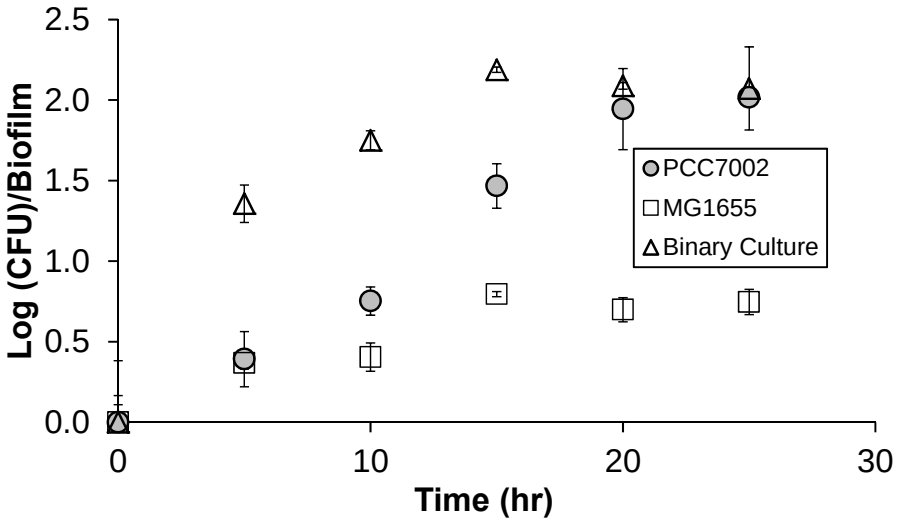

Figure A. 2. Colony biofilm growth over one light:dark cycle. The binary and control PCC7002 cultures were enumerated on cyanobacteria specific medium (A+ agar) while the *E.coli* MG1655 was cultured on A+ with Synechococcus PCC7002 but enumerated on Luria-Bertani agar. Individual data points are averages from 2-4 experimental replicates. Error bars represent ± 1 standard deviation.

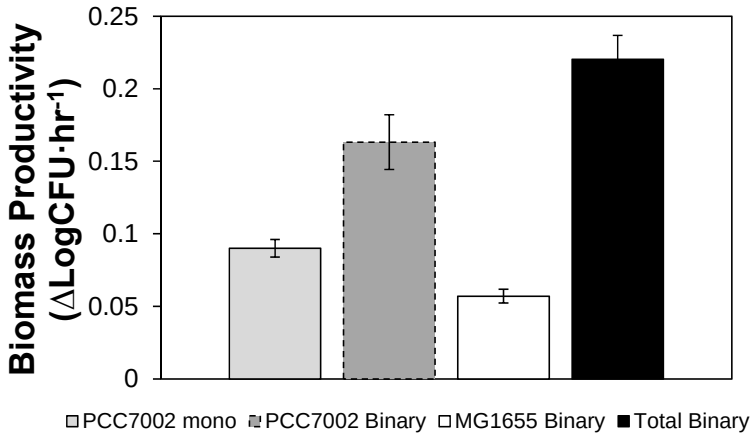

Figure A. 3. Comparison of biomass productivity during the first 15 hrs of growth, defined here as the log change in colony forming units (CFU) per hour. Data for specific for Synechococcus PCC7002 and E.coli MG1655 were collected using strain specific enumeration medium. Error bars represent plus or minus one standard error from the linear regression.

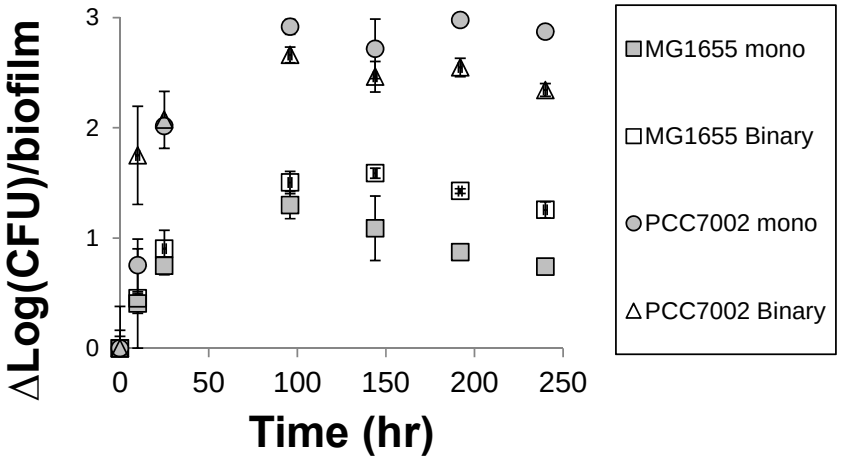

Figure A. 4. Colony biofilm growth over ten light:dark cycles. The binary and control PCC7002 cultures were enumerated on cyanobacteria specific medium (A+ agar) while the E. coli MG1655 was cultured on A+ with Synechococcus PCC7002 but enumerated on Luria-Bertani agar. Individual data points are averages from 2-4 experimental replicates. Error bars represent ± 1 standard deviation.

Vitamin B12 Competition. *Synechococcus* PCC 7002 has an obligate requirement for extracellular cobalamin (vitamin B12) (Wilhelm and Trick 1995). *E.coli* also has a requirement for B12 and has been shown in some cases to compete for B12 with its host and other community members (Booth and Heath 1962; Davis and Mingioli 1950; Roth et al. 1996). Biomass productivity of the binary biofilm cultures was not affected by B12 reduction in the growth media (no added B12 to A+ agar). This result confirms that there was no experimental evidence of competition. However, the *Synechococcus* monocultures did show reduced total CFU counts under B12 reduced conditions (Figure. A.4). This result was confirmed in one 25 hr growth cycle. CSLM images did not show observable changes in biofilm morphology when cultured with or without added B12 (data not shown).

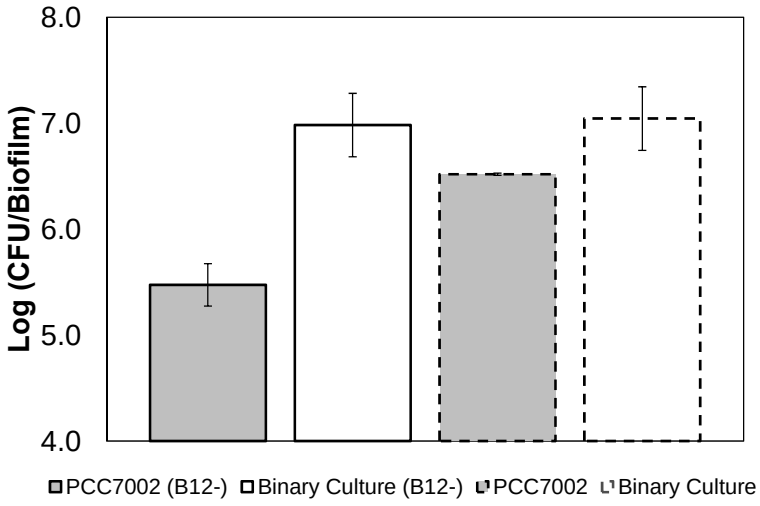

Figure A. 5. Cyanobacteria specific enumeration data for 25 hr samples which compares the effect of biofilm growth with and without vitamin B12 additions to the growth medium. Individual data points are averages from five experimental replicates. Error bars represent ± 1 standard deviation.

Oxygen Gradients and Transport. Mature binary biofilm cultures showed decreased localized O_2 concentrations compared to the *Synechococcus* monocultures. This result was observed during steady-state diffusion under both light and dark conditions (Figure. A.6). The colony biofilms and agar substrata were completely penetrable by light. Hence, the biofilm thickness was equal to the depth of the active zone of photosynthesis (discussed further below) and was determined to be 200 ± 25 μm for both sample types (Binary and monoculture). The flux of O_2 from the surface of the mat, interpreted as the net areal rate of photosynthesis ($J_{ox\text{-}surface} = P_n$), was near identical between the binary and *Synechococcus* illuminated biofilms. The observed O_2 flux into the biofilms under dark conditions, interpreted as the areal rate of respiration ($J_{ox\text{-}surface} = R_{dark}$), was higher for the binary culture. A summary for the different biofilm O_2 fluxes is shown in Table A.1.

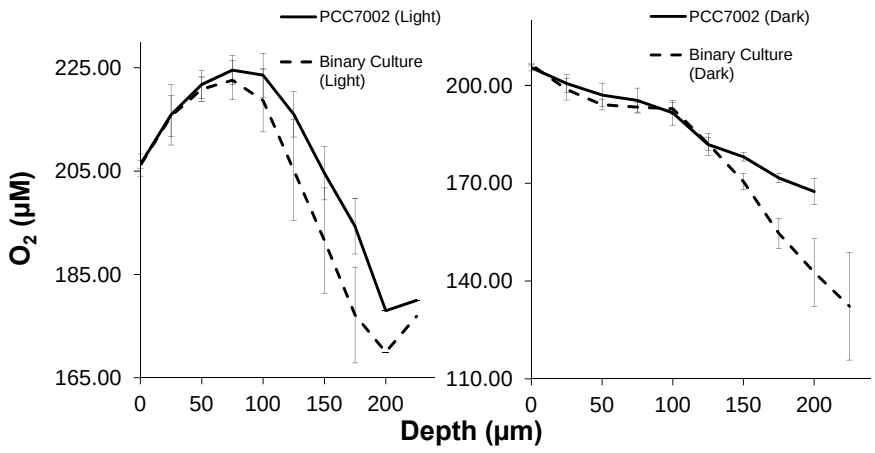

Figure A. 6. Steady-state oxygen microprofiles measured inside binary and mono culture (PCC 7002) colony biofilms under light and dark conditions. Each data point plotted represents averages from 4-6 individual measurements taken near the center of the biofilms. Error bars represent ± 1 standard deviation.

Photosynthesis and Coupled-respiration. The areal gross photosynthesis rates (P_g) were effectively identical between the binary and monoculture biofilm samples measured (Table A.2). However, the photosynthesis profiles exhibited slightly different shapes corresponding to maximum volumetric photosynthesis [$P_g(z)$] magnitude and position (Figure. A 7). The light:dark shift measurements taken at the position above the biofilm showed no dynamic change in O_2 concentration.

Table A. 1. Summary of calculated oxygen flux values into (consumption, negative values) and out-of (production, positive values) the biofilm samples. Flux into the bottom of the illuminated biofilm samples (Jox-bottom) was calculated from the average slopes from all profiles showing the positive slope shift at the biofilm-substratum interface (see also Figure. A. 6). The effective diffusion was assumed to be constant at the top and bottom of each sample. Values are expressed within ± 1 standard error.

	$J_{ox\text{-}surface}$ Light production ($\mu mol\ O_2 \cdot cm^{-2} \cdot sec^{-1}$)	$J_{ox\text{-}bottom}$ Light consumption ($\mu mol\ O_2 \cdot cm^{-2} \cdot sec^{-1}$)	$J_{ox\text{-}surface}$ Dark consumption ($\mu mol\ O_2 \cdot cm^{-2} \cdot sec^{-1}$)	$J_{ox\text{-}bottom}$ Dark consumption ($\mu mol\ O_2 \cdot cm^{-2} \cdot sec^{-1}$)
PCC 7002	$(3.2\pm0.4)\cdot10^{-5}$	$(-0.8\pm0.2)\cdot10^{-5}$	$(-1.7\pm0.2)\cdot10^{-5}$	$(-2.1\pm0.3)\cdot10^{-5}$
Binary-culture	$(3.0\pm0.5)\cdot10^{-5}$	$(-0.8\pm0.2)\cdot10^{-5}$	$(-2.5\pm0.3)\cdot10^{-5}$	$(-4.5\pm0.2)\cdot10^{-5}$

Table A. 2. Areal rates of photosynthesis and coupled-respiration. The net areal biofilm photosynthesis rate is defined here as the sum of oxygen fluxes to and from the bottom and surfaces of the biofilm samples. The areal photo-respiration rate is the difference between the gross and net rates of photosynthesis and represents the amount of oxygen being consumed inside the biofilm during illumination.

	Gross Areal Photosynthesis Rate ($\mu mol\ O_2 \cdot cm^{-2} \cdot sec^{-1}$)	Net areal Biofilm Photosynthesis Rate ($\mu mol\ O_2 \cdot cm^{-2} \cdot sec^{-1}$)	Areal Biofilm Photo-Respiration Rate ($\mu mol\ O_2 \cdot cm^{-2} \cdot sec^{-1}$)
PCC 7002	$4.0 \cdot 10^{-5}$	$2.4 \cdot 10^{-5}$	$1.6 \cdot 10^{-5}$
Binary culture	$3.9 \cdot 10^{-5}$	$2.2 \cdot 10^{-5}$	$1.7 \cdot 10^{-5}$

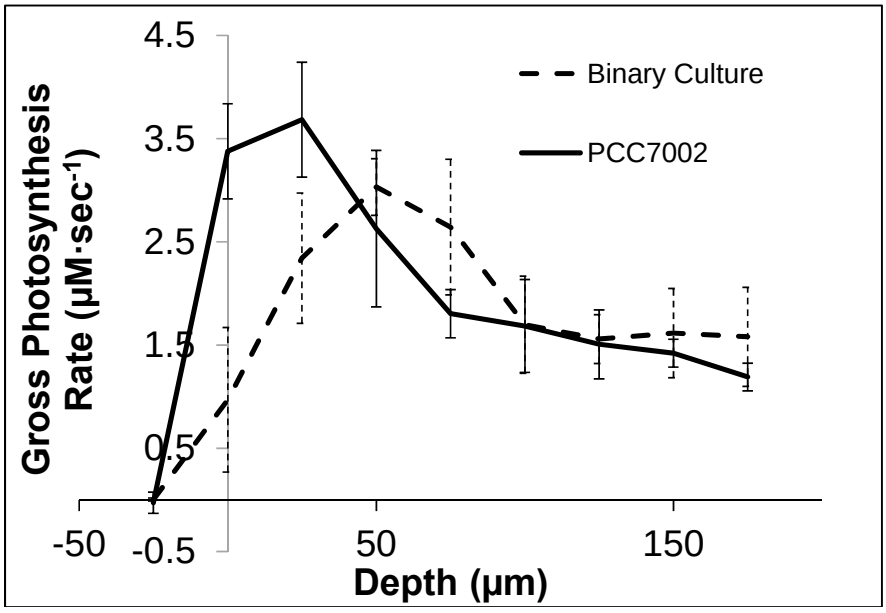

Figure A. 7. Photosynthesis profile composed of rates for depth positions directly above and inside the colony biofilms. Profiles are averages from 3-4 replicates taken near the radial-center of the biofilms under illuminated conditions. Photosynthesis rates were determined at 1-2 seconds immediately following the light:dark shift. Error bars represent ± 1 standard deviation.

Appendix A: Specific Project Discussion

The manuscript presented here in Appendix A is both incomplete and in rough-draft form. Additional data analysis and experimentation is required to finalize this document for submission to a peer-reviewed journal. This discussion section serves two purposes; 1) critically evaluate the current data sets and scientific interpretations and 2) consider additional experimental approaches that may be used to finalize this project.

The colony biofilm culturing system was logistically advantageous for processing and analyzing a relatively high number of samples. However, the selective drop-plate method developed and used here to quantify *Synechococcus* and *E. coli* colony CFUs was not independently conclusive. A number of control experiments confirmed that *E. coli* monoculture colonies could be obtained on A+ media, even in the absence of an added viable carbon source. Hence, selective plating for *Synechococcus* from the binary culture could be influenced by the presence of *E. coli*. Additionally, the total binary counts (Figure. A. 3), which is a sum of the selective plate counts, may double-account for some CFU's. Additionally, *E. coli* monoculture biofilms grew on A+ agar plates and persisted at CFU values very near to the *E. coli* binary numbers until ~ 4 light-dark cycles (4 days). The time dependent selective drop-plate data may still be representative of cell production and be used to calculate cell productivity; however, an alternative method such as strain-specific qPCR should be used to verify the accuracy of the current data sets.

Both *Synechococcus and E. coli* are vitamin B12 auxotrophs and (as mentioned in the results) could potentially compete for this essential nutrient in binary culture. The

data from the current study confirms that there are no statistical differences between binary cultures grown with and without the addition of B12. There was a measureable decrease in the PCC 7002 monocultures grown without the addition of B12 when compared to the typical A+ media samples. These data sets imply that there is not a B12 competition scenario taking place between *Synechococcus* and *E. coli.* However, the data presented here is likely not representative of perfectly vitamin B12 deficit culturing since B12 was not actively removed from the media components. It is beyond the scope of this study to thoroughly characterize the growth response (both binary and monoculture) to vitamin B12 limitation. A greater consideration of culturing materials and purities would be needed to limit microbial growth (in this study) by vitamin B12 availability.

The steady-state oxygen microprofiles spanned the entire depth of the biofilm samples and did not reveal anoxic zones. This was expected since light penetration through the biofilm samples and agar substrata was visually detectable. The entire biofilm volume remained near media saturation (~206 µM for A+ media at 37 ºC). In fact, only a small degree of supersaturation was observed (only about 1.1X saturation) as compared to previously reported measurements in cyanobacteria biofilms reaching up to 5X saturation (Glud et al. 1992; Kuhl et al. 1996). The low dissolved oxygen concentrations observed in the current study are due to a combination of relatively thin biofilms and low level of applied irradiance (profile measurement PAR values = 43 µmol photon$\cdot m^{-2} \cdot sec^{-1}$). Different culturing and illumination strategies, such previously described agar-liquid-flow systems (Glud et al. 1992; Kuhl et al. 1996; also see Appendix

C) in combination with LED light banks, could and should be investigated to establish better control of illumination, oxygen transport and biofilm growth.

The flux of oxygen and the integrated photosynthesis profiles were used to establish differences in photosynthesis and photosynthesis-coupled respiration processes between the binary and monocultures. However, only small changes between the two systems were observable. This may be in-part due to the experimental design. Thicker biofilms could result in with more defined regions of respirations and anoxia and would likely show that the binary cultures exhibit higher degrees of respiration. Additionally, oxygen flux was observed into the bottom of the biofilms from the biofilm-substratum interface. This was an unexpected result and needs to be carefully re-analyzed to establish the accuracy and importance of this phenomenon. That observation may be due to artifacts involved with microsensor measurements at and/or in the poly-carbonate filter (see materials and methods section). The flux of oxygen to and from the biofilm may be more accurately accounted for in the absence of the poly-carbonate filter and covering the surface of the biofilm with agar should also be considered as an option to yield accurate measurements though an artificially induced diffusive boundary layer.

This study could be expanded by considering combinations of metabolically engineered strains. For example, cyanobacteria have previously been retro-engineered to export sugars (sucrose) and act as more efficient primary producers (Ducat et al. 2012). It is hypothesized that *E. coli* benefits the *Synechococcus* strain by aerobically oxidizing photosynthates and concurrently reducing two inhibitory byproducts (oxygen and photosynthate). The photosynthate compounds need to be confirmed and identified since

they are thought to be inhibitory organic acid compounds such as acetate and/or formate (depending on light cycle). If the composition of organic compounds in the cultures was known, then *E. coli* strains could be engineered for more efficient heterotrophic-aerobic oxidization. However, analytical identification of extracellular small molecules is technically challenging for these systems especially considering that these are biofilm samples with relatively small volumes. Larger scale suspended culture experiments, such as 5-10 L turbidostat photo-reactor cultures, could significantly expand the quality and amount of data available on this system and allow for more tractable analytical chemistry analysis.

Appendix A: Current Conclusions

This manuscript-in-preparation outlines an artificial biofilm consortium composed of primary producer *Synechococcus* strain PCC 7002 and consumer strain *Escherichia coli* MG1655. The binary system exhibits enhanced culture-productivity during early exponential phase. More data analysis and additional experimentation is required to establish all of the benefits of the described artificial binary culture.

APPENDIX B

DESIGN, CONSTRUCTION AND OPERATION OF A BIOFILM FLOW-CELL REACTOR FOR SIMULATING ACIDIC IRON-OXIDE HOT SPRING ENVIRONMENTS

Front Matter Details

IGERT Internship report –Hans C. Bernstein

December 1st 2012

Host Mentor: Dr. Helen Kreuzer, Pacific Northwest National Laboratories, Richland WA, USA

Internship Location: Microbial Cell Dynamics Laboratory, Pacific Northwest National Laboratories, Richland WA, USA

Internship Dates: Month of July 2012 plus additional and supporting field dates in Yellowstone National Park

MSU Course: DGED 676, Instructor—Robin Gerlach

Introduction

Yellowstone National Park (YNP), Wyoming, USA contains a diverse collection of pristine high-temperature environments containing stable thermophilic microbial communities. Acidic (pH ~3), amorphous Fe(III)-oxyhydroxide microbial mats located in Norris Geyser Basin (NGB) are of particular interest due to the interplay between geochemical cycling, nutrient transport, and unique microbial metabolic capabilities associated with dominant community members of the domain *Archaea* (Bernstein et al. In-Review; Inskeep and McDermott 2005; Inskeep et al. 2010). Of these, Fe-oxidizing *Metallosphaera yellowstonensis*-like organisms have been shown to comprise greater than 20% of the total archaeal community in numerous Fe(III)-oxide microbial mats and are believed to play a central role in the formation of the Fe(III)-oxide mat structure (Kozubal et al. 2008). Although, *M. yellowstonensis* and other organisms have been

isolated and cultured in a laboratory environment, Fe(III)-oxide microbial mat formation (analogous to the NGB sites) has never been observed *ex situ*.

Amorphous Fe(III)-As(V) oxyhydroxide microbial mats from NGB have been shown to form as a result of microbial activity (Inskeep et al. 2004). The rate of abiotic Fe(II)-oxidation is very slow and constrained by low pH (<4.5) (Konhauser 1998; Singer and Stumm 1970). These microbial mats are comprised of fairly porous Fe(III)-oxides that form on rhyolitic parent material and are essentially equivalent to biofilms by an accepted definition; *matrix enclosed accretions of microbial cells adhered to biotic or abiotic surfaces* (Hall-Stoodley et al. 2004). These biofilms are unique because they are partially comprised of a bio-mineralized component (Fe(III)-oxide and adsorbed As(V)). This mineral phase, mediated by chemolithotrophic microorganisms, forms *via* redox reactions of O_2 as the anode and biological terminal electron acceptor reacting with Fe(II) as the cathode and biological electron donor.

Previously, some biofilms have been successfully cultured and characterized utilizing a variety of continuous flow reactor methods (Goeres et al. 2009; Goeres et al. 2005; Hamilton 2003). Of these, flow-cell reactor designs can be used to simulate selected elements that correspond to flowing and/or hot spring environments, such as: directional flow, air-liquid-biofilm interfacial geometry, pseudo-constant velocity and low shear stress distributions. However, *ex situ* representation of the NGB hot spring or any other natural environment in continuous flow biofilm reactors presents certain technical challenges. One of the major challenges, with respect to simulating the NGB hot spring environments, arises from the gradient geometry intrinsic to the native springs.

These springs originate from anoxic, highly-reduced source water (~80-85ºC). The springs become oxygenated and exhibit temperature decreases.as they travel down the stream channel. The microbial population and mineral composition in the microbial mats change along with the dissolved oxygen concentration (DO), temperature and stream-channel-position. Additionally, vertical oxygen and *M. yellowstonensis* abundance gradients exist (*in situ*) within the microbial mats and are partially attributed to mass transfer limitations of oxygen (Bernstein et al. In-Review).

A project has been initiated to design, construct and characterize a flow-cell reactor that has the potential to simulate some of the key environmental parameters present in select NGB hot spring sites. This is a multi-institution project involving Montana State University (MSU) and Pacific Northwest National Laboratories (PNNL). Dr. Helen Kreuzer is the project lead for the PNNL portion of the chemosynthetic hot springs project, which is part of their DOE Genome Science Program, microbial interactions Foundational Scientific Focus Area (FSFA). The flow-cell reactor project was initiated and partially completed during an internship (July 2012) and benefitted from the resource and expertise available at PNNL within the Microbial Cell Dynamics Laboratory (MCDL).

Objectives of the Internship

PNNL's (Dr. Kreuzer, Dr. James Moran, Dr. Janine Hutchison and other PNNL staff) primary research interest, regarding the NGB chemosynthetic hot springs, is to investigate the ecophysiological characteristics of the NGB microbial mat communities. Their experiments have relied on the limited and seasonal access to the field sites.

Additionally, their experiments often require harvesting of microbial mat material which can have a significant impact on the sites and available material is limited. *The objective of this project was to develop a flow-cell biofilm reactor that a can simulate some of the environmental conditions from the NGB hot spring sites and be used as an acceptable surrogate for some of the field experiments.* This PNNL internship portion of the project was separated into three tasks:

Task 1. Design a prototype flow-cell biofilm reactor to simulate and control some of the key environmental conditions native to the NGB hot springs research sites.

Task 2. Construct the prototype flow-cell biofilm reactor and implement it at the MCDL/PNNL facility.

Task 3. Characterize the operational parameters of the reactor and develop an experimental protocol.

Research Design and Methods

Task 1: The prototype flow-cell biofilm reactor designed for this project was modified from the previously reported and commercially available, drip-flow-reactor (DFR) (Biosurface Technologies Bozeman, MT). Biofilm culturing in the DFR has been well characterized and is best suited for continuous flow under low-shear (Goeres et al. 2009). The original DFR apparatus consists of 4-6 flow chambers (in parallel) which are loaded with a coupon substratum such as borosilicate glass slides. The reactor is set at an angle (typically 10º) to facilitate flow across the biofilm/substratum which enters from a hypodermic needle and septum built into a removable cover. The influent consists of fresh culturing media and is discharged through an effluent port set at the end of each

flow chamber. Figure B. 1 contains a schematic diagram which illustrates the DFR experimental apparatus and typical configuration.

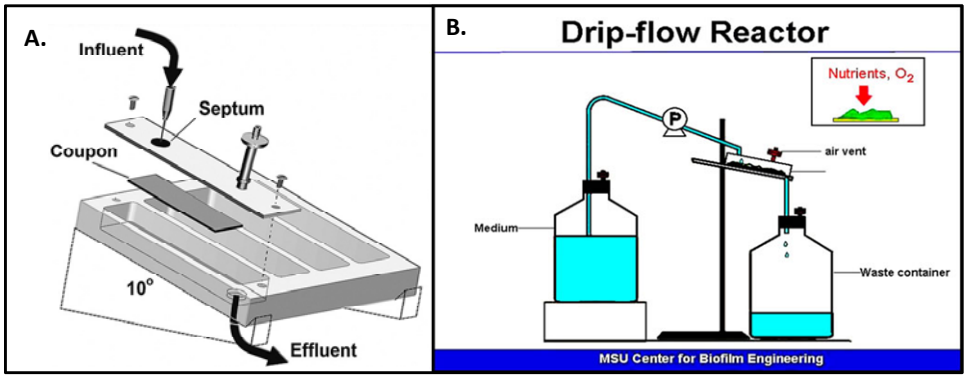

Figure B. 1. Illustrated schematics of the original drip-flow reactor. A.) flow-cell apparatus and B.) typical experimental configuration. © CBE.

The key controllable environmental inputs, simulated from the NGB hot spring sites, were determined to be: 1) directional low-velocity/low-shear flow, 2) vertical air-liquid-biofilm interfacial geometry, 3) constant and high temperature (68ºC) 4) constant and low pH (2-3) and 5) capacity for relatively long term operation to accommodate for the slow Fe(III)-oxide mat accumulation rates measured *in situ* (0.35-2.6 µmol $Fe \cdot cm^{-2} \cdot day^{-1}$) (Bernstein et al. In-Review). The original DFR apparatus and typical experimental configuration (Figure B. 1) is not well suited for control of these parameters. However, the DFR served as an appropriate starting platform and was retro-fitted for this project.

The modified DFR used for this project has been unofficially named, the *multi-channel biofilm flow reactor* (MCFBR). The MCFBR has been modified to have identical influent and effluent ports at both ends of each flow chamber. Additionally, the chambers

(dimensions; 10 x 2.5 x 1.5 cm) are no longer constrained to be set at an angle to induce flow. Directional flow was designed to be controlled by integrating matching peristaltic pump drives in the influent and effluent tubing lines corresponding to each flow chamber. The majority of the modifications from the typical DFR system were made to the experimental configuration. Figure B. 2 illustrates the prototype MCFBR experimental configuration. Similar to the DFR, four flow-cells were operated in parallel; however, pre-and post-mixing chambers were designed and coupled with a recycle stream. The recycle stream was designed to facilitate long term operation with respect to media consumption. It is important to note that media recycle can be achieved without dual-mixing chambers. However, the dual-mixing chamber design was implemented to allow this experimental configuration to be coupled with identical modular-reactors in series, which can be used to simulate the stream-channel gradients in temperature and DO (observed *in situ*). One reactor module (as shown in Figure B. 2) is designed to represent a single position or transect in the spring channel by maintaining constant temperature and DO in the flow-cell apparatus feed (flow from mixing upstream mixing chamber).

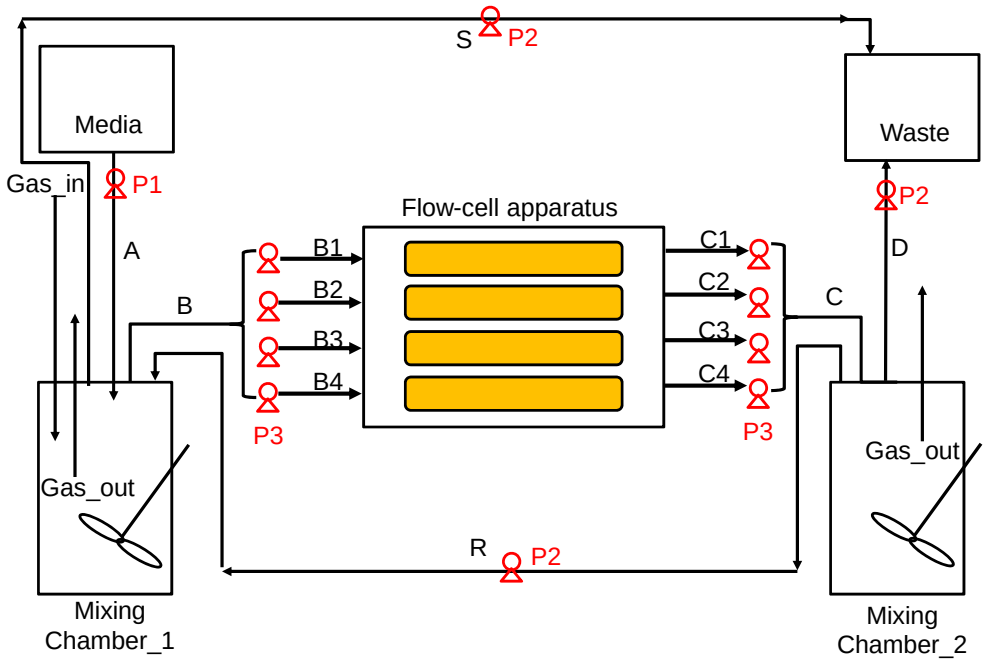

Figure B. 2. Illustrated schematic for the prototype multi-channel flow biofilm reactor. The flow streams are labeled accordingly: (A) fresh media influent to mixing chamber 1 (MC1), (B) flow-cell influent from MC1 (divided into four streams), (C) effluent from flow-cell reactor to MC2 (also divided into four streams), (D) waste stream effluent from MC2, (R) recycle stream from MC2 to MC1, and (S) "safety" stream from MC1 used to set a maximum contained media volume for MC1 and prevent overflow. The pumps are labeled P1-P3 which is discussed in more detail in this document under sections tasks 2 and 3.

Task 2: Construction and parts allocation for the MCFBR was done at MSU and PNNL prior and during the July 2012 PNNL internship. The flow-cell apparatus was constructed by special order from Biofsurface Technologies (Bozeman, MT). The flow-cell in-and out-flow ports were built with 1", barbed fittings. Various sizes of Masterflex L/S silicon tubing (Cole-Parmer) were used for all flow-lines. The mixing chambers were constructed from 1 L cylindrical glass flasks fitted with a size 15 rubber stopper containing 5-ports tailored with ¼" glass tubing. The glass tubing ports were built to be adjustable with respect to vertical position allowing them to either draw from the liquid

control volume (dip-stick configuration) or make material exchanges in the head space. Gas delivery in mixing chamber 1 (upstream of flow-cell apparatus) was facilitated with a generic air stone submerged in the liquid. Agitation capabilities were built into the mixing-chambers with magnetic stir bars and by placing the chambers on compact magnetic stir-plates (VWR Lab Disc Magnetic Stirrer). Three Masterflex L/S variable speed modular peristaltic pump drives (designated P1-P3) were used in conjunction with Masterflex L/S two-channel Easy-Load rotors. Mixing chambers and flow-cell apparatus were assembled together in close proximity required for incubator housing. A basic drying oven (capable of maintaining 68º C) was used for temperature control. Large polypropylene carboys (20-50 L) were used for the media and waste containers. The media carboy was outfitted with a large magnetic stir bar and constantly mixed with a large volume magnetic stirrer (Cool-Stir).

Task 3: Development of a basic protocol for MCFBR operation was accomplished at PNNL in the MCDL. The following people directly contributed to the protocol and method development: Helen Kreuzer, Bill Inskeep, James Moran, Janine Hutchison, Will Chrisler and Eric Hill. The experimental system was first tested in a non-biological run (DI water) and then tested/developed by attempting to culture *M. yellowstonensis*, autotrophically. The culturing conditions, specific for the *M. yellowstonensis* initial experiment, were chosen to attempt simulation for some of the conditions found in the Beowulf east spring at transect D (specifics discussed below).

Pumps and Media Delivery Specifics. Three peristaltic pumps (P1-P3) were used for continuous, open-system media flow. Fresh media delivery to mixing chamber 1 (stream A) was pumped with P1 equipped with a single pump head and size 14 Masterflex L/S tubing to achieve a desired flow rate of 1.2 $ml \cdot min^{-1}$. The recycle, safety and waste streams (streams R, S and D respectively) were pumped with P2 equipped with three pump heads. Flow through P2 was pumped and delivered with size 16 Masterflex L/S tubing to achieve a desired flow rate of 22 $ml \cdot min^{-1}$. Media delivery to and from the flow-cell apparatus (streams B and C) was pumped with P3 equipped with four dual-drive pump heads (total of 8 drives). Each P3-drive was fitted with size 16 tubing to achieve a desired flow rate of 6 $ml \cdot min^{-1}$ to each flow chamber, resulting in a total flow of 24 $ml \cdot min^{-1}$ to and from the flow cell apparatus. The volumetric flow rate achievable for each tubing size is proportional to the RPM of the pump drive. Four-point calibrations and standard curves were determined for each pump-tubing size combination used in this experiment (Equations B. 1-3) (*Note: small differences between P2 and P3 for size 16 tubing*). These calibrations and standard curves were used to non-invasively check the accuracy of each pump during operation by simply measuring the RPM.

$$P1: RPM = 0.2255 \cdot F_{size\_14}(ml \cdot min^{-1}) + 0.162 \quad \text{Eq. B.1}$$

$$P2: RPM = 1.0498 \cdot F_{size\_16}(ml \cdot min^{-1}) + 0.113 \quad \text{Eq. B.2}$$

$$P3: RPM = 1.0724 \cdot F_{size\_16}(ml \cdot min^{-1}) + 0.051 \quad \text{Eq. B.3}$$

Media flow in each chamber was set with matching in and out flow rates which maintained constant liquid depth and volume (0.5 cm and 12.75 cm^3 respectively). It should be noted that these constant values were achieved by charging each flow cell with

the respective 12.75 cm^3 of media before inducing continuous flow. The constant liquid depth in each flow cell permitted 1 cm of head space which effectively simulates the air-liquid-biofilm interfacial geometry observed in the natural springs. The calculated average velocity and residence time (single pass) for media flow in each chamber was 0.32 $cm \cdot sec^{-1}$ and 31.9 sec respectively. These values may under-represent the conditions observed in the springs (v_{max} = 5-20 $cm \cdot sec^{-1}$ in Beowulf east, transect D); however, the exact velocity distribution and average velocity of the representative spring position is not known.

Each mixing chamber was set to a constant volume of 300 ml by setting the dip-stick glass tubing positions and maintaining higher out-flows (the sums of streams [S + B] and [R + D] for mixing chambers 1 and 2 respectively) compared to in-flows. The resident liquid control volume for the entire system was calculated to be 950 ml (sum of 4-flow-chambers, both mixing chambers and tubing volume). The dilution rate and residence volume for the reactor system (dilution rate = in-flow(A)$\cdot$system_vol^{-1}) was set to 0.076 hr^{-1} and 13.2 hr respectively. The media-recycle ratio (MRr = flow(R)$\cdot$flow$(B)^{-1}$) was set to 0.92.

Culturing media. The *M. yellowstonensis* initial experiment was run with Beowulf synthetic media (BS) (400 µM $NaNO_3$, 1200 µM Na_2SO_4, 1200 µM KCl, 114 µM $AlCl_3 \cdot 6H_2O$, 717 µM H_3BO_3, 12 µM $MgSO_4$, 100 µM K_2HPO_4, 147 µM KF, 600 µM NH_4Cl, 250 µM $CaCl_2$, 5000 µM $NaHCO_3$) plus 1 ml of ATCC vitamin solution (Whole's solution). Media was adjusted with HCl to a pH of 3.The BS media was also supplemented with 50 $\mu g \cdot L^{-1}$ kanamycin (antibiotic used to facilitate axenic culturing),

0.025 yeast extract and 200 μM Fe(II)SO_4 (electron donor for *M. yellowstonensis*). The concentration of Fe(II) was set roughly 4 times higher than values measured at the representative spring site. This increase and the addition of yeast extract was done to raise the amount of available electron donor to *M. yellowstonensis*.

Reactor Start-Up and Culturing Conditions. All reactor components and media were autoclaved and sterilized prior to experimental start-up. The internal reactor control volume (mixing chambers and flow-cell apparatus loaded with borosilicate glass slides) was charged with 400 ml of *M. yellowstonensis* inoculum cultured in BS media (cell density unknown). Internal flow (flow-cell and recycle flow only) was induced for 24 hrs to facilitate microbial adhesion inside the flow cell. After the 24 hr inoculation step, continuous system flow (fresh media and waste flow, streams A and D) was turned on for a total of 10 days. The reactor system control volume was incubated at 68ºC and the target DO and DIC (*note: all CO_2 at this pH*) levels were 60 and 800 μM respectively.

Gas Control. The target dissolved gas concentrations (DO and DIC) were not obtainable by simply sparging the media with air. A three-gas-mixing system (illustrated in Figure B. 3) was devised with the help of Eric Hill and the resources available in the MDCL. Its purpose was to deliver a gas stream with the correct composition to achieve the target dissolved gas concentrations. The final gas stream was delivered at 1 volume-per-minute (mixing chamber liquid volume-300 $ml \cdot min^{-1}$). The dissolved gas concentrations were estimated from Henry's law using published coefficients ($k_{cp}(std) = 1.3 \cdot 10^{-3}$ and $3.4 \cdot 10^{-2}$ $mol \cdot L^{-1} \cdot atm^{-1}$ for O_2 and CO_2 respectively) scaled for temperature

by the Van't Hoff equation (equation B.4) (C_{sol} = 1700 and 2400 for O_2 and CO_2 respectively) (Perry et al. 1973).

$$k_{cp}(T) = k_{cp}(278\ K) \cdot exp\left[C_{sol}\left(\frac{1}{T} - \frac{1}{278\ K}\right)\right] \quad \text{Eq. B.4}$$

The gas composition for the off-gas and in-stream to mixing chamber 1 (Fg_mix) was measured during the experiment with an off-gas detector (BlueSense).

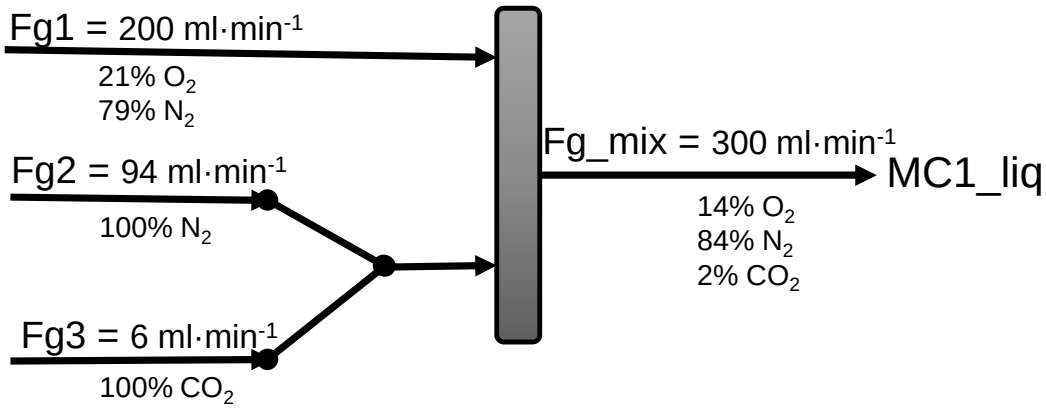

Figure B. 3. Illustrated schematics of the three-gas-mixing system. This was assembled to deliver the calculated gas composition required to obtain the target O2 and CO2 concentrations in the flow-chamber feed stream (stream B and mixing chamber 1). The CO2 concentration in the air stream (~0.04% in Fg1) was considered negligible in the mass balance calculations.

Break-Down Procedure and Sampling. Flow was stopped in the MCFBR after 10 days of operation and the glass slide substrates were processed for microscopy. The four glass slides were removed from the chambers in the reactor. Two of the slides were submerged in 50 ml fresh 2.5 % glutaraldehyde in PBS and stored at 4ºC for transmission electron microscopy analysis (TEM) in EMSL. The other two slides were fixed in fresh 4% paraformaldehyde (PFA) in PBS for 1 hr at room temperature. The PFA fixed slides

were processed in an ethanol dehydration step which included consecutive 3 minute washes in 50, 80 and 100% EtOH followed by an air drying step. These slides were stored at -20ºC. Controls were prepared by incubating slides in glass bottles containing the BS media (described above) and the *M. yellowstonensis* culture. Batch culture controls were processed identically to the MCFBR glass slides. The PFA slides were stained/incubated in 1:1000 DAPI and 1:10000 SYBR Gold solutions at 65ºC for 1 hr, rinsed with fresh PBS and air-dried prior to confocal imaging. Non-stain controls were also prepared from the batch culture controls.

Results and Discussion

The primary goal for the internship portion of this project was to design, construct and characterize a continuous, flow-cell biofilm reactor capable of simulating some of the environmental conditions found in the representative NGB hot springs. This was accomplished with the prototype MCFBR. Figure B. 4 depicts a photograph of the experimental system in operation at PNNL.

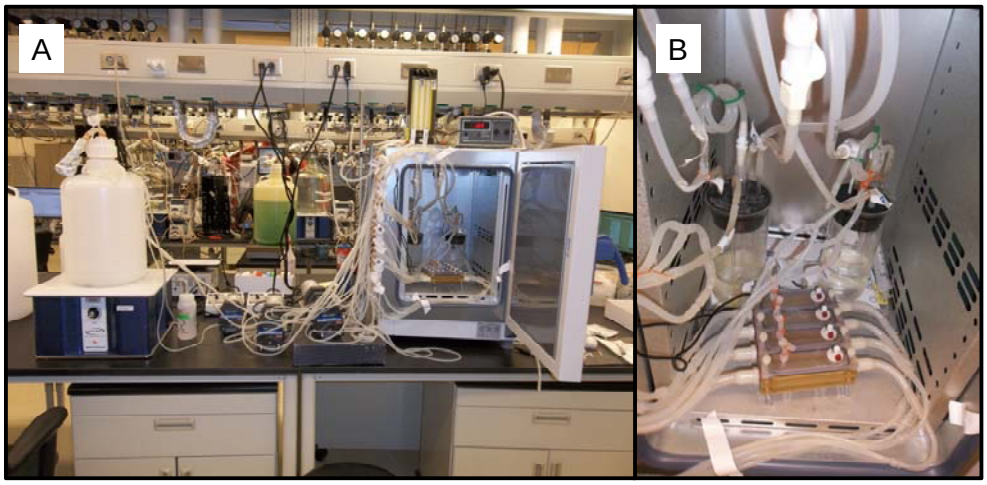

Figure B. 4. Photographs of the MCFBR in operation at PNNL. A) Whole experimental configuration including feed carboy, pump and incubator configuration. B) Mixing chambers and flow-cell apparatus contained in the incubator housing.

The MCFBR was partially characterized by attempting to grow *M. yellowstonensis,* autotrophically in biofilm phase. After 10 days of flow, the glass slide substrates (in the flow-cell apparatus) showed accumulated and attached biofilm-like material. The biofilm-like material attached to the slides did not visually show the same morphology of the Fe(III)-oxide microbial mats from the springs. This was further investigated with confocal and electron microscopy efforts in EMSL. The microscopy results verified attached biofilm and cell-like material (CLM) but did not directly confirm that it was a *M. yellowstonensis* biofilm. Figure B. 5 contains some of the microscopy results from this experiment.

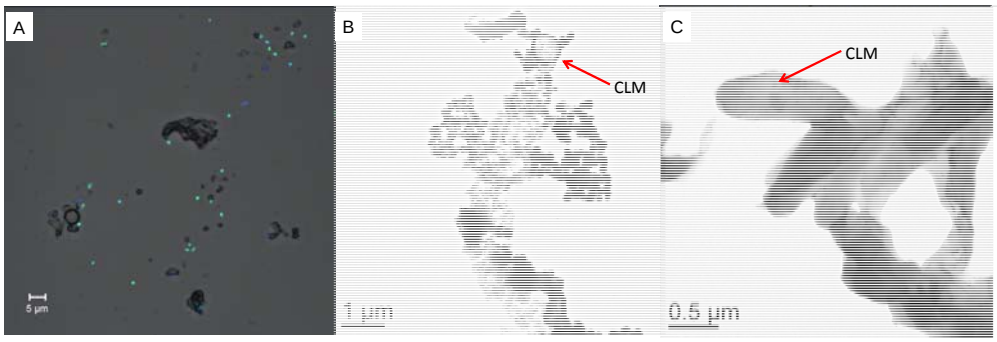

Figure B. 5. Microscopy images of samples taken from the MCFBR experiment showing cell-like-material (CLM) attached to the glass substratum. A) Confocal image of MCFBR slide stained with DAPI and SYBR Gold. B) TEM image showing CLM with the cocci morphology similar to M. yellowstonensis. C) TEM image showing CLM aggregates displaying bacilli morphology.

Conclusions and Future Work

A continuous flow-cell reactor was designed, constructed and characterized at PNNL. Its purpose was to simulate some of the key environmental characteristics found in the NGB hot spring sites; specifically the Beowulf east Fe(III)-oxide microbial mats. Characterization and protocol development was done by attempting to culture iron-oxidizing *M. yellowstonensis* autotrophically. Biofilm-like material was observed in the MCFBR after 10 days of operation. However, it was not deemed analogous to the Fe(III)-oxide microbial mats from NGB. It should be stated that *ex situ* Fe(III)-oxide microbial mats, analogous to the NGB sites, have *still* never been cultured *ex situ*. However, potential methodology to accomplish this has now been developed.

Table 1. Proof of concept experimental design

***In vitro* culture from native mat inoculum**	**Aerobic-heterotrophic isolate culture (*ex. NAG1)***
Step1) harvest slides from springs incubated *in situ*	**Step1)** Culture isolate with slide section substratum
Step2) inoculate MCFBR with sectioned Fe(III)-mat slide placed adjacent to clean-sterile slides	**Step2)** inoculate MCFBR with sectioned slide (with isolate attached) placed adjacent to clean-sterile slides. Analyze replicate slides from inoculum culture as t=0 data point
Step3) incubate under flow until slides placed adjacent to inoculum slide support microbial mat	**Step3)** Carry-out steps 3 and 4 from left column.
Step4) transfer in-chamber grown slides to new, clean and sterile chamber and subject to new flow	**Step4)** analyze isolate biofilm for oxygen and carbon-dioxide reactions with microsensors and/or gas analyzers in MCFBR prototype 2 configuration. Compare results to suspended cultures grown in batch.
Step5) analyze *in vitro* mat culture metagenome and compare to *in situ* mat	

Future experiments are being devised to more thoroughly test *ex situ* Fe(III)-microbial mat culturing with the MCFBR system. The illustration above (Table 1) summarizes these experimental designs. Additionally, the MCFBR is being further developed for these and other biofilm experiments. Specifically, the removable lids to the flow-cell apparatus have been re-designed, since the July 2012 PNNL internship, for better control of the head space overlaying the liquid-biofilm interface. Additionally, the MCFBR prototype conceived during this internship has been used as a starting platform for designing a flow-cell reactor specific for photoautotrophic biofilm cultivation.

Impact of Personal and Professional Development

This internship opportunity was provided to me by the Integrated Graduate Education and Research Traineeship (IGERT) fellowship and by PNNL. It has positively impacted my professional and personal development in many ways. Here, I will specifically describe some of the ways this experience has impacted me. *First,* PNNL is, in my eyes, the mecca for interdisciplinary science. I was able to expand my own interdisciplinary proficiency by interacting with specialists in microbial physiology (FSFA research team), microscopy (EMSL research team) and bioreactors (MCDL research team). *Second,* I became familiar with the world-class scientific and research culture at PNNL. I had the opportunity to meet with scientists about topics other than my internship research objectives and also became familiar with the important safety standards of a national laboratory environment. *Third,* I learned how to contribute my skills in biofilm science and engineering towards problem solving efforts within new teams of professionals. I became aware, perhaps for the first time, that I have a certain set of skills that can be used in environments other than my home institution at MSU.

I would also like to emphasis that this internship experience gave me the opportunity to create personal relationships with scientific professionals who are also very kind and congenial people. The relationships forged while at PNNL and in the field with PNNL staff has already proven to go beyond just the internship experience. As mentioned I am pursuing a potential postdoctoral position at PNNL to continue doing

work directly related to this internship and expect to continue collaborating with these people during my career.

Project Specific Acknowledgements

This research internship at Pacific Northwest National Laboratory was made possible by the time and resource commitment of Dr. Helen Kreuzer who acted as the internship advisor. I would also like to thank the IGERT program director, Dr. Bill Inskeep for his efforts and contribution and for facilitating the initial discussions. While at PNNL I worked closely with Eric Hill who directly contributed his expertise in bioreactors to the project. Dr. Janine Hutchison also contributed time and expertise in microbial culturing methods as well as the experimental design. I would also like to acknowledge the microscopy expertise at EMSL, Will Chrisler and Alice Dohnalkova, for their contributions. Dr. James Moran helped with the project described above and contributed to the initial field studies that served as a basis. He and Dr. Kreuzer also introduced me to other projects of interest being conducted at PNNL which significantly enriched my experience.

This project was funded by the National Science Foundation- IGERT Program (DGE 0654336) and the DOE-FSFA program at PNNL.

APPENDIX C

SYNTHETIC ESCHERICHIA COLI CONSORTIA ENGINEERED FOR SYNTROPHIC METABOLITE EXCHANGE AND PARTITIONED TERMINAL ELECTON ACCEPTOR FUNCTIONALITY

Synopsis

The previously described *E. coli* consortia (Chapter 4) exhibit enhanced biomass productivity based on engineered syntrophic metabolite exchanges (Bernstein et al. 2012). The primary exchange compound was hypothesized and experimentally determined to be acetate which is produced via fermentation reactions associated with substrate (glucose) over-flow and/or low oxygen availability (Alexeeva et al. 2002; Xu et al. 1999). The enhanced biomass productivity observed in the synthetic system was attributed to acetic acid scavenging by an acetate-specialist strain 403G100. Acetate oxidative catabolism, in *E. coli,* requires a terminal electron acceptor (TEA) such as oxygen and the previously reported consortia designs create the potential for TEA competition under aerobic or micro-aerobic conditions such as those typically found in biofilms. An alternative consortium design has been considered and constructed which permits acetate scavenging in a non-competitive manner under anaerobic conditions in which utilize nitrate as the sole TEA available to the 403G100 strain. Figure C.1 contains a schematic of the anaerobic, nitrate-reducing consortium.

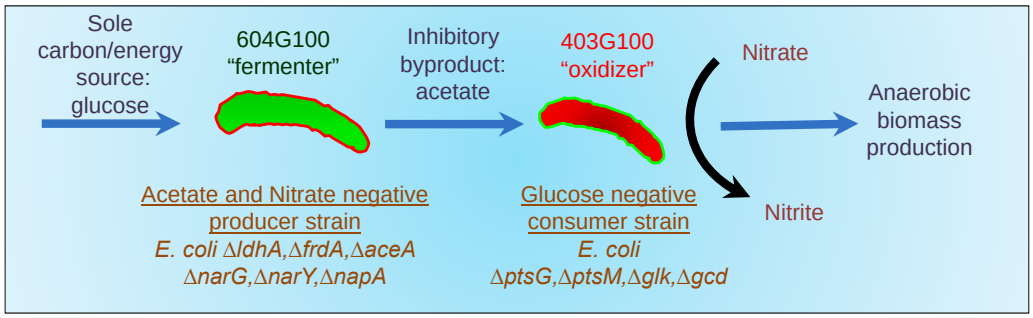

Figure C. 1. Schematic illustration of the anaerobic, nitrate-reducing synthetic consortium. The coupling of the two deletion mutants, 604G100 and 403G100, is hypothesized to allow concurrent glucose fermentation and catabolic acetate oxidation under anoxic conditions.

Preliminary Data

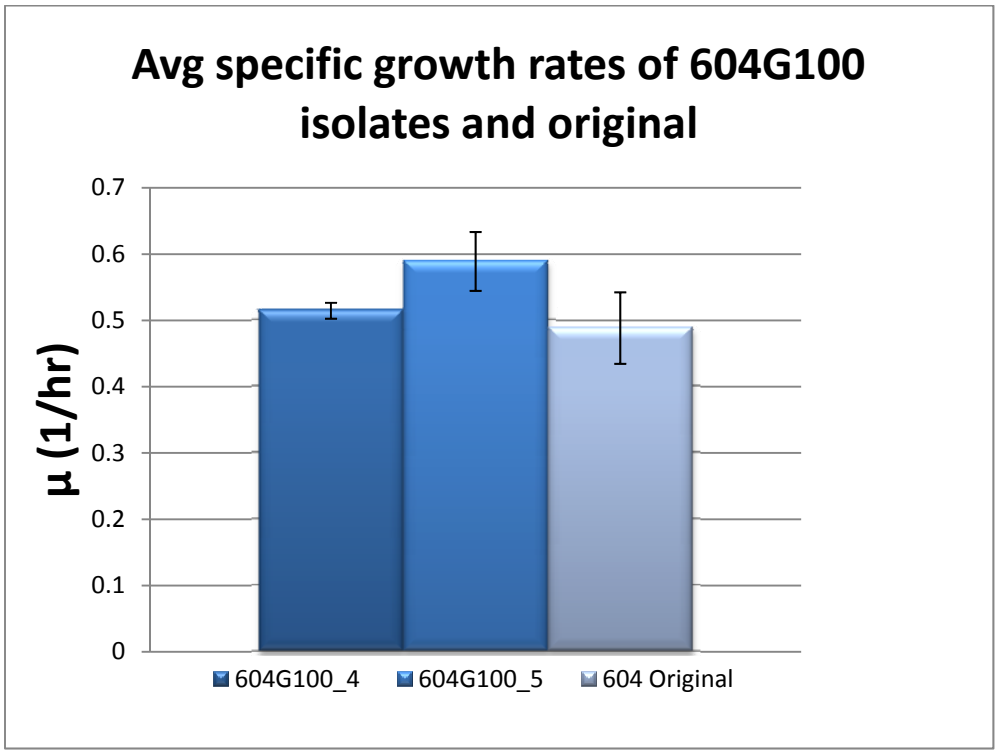

Figure C. 2. Maximum specific growth rates of two 604G100 isolates taken from the 100-generation chemostat adaptation experiment compared to the un-adapted, original 604 strain (methodology described in Bernstein et al. 2012). Data points represent averages from at least three independent batch reactor experiments. Error bars represent ± 1 standard deviation.

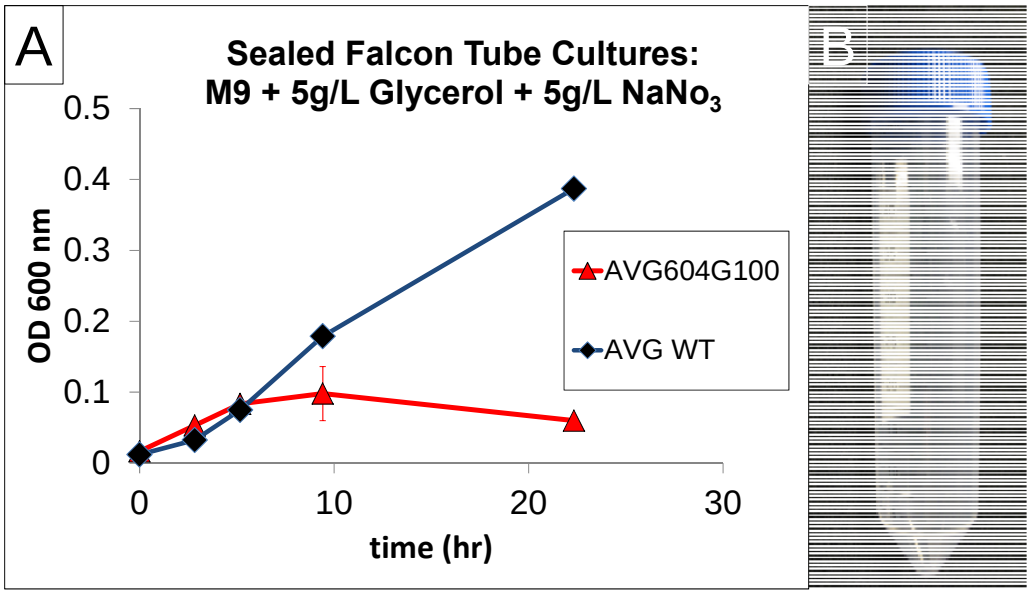

Figure C. 3. Preliminary growth experiment comparing the *E. coli* 604G100 deletion mutant to the MG1655 wild-type under micro-aerobic to anoxic conditions (panel A). Cultures were grown in tightly sealed 50 ml falcon tubes (panel B), with effectively no head space. Cultures were assumed to reach anoxic conditions though aerobic oxidation of glycerol which typically a non-fermentable substrate for *E. coli*. This data is preliminary evidence that the 604G100 strain does not utilize nitrate as a viable terminal election acceptor.

APPENDIX D

SELECTED ABSTRACTS

This appendix contains selected abstracts from previously published, peer-reviewed manuscripts directly related to the technical content in this dissertation. Abstracts are listed in chronological order of publication.

1) Robustness analysis of culturing perturbations on *Escherichia coli* colony biofilm beta-lactam and aminoglycoside antibiotic tolerance

Trevor R. Zuroff, Hans C. Bernstein, Jenna Lloyd-Randolfi, Lourdes Jimenez-Taracido, Philip S. Stewart and Ross P. Carlson. (2010). BMC Microbiology 10: 185.

Abstract

Biofilms are ubiquitous. For instance, the majority of medical infections are thought to involve biofilms. However even after decades of investigation, the in vivo efficacy of many antimicrobial strategies is still debated suggesting there is a need for better understanding of biofilm antimicrobial tolerances. The current study's goal is to characterize the robustness of biofilm antibiotic tolerance to medically and industrially relevant culturing perturbations. By definition, robust systems will return similar, predictable responses when perturbed while non-robust systems will return very different and potentially unpredictable responses. The predictability of an antibiotic tolerance response is essential to developing, testing, and employing antimicrobial strategies. The antibiotic tolerance of Escherichia coli colony biofilms was tested against beta-lactam and aminoglycoside class antibiotics. Control scenario tolerances were compared to tolerances under culturing perturbations including 1) different nutritional environments 2)

different temperatures 3) interruption of cellular quorum sensing and 4) different biofilm culture ages. Here, antibiotic tolerance was defined in terms of culturable biofilm cells recovered after a twenty four hour antibiotic treatment. Colony biofilm antibiotic tolerances were not robust to perturbations. Altering basic culturing parameters like nutritional environment or temperature resulted in very different, non-intuitive antibiotic tolerance responses. Some minor perturbations like increasing the glucose concentration from 0.1 to 1 g/L caused a ten million fold difference in culturable cells over a twenty four hour antibiotic treatment. The current study presents a basis for robustness analysis of biofilm antibiotic tolerance. Biofilm antibiotic tolerance can vary in unpredictable manners based on modest changes in culturing conditions. Common antimicrobial testing methods, which only consider a single culturing condition, are not desirable since slight culturing variations can lead to very different outcomes. The presented data suggest it is essential to test antimicrobial strategies over a range of culturing perturbations relevant to the targeted application. In addition, the highly dynamic antibiotic tolerance responses observed here may explain why some current antimicrobial strategies occasionally fail.

2) Laser desorption VUV postionization MS imaging of a cocultured biofilm

Chhavi Bhardwaj, Jerry F. Moore, Yang Cui, Gerald L. Gasper, Hans C. Bernstein, Ross P. Carlson, Luke Hanley. (2012). Analytical and Bioanalytical Chemistry: 1-9.

Abstract

Laser desorption postionization mass spectrometry (LDPI-MS) imaging is demonstrated with a 10.5 eV photon energy source for analysis and imaging of small endogenous molecules within intact biofilms. Biofilm consortia comprised of a synthetic Escherichia coli K12 coculture engineered for syntrophic metabolite exchange are grown on membranes and then used to test LDPI-MS analysis and imaging. Both E. coli strains displayed many similar peaks in LDPI-MS up to m/z 650, although some observed differences in peak intensities were consistent with the appearance of byproducts preferentially expressed by one strain. The relatively low mass resolution and accuracy of this specific LDPI-MS instrument prevented definitive assignment of species to peaks, but strategies are discussed to overcome this shortcoming. The results are also discussed in terms of desorption and ionization issues related to the use of 10.5 eV single-photon ionization, with control experiments providing additional mechanistic information. Finally, 10.5 eV LDPI-MS was able to collect ion images from intact, electrically insulating biofilms at ~100 μm spatial resolution. Spatial resolution of ~20 μm was possible, although a relatively long acquisition time resulted from the 10 Hz repetition rate of the single-photon ionization source.

3) Iron induces bimodal population development by *Escherichia coli*

William H. DePas, David A. Hufnagel, John S. Lee, Luz P. Blanco, Hans C. Bernstein, Steve T. Fisher, Garth A. James, Philip S. Stewart, and Matthew R. Chapman. (2013). Proceedings of the National Academy of Sciences of the United States of America. Doi:10.1073/pnas.1218703110

Abstract

Bacterial biofilm formation is a complex developmental process involving cellular differentiation and the formation of intricate 3D structures. Here we demonstrate that exposure to ferric chloride triggers rugose biofilm formation by the uropathogenic Escherichia coli strain UTI89 and by enteric bacteria Citrobacter koseri and Salmonella enterica serovar typhimurium. Two unique and separable cellular populations emerge in iron-triggered, rugose biofilms. Bacteria at the air–biofilm interface express high levels of the biofilm regulator csgD, the cellulose activator adrA, and the curli subunit operon csgBAC. Bacteria in the interior of rugose biofilms express low levels of csgD and undetectable levels of matrix components curli and cellulose. Iron activation of rugose biofilms is linked to oxidative stress. Superoxide generation, either through addition of phenazine methosulfate or by deletion of sodA and sodB, stimulates rugose biofilm formation in the absence of high iron. Additionally, overexpression of Mn-superoxide dismutase, which can mitigate iron-derived reactive oxygen stress, decreases biofilm formation in a WT strain upon iron exposure. Not only does reactive oxygen stress promote rugose biofilm formation, but bacteria in the rugose biofilms display increased

resistance to H_2O_2 toxicity. Altogether, we demonstrate that iron and superoxide stress trigger rugose biofilm formation in UTI89. Rugose biofilm development involves the elaboration of two distinct bacterial populations and increased resistance to oxidative stress.

REFERENCES CITED

Abd-Alla MH, Elsadek El-Enany A-W. 2012. Production of acetone-butanol-ethanol from spoilage date palm (Phoenix dactylifera L.) fruits by mixed culture of Clostridium acetobutylicum and Bacillus subtilis. Biomass and Bioenergy 42(0):172-178.

Alexeeva S, Hellingwerf KJ, Teixeira de Mattos MJ. 2002. Quantitative assessment of oxygen availability: perceived aerobiosis and its effect on flux distribution in the respiratory chain of Escherichia coli. J Bacteriol 184(5):1402-6.

Anderl JN, Franklin MJ, Stewart PS. 2000. Role of antibiotic penetration limitation in Klebsiella pneumoniae biofilm resistance to ampicillin and ciprofloxacin. Antimicrob Agents Chemother 44(7):1818-24.

Anderl JN, Zahller J, Roe F, Stewart PS. 2003. Role of nutrient limitation and stationary-phase existence in Klebsiella pneumoniae biofilm resistance to ampicillin and ciprofloxacin. Antimicrob Agents Chemother 47(4):1251-6.

Angenent LT, Karim K, Al-Dahhan MH, Wrenn BA, Domíguez-Espinosa R. 2004. Production of bioenergy and biochemicals from industrial and agricultural wastewater. Trend in Biotechnol 22(9):477-485.

Aristidou AA, San KY, Bennett GN. 1994. Modification of central metabolic pathway in escherichia coli to reduce acetate accumulation by heterologous expression of the bacillus subtilis acetolactate synthase gene. Biotechnology and Bioengineering 44(8):944-51.

Atsumi S, Hanai T, Liao JC. 2008. Non-fermentative pathways for synthesis of branched-chain higher alcohols as biofuels. Nature 451(7174):86-U13.

Atsumi S, Higashide W, Liao JC. 2009. Direct photosynthetic recycling of carbon dioxide to isobutyraldehyde. Nature Biotechnology 27(12):1177-U142.

Auernik KS, Kelly RM. 2008. Identification of components of electron transport chains in the extremely thermoacidophilic crenarchaeon Metallosphaera sedula through iron and sulfur compound oxidation transcriptomes. Applied and Environmental Microbiology 74(24):7723-7732.

Baba T, Ara T, Hasegawa M, Takai Y, Okumura Y, Baba M, Datsenko KA, Tomita M, Wanner BL, Mori H. 2006. Construction of Escherichia coli K-12 in-frame, single-gene knockout mutants: the Keio collection. Mol Syst Biol 2.

Bader J, Mast-Gerlach E, Popović MK, Bajpai R, Stahl U. 2010. Relevance of microbial coculture fermentations in biotechnology. J of Appl Microbiol 109(2):371-387.

Bagi Z, Ács N, Bálint B, Horváth L, Dobó K, Perei K, Rákhely G, Kovács K. 2007. Biotechnological intensification of biogas production. Applied Microbiology and Biotechnology 76(2):473-482.

Baker BJ, Banfield JF. 2003. Microbial communities in acid mine drainage. Fems Microbiology Ecology 44(2):139-152.

Balagadde FK, Song H, Ozaki J, Collins CH, Barnet M, Arnold FH, Quake SR, You L. 2008. A synthetic Escherichia coli predator-prey ecosystem. Mol Syst Biol 4.

Bateson MM, Ward DM. 1988. Photoexcretion and Fate of Glycolate in a Hot-Spring Cyanobacterial Mat. Applied and Environmental Microbiology 54(7):1738-1743.

Bathe S, Norris PR. 2007. Ferrous iron- and sulfur-induced genes in Sulfolobus metallicus. Applied and Environmental Microbiology 73(8):2491-2497.

Bayer TS, Widmaier DM, Temme K, Mirsky EA, Santi DV, Voigt CA. 2009. Synthesis of methyl halides from biomass using engineered microbes. J Am Chem Soc 131(18):6508-6515.

Beam JP, Jay, Z.J., Kozubal, M.A., Inskeep, W.P. Distribution and ecology of Thaumarchaea in geothermal enviroments; 2011; Big Sky, Montana USA.

Beardall J, Raven JA. 1981. Transport of inorganic carbon and the 'CO2 concentrating mechanism' in Chlorella emersonii (Chlorophyceae)1. J. Phycol 17(2):134-141.

Bender J, Phillips P. 2004. Microbial mats for multiple applications in aquaculture and bioremediation. Bioresource Technology 94(3):229-238.

Bernstein HC, Beam JP, Kozubal MA, Carlson RP, Inskeep WP. 2013. In situ analysis of oxygen consumption and diffusive transport in high-temperature acidic iron-oxide microbial mats. Environl Microbiol.

Bernstein HC, Carlson RP. 2012. Microbial consortia engineering for cellular factories: in vitro to in silico systems. Comput Struct Biotechnol J. 3.

Bernstein HC, Paulson SD, Carlson RP. 2012. Synthetic Escherichia coli consortia engineered for syntrophy demonstrate enhanced biomass productivity. Journal of Biotechnology 157(1):159-166.

Beyenal H, Lewandowski Z, Harkin G. 2004. Quantifying biofilm structure: Facts and fiction. Biofouling 20(1):1-23.

Bhardwaj C, Cui Y, Hofstetter T, Liu S, Bernstein HC, Carlson RP, Ahmed M, Hanley L. (In-Prep). Differentiation of Microbial Species and Strains in Cocultured Biofilms using Laser Desorption Postionization Mass Spectrometry and Multivariate Analysis.

Bhardwaj C, Moore J, Cui Y, Gasper G, Bernstein H, Carlson R, Hanley L. 2012. Laser desorption VUV postionization MS imaging of a cocultured biofilm. Anal Bioanal Chem:1-9.

Bigelow NW, Hardin WR, Barker JP, Ryken SA, MacRae AC, Cattolico RA. 2011. A comprehensive GC–MS sub-microscale assay for fatty acids and its applications. J. American Oil Chemists' Society 88(9):1329-1338.

Bizukojc M, Dietz D, Sun J, Zeng A-P. 2010. Metabolic modelling of syntrophic-like growth of a 1,3-propanediol producer Clostridium butyricum and a methanogenic archeon;Methanosarcina mazei under anaerobic conditions. Bioprocess Biosyst Eng 33(4):507-523.

Boelee NC, Temmink H, Janssen M, Buisman CJN, Wijffels RH. 2012. Scenario analysis of nutrient removal from municipal wastewater by microalgal biofilms. Water 4(2):460-473.

Boonchan S, Britz ML, Stanley GA. 2000. Degradation and mineralization of high-Molecular-weight polycyclic aromatic hydrocarbons by defined fungal-bacterial cocultures. Appl and environ microbiol 66(3):1007-1019.

Booth CC, Heath J. 1962. Effect of E coli on Absorption of Vitamin B12. Gut 3(1):70-&.

Brauer VS, Stomp M, Huisman J. 2012. The nutrient-lad hpothesis: ptterns of rsource limitation and community structure driven by competition for nutrients and light. American Naturalist 179(6):721-740.

Brenner K, Arnold FH. 2011. Self-organization, layered structure, and aggregation enhance persistence of a synthetic biofilm consortium. PLoS ONE 6(2):e16791.

Brenner K, Karig DK, Weiss R, Arnold FH. 2007. Engineered bidirectional communication mediates a consensus in a microbial biofilm consortium. Proc Natl Acad Sci USA 104(44):17300-17304.

Brenner K, You L, Arnold FH. 2008. Engineering microbial consortia: a new frontier in synthetic biology. Trends Biotechnol 26(9):483-9.

Briones A, Raskin L. 2003. Diversity and dynamics of microbial communities in engineered environments and their implications for process stability. Curr Opin Biotechnol 14(3):270-276.

Brune KD, Bayer TS. 2012. Engineering microbial consortia to enhance biomining and bioremediation. Frontiers in microbiology 3:203.

Calhoun MW, Oden KL, Gennis RB, de Mattos MJ, Neijssel OM. 1993. Energetic efficiency of Escherichia coli: effects of mutations in components of the aerobic respiratory chain. J Bacteriol 175(10):3020-5.

Caplice E, Fitzgerald GF. 1999. Food fermentations: role of microorganisms in food production and preservation. Int J of Food Microbiol 50(1–2):131-149.

Canfield DE, Marais DJD. 1993. Biogeochemical Cycles of Carbon, Sulfur, and Free Oxygen in a Microbial Mat. Geochimica Et Cosmochimica Acta 57(16):3971-3984.

Carlson R, Srienc F. 2004. Fundamental Escherichia coli biochemical pathways for biomass and energy production: Identification of reactions. Biotechnology and Bioengineering 85(1):1-19.

Carlson R, Wlaschin A, Srienc F. 2005. Kinetic studies and biochemical pathway analysis of anaerobic poly-(R)-3-hydroxybutyric acid synthesis in Escherichia coli. Applied and Environmental Microbiology 71(2):713-720.

Carlson RP. 2007. Metabolic systems cost-benefit analysis for interpreting network structure and regulation. Bioinformatics 23(10):1258-1264.

Carlson RP. 2009. Decomposition of complex microbial behaviors into resource-based stress responses. Bioinformatics 25(1):90-97.

Carlson RP, Taffs R. 2009. Molecular level in silico analysis of mass and energy flows in microbial communities. Geochim Cosmochim Acta 73(13):A193-A193.

Carlson RP, Taffs RL. 2010. Molecular-level tradeoffs and metabolic adaptation to simultaneous stressors. Current opinion in biotechnology 21(5):670-6.

Characklis W, Cooksey K. 1983. Biofilms and microbial fouling. Adv Appl Microbiol 29:93-138.

Chisti Y. 2007a. Biodiesel from microalgae. Biotechnology Adv 25(3):294-306.

Chisti Y, Yan JY. 2011. Energy from algae: Current status and future trends algal biofuels - A status report. Appl Energy 88(10):3277-3279.

Christenson L, Sims R. 2011. Production and harvesting of microalgae for wastewater treatment, biofuels, and bioproducts. Biotechnol Adv 29(6):686-702.

Christenson LB, Sims RC. 2012. Rotating algal biofilm reactor and spool harvester for wastewater treatment with biofuels by-products. Biotechnology and Bioengineering 109(7):1674-1684.

Conrad TM, Joyce AR, Applebee MK, Barrett CL, Xie B, Gao Y, Palsson BO. 2009. Whole-genome resequencing of Escherichia coli K-12 MG1655 undergoing short-term laboratory evolution in lactate minimal media reveals flexible selection of adaptive mutations. Genome Biol 10(10):R118.

Converti A, Casazza AA, Ortiz EY, Perego P, Del Borghi M. 2009. Effect of temperature and nitrogen concentration on the growth and lipid content of Nannochloropsis oculata and Chlorella vulgaris for biodiesel production. Chem Eng Process: Process Intensification 48(6):1146-1151.

Cooper MS, Hardin WR, Petersen TW, Cattolico RA. 2010. Visualizing "green oil" in live algal cells. J. biosci bioeng 109(2):198-201.

Cowan SE, Gilbert E, Liepmann D, Keasling JD. 2000. Commensal interactions in a dual-species biofilm exposed to mixed organic compounds. Appl Environ Microbiol 66(10):4481-4485.

Crespi BJ. 2001. The evolution of social behavior in microorganisms. Trends Ecol Evol 16(4):178-183.

Cueto M, Jensen PR, Kauffman C, Fenical W, Lobkovsky E, Clardy J. 2001. Pestalone, a new antibiotic produced by a marine fungus in response to bacterial challenge. J Nat Prod 64(11):1444-1446.

Datsenko KA, Wanner BL. 2000. One-step inactivation of chromosomal genes in Escherichia coli K-12 using PCR products. Proc Natl Acad Sci U S A 97(12):6640-5.

Davis BD, Mingioli ES. 1950. Mutants of Escherichia-Coli Requiring Methionine or Vitamin-B12. Journal of Bacteriology 60(1):17-28.

de Beer D, Stoodley P, Roe F, Lewandowski Z. 1994. Effects of biofilm structures on oxygen distribution and mass-transport. Biotechnology and Bioengineering 43(11):1131-1138.

De Mazancourt C, Schwartz MW. 2010. A resource ratio theory of cooperation. Ecol Lett 13(3):349-359.

De Mey M, De Maeseneire S, Soetaert W, Vandamme E. 2007. Minimizing acetate formation in E-coli fermentations. Journal of Industrial Microbiology & Biotechnology 34(11):689-700.

DeLong JP. 2008. The maximum power principle predicts the outcomes of two-species competition experiments. Oikos 117(9):1329-1336.

Dias J, Oehmen A, Serafim L, Lemos P, Reis M, Oliveira R. 2008. Metabolic modelling of polyhydroxyalkanoate copolymers production by mixed microbial cultures. BMC Syst Biol 2(1):59.

Dittrich CR, Vadali RV, Bennett GN, San KY. 2005. Redistribution of metabolic fluxes in the central aerobic metabolic pathway of E. coli mutant strains with deletion of the ackA-pta and poxB pathways for the synthesis of isoamyl acetate. Biotechnol Prog 21(2):627-31.

Druschel GK, Emerson D, Sutka R, Suchecki P, Luther GW. 2008. Low-oxygen and chemical kinetic constraints on the geochemical niche of neutrophilic iron(II) oxidizing microorganisms. Geochimica Et Cosmochimica Acta 72(14):3358-3370.

Ducat DC, Avelar-Rivas JA, Way JC, Silver PA. 2012. Rerouting carbon flux to enhance photosynthetic productivity. Appl Environ Microbiol 78(8):2660-2668.

Ducat DC, Way JC, Silver PA. 2011. Engineering cyanobacteria to generate high-value products. Trends in biotechnology 29(2):95-103.

Egland PG, Palmer RJ, Jr., Kolenbrander PE. 2004. Interspecies communication in Streptococcus gordonii-Veillonella atypica biofilms: signaling in flow conditions requires juxtaposition. Proc Natl Acad Sci U S A 101(48):16917-22.

Eiteman MA, Altman E. 2006. Overcoming acetate in Escherichia coli recombinant protein fermentations. Trends Biotechnol 24(11):530-6.

Eiteman MA, Lee SA, Altman E. 2008. A co-fermentation strategy to consume sugar mixtures effectively. J Biol Eng 2:3.

Eiteman MA, Lee SA, Altman R, Altman E. 2009. A substrate-selective co-fermentation strategy with Escherichia coli produces lactate by simultaneously consuming xylose and glucose. Biotechnol Bioeng 102(3):822-7.

El-Mansi M, Stephanopoulos G, Carlson RP. 2011. Flux Control Analysis and Stoichiometric Network Modeling: Basic Principles and Industrial Applications. In: El-Mansi M, Bryce CFA, Demian AL, Allman AR, editors. ermentation Microbiology and Biotechnology: CRC/Taylor and Francis Inc. p 150-190.

Emerson D, Moyer CL. 2002. Neutrophilic Fe-oxidizing bacteria are abundant at the Loihi Seamount hydrothermal vents and play a major role in Fe oxide deposition. Applied and Environmental Microbiology 68(6):3085-3093.

Emerson D, Revsbech NP. 1994a. Investigation of an Iron-oxidizing microbial mat community located near Aarhus, Denmark: field studies. Appl Environ Microbiol 60(11):4022-31.

Emerson D, Revsbech NP. 1994b. Investigation of an iron-oxidizing microbial mat community located near Aarhus, Denmark: laboratory studies. Appl Environ Microbiol 60(11):4032-8.

Eustance E, Gardner RD, Moll KM, Menicucci J, Gerlach R, Peyton BM. 2013. Growth, nitrogen utilization and biodiesel potential for two chlorophytes grown on ammonium, nitrate or urea. J. Appl Phycol:1-15.

Farooq W, Lee Y-C, Ryu B-G, Kim B-H, Kim H-S, Choi Y-E, Yang J-W. 2013. Two-stage cultivation of two Chlorella sp. strains by simultaneous treatment of brewery wastewater and maximizing lipid productivity. Bioresour Technol 132(0):230-238.

Fong SS, Palsson BO. 2004. Metabolic gene-deletion strains of Escherichia coli evolve to computationally predicted growth phenotypes. Nat Genet 36(10):1056-8.

Freilich S, Zarecki R, Eilam O, Segal ES, Henry CS, Kupiec M, Gophna U, Sharan R, Ruppin E. 2011. Competitive and cooperative metabolic interactions in bacterial communities. Nat Commun 2:589.

Gardner R, Cooksey K, Mus F, Macur R, Moll K, Eustance E, Carlson R, Gerlach R, Fields M, Peyton B. 2012. Use of sodium bicarbonate to stimulate triacylglycerol accumulation in the chlorophyte Scenedesmus; sp. and the diatom Phaeodactylum tricornutum</i&gt. J Appl Phycol:1-10.

Gardner R, Peters P, Peyton B, Cooksey KE. 2011. Medium pH and nitrate concentration effects on accumulation of triacylglycerol in two members of the chlorophyta. J. Appl Phycol 23(6):1005-1016.

Gardner RD, Lohman E, Gerlach R, Cooksey KE, Peyton BM. 2013. Comparison of CO2 and bicarbonate as inorganic carbon sources for triacylglycerol and starch accumulation in Chlamydomonas reinhardtii. Biotechnology and Bioengineering 110(1):87-96.

Gilbert ES, Walker AW, Keasling JD. 2003. A constructed microbial consortium for biodegradation of the organophosphorus insecticide parathion. Applied Microbiology and Biotechnology 61(1):77-81.

Girvan MS, Campbell CD, Killham K, Prosser JI, Glover LA. 2005. Bacterial diversity promotes community stability and functional resilience after perturbation. Environ Microbiol 7(3):301-13.

Glud RN, Kühl M, Kohls O, Ramsing NB. 2002. Heterogeneity of oxygen production and consumption in a photosynthetic microbial mat as studied by planar optodes. Journal of Phycology 35(2):270-279.

Glud RN, Ramsing NB, Revsbech NP. 1992. Photosynthesis and photosynthesis-coupled respiration in natural biofilms quantified with oxygen microsensors. J. Phycol 28(1):51-60.

Glud RN, Ramsing NB, Revsbech NP. 2004. Photosyntesis and photosynthesis-coupled respiration in natural biofilms quantified with oxygen microsensors. Journal of Phycology 28(1):51-60.

Gore J, Youk H, van Oudenaarden A. 2009. Snowdrift game dynamics and facultative cheating in yeast. Nat Commun 459(7244):253-256.

Gross R, Hauer B, Otto K, Schmid A. 2007. Microbial biofilms: new catalysts for maximizing productivity of long-term biotransformations. Biotechnology and Bioengineering 98(6):1123-34.

Guckert JB, Cooksey KE. 1990. Triglyceride accumulation and fatty acid profile changes in Chlorella (Chlorophyta) during high pH-induced cell cycle inhibtion. J. Phycol 26(1):72-79.

Hall-Stoodley L, Costerton JW, Stoodley P. 2004. Bacterial biofilms: from the Natural environment to infectious diseases. Nat Rev Micro 2(2):95-108.

Hamamura N, Macur RE, Korf S, Ackerman G, Taylor WP, Kozubal M, Reysenbach AL, Inskeep WP. 2009. Linking microbial oxidation of arsenic with detection and phylogenetic analysis of arsenite oxidase genes in diverse geothermal environments. Environmental Microbiology 11(2):421-431.

Hamilton M. 2003. The Biofilm Laboratory Step-By-Step Protocols for Experimental Design, Analysis, and Data Interpretation. Hamilton M, Heerisink J, Buckingham-Meyer K, Goeres D, editors. Bozeman MT: Cytergy Publishing.

Handelsman J, Rondon MR, Brady SF, Clardy J, Goodman RM. 1998. Molecular biological access to the chemistry of unknown soil microbes: a new frontier for natural products. Chem Biol 5(10):R245-R249.

Hanly TJ, Henson MA. 2011. Dynamic flux balance modeling of microbial co-cultures for efficient batch fermentation of glucose and xylose mixtures. Biotechnol Bioeng 108(2):376-385.

Herigstad B, Hamilton M, Heersink J. 2001. How to optimize the drop plate method for enumerating bacteria. J Microbiol Methods 44(2):121-9.

Holmes EE, Lewis MA, Banks JE, Veit RR. 1994. Partial-differential equations in ecology - spatial interactions and population-dynamics. Ecology 75(1):17-29.

Hu Q, Sommerfeld M, Jarvis E, Ghirardi M, Posewitz M, Seibert M, Darzins A. 2008. Microalgal triacylglycerols as feedstocks for biofuel production: perspectives and advances. The Plant J. 54(4):621-639.

Hua Q, Yang C, Baba T, Mori H, Shimizu K. 2003. Responses of the central metabolism in Escherichia coli to phosphoglucose isomerase and glucose-6-phosphate dehydrogenase knockouts. J Bacteriol 185(24):7053-67.

Ibarra RU, Edwards JS, Palsson BO. 2002. Escherichia coli K-12 undergoes adaptive evolution to achieve in silico predicted optimal growth. Nature 420(6912):186-9.

Inskeep WP, Ackerman GG, Taylor WP, Kozubal M, Korf S, Macur RE. 2005. On the energetics of chemolithotrophy in nonequilibrium systems: case studies of geothermal springs in Yellowstone National Park. Geobiology 3(4):297-317.

Inskeep WP, Macur RE, Harrison G, Bostick BC, Fendorf S. 2004. Biomineralization of As(V)-hydrous ferric oxyhydroxide in microbial mats of an acid-sulfate-chloride geothermal spring, Yellowstone National Park. Geochimica Et Cosmochimica Acta 68(15):3141-3155.

Inskeep WP, McDermott TR. 2005. Geomicrobiology of acidsulfate-chloride springs in Yellowstone National Park. Inskeep WP, McDermott TR, editors. Bozeman, MT: Montana State University.

Inskeep WP, Rusch DB, Jay ZJ, Herrgard MJ, Kozubal MA, Richardson TH, Macur RE, Hamamura N, Jennings RD, Fouke BW and others. 2010. Metagenomes from high-temperature chemotrophic systems reveal geochemical controls on microbial community structure and function. Plos One 5(3).

Jackson CR, Langner HW, Donahoe-Christiansen J, Inskeep WP, McDermott TR. 2001. Molecular analysis of microbial community structure in an arsenite-oxidizing acidic thermal spring. Environmental Microbiology 3(8):532-542.

Jay ZJ, Planer-Friedrich B, Rusch DB, Inskeep WP. Linking geochemistry to microbial community structure and function in sulfidic geothermal systems of Yellowstone National Park; 2011; Prague, Czech Rep. Mineralogical Magazine. p 1104.

Jensen J, Revsbech NP. 1989. Photosynthesis and respiration of a diatom biofilm cultured in a new gradient growth chamber. FEMS Microbiol Lett 62(1):29-38.

Jorgensen BB, Marais DJD. 1990. The diffusive boundary layer of sediments: oxygen microgradients over a microbial mat. Limnol Oceanograph 35(6):1343-1355.

Jorgensen BB, Revsbech NP. 1985. Diffusive boundary layers and the oxygen uptake of sediments and detritus. Limnol Oceanograph 30(1):111-122.

Jorgensen BB, Revsbech NP, Blackburn TH, Cohen Y. 1979. Diurnal Cycle of Oxygen and Sulfide Microgradients and Microbial Photosynthesis in a Cyanobacterial Mat Sediment. Applied and Environmental Microbiology 38(1):46-58.

Joset-Espardellier F, Astier C, Evans E, Carr N. 2006. Cyanobacteria grown under photoautotrophic, photoheterotrophic, and heterotrophic regimes: sugar metabolism and carbon dioxide fixation. FEMS Microbiology Letters 4(5):261-264.

Kapley A, Purohit HJ, Chhatre S, Shanker R, Chakrabarti T, Khanna P. 1999. Osmotolerance and hydrocarbon degradation by a genetically engineered microbial consortium. Bioresour Technol 67(3):241-245.

Kappler U, Sly LI, McEwan AG. 2005. Respiratory gene clusters of Metallosphaera sedula – differential expression and transcriptional organization. Microbiology 151(1):35-43.

Karel SF, Robertson CR. 1987. Reaction-rate calculations for cosubstrates diffusing into catalyst layer from opposite sides. Biotechnology and Bioengineering 30(3):427-438.

Kato S, Haruta S, Cui ZJ, Ishii M, Igarashi Y. 2008. Network relationships of bacteria in a stable mixed culture. Microb Ecol 56(3):403-11.

Kim HJ, Boedicker JQ, Choi JW, Ismagilov RF. 2008. Defined spatial structure stabilizes a synthetic multispecies bacterial community. Proc Natl Acad Sci USA 105(47):18188-18193.

Kinnersley MA, Holben WE, Rosenzweig F. 2009. E Unibus Plurum: genomic analysis of an experimentally evolved polymorphism in Escherichia coli. PLoS Genet 5(11):e1000713.

Klamt S, Stelling J, Ginkel M, Gilles ED. 2003. FluxAnalyzer: exploring structure, pathways, and flux distributions in metabolic networks on interactive flux maps. Bioinformatics 19(2):261-269.

Klein AH, Shulla A, Reimann SA, Keating DH, Wolfe AJ. 2007. The intracellular concentration of acetyl phosphate in Escherichia coli is sufficient for direct phosphorylation of two-component response regulators. Journal of Bacteriology 189(15):5574-5581.

Klitgord N, Segrè D. 2010. Environments that Induce Synthetic Microbial Ecosystems. PLoS Comput Biol 6(11):e1001002.

Klitgord N, Segrè D. 2011. Ecosystems biology of microbial metabolism. Curr Opin Biotechnol 22(4):541-546.

Kneitel JM, Chase JM. 2004. Trade-offs in community ecology: linking spatial scales and species coexistence. Ecol Lett 7(1):69-80.

Kondo S, Miura T. 2010. Reaction-Diffusion Model as a Framework for Understanding Biological Pattern Formation. Science 329(5999):1616-1620.

Konhauser KO. 1998. Diversity of bacterial iron mineralization. Earth-Science Reviews 43(3-4):91-121.

Kozubal M, Macur RE, Korf S, Taylor WP, Ackerman GG, Nagy A, Inskeep WP. 2008. Isolation and distribution of a novel iron-oxidizing crenarchaeon from acidic geothermal springs in Yellowstone National Park. Applied and Environmental Microbiology 74(4):942-9.

Kozubal M, Romine M, Jennings R, Jay ZJ, Tringe SG, Rusch DB, Beam JP, McCue L, Inskeep* WP. 2012a. Deeply-rooted archaeal lineage discovered in high-temperature acidic iron mats supports the importance of oxygen in the early evolution of Archaea. ISM, 2013.

Kozubal MA, Dlakic M, Macur RE, Inskeep WP. 2011. Terminal oxidase diversity and function in "Metallosphaera yellowstonensis": gene expression and protein modeling suggest mechanisms of Fe(II) oxidation in the Sulfolobales. Applied and Environmental Microbiology 77(5):1844-1853.

Kozubal MA, Macur RE, Jay ZJ, Beam JP, Malfatti SA, Tringe SG, Kocar BD, Borch T, Inskeep WP. 2012b. Microbial iron cycling in acidic geothermal springs of yellowstone national park: integrating molecular surveys, geochemical processes, and isolation of novel fe-active microorganisms. Frontiers in microbiology 3:109.

Kuhl M, Glud RN, Ploug H, Ramsing NB. 1996. Microenvironmental control of photosynthesis and photosynthesis-coupled respiration in an epilithic cyanobacterial biofilm. J. Phycol 32(5):799-812.

Langner HW, Jackson CR, Mcdermott TR, Inskeep WP. 2001. Rapid oxidation of arsenite in a hot spring ecosystem, Yellowstone National Park. Environmental Science & Technology 35(16):3302-3309.

Lasko DR, Zamboni N, Sauer U. 2000. Bacterial response to acetate challenge: a comparison of tolerance among species. Applied Microbiology and Biotechnology 54(2):243-247.

Lassen C, Glud RN, Ramsing NB, Revsbech NP. 1998. A method to improve the spatial resolution of photosynthetic rates obtained by oxygen microsensors. J. Phycol 34(1):89-93.

Law R. 1979. Optimal life histories under age-specific predation. American Naturalist 114(3):399-417.

Lee PR, Ong YL, Yu B, Curran P, Liu SQ. 2010. Profile of volatile compounds during papaya juice fermentation by a mixed culture of Saccharomyces cerevisiae and Williopsis saturnus. Food Microbiol 27(7):853-861.

Lin WC, Coppi MV, Lovley DR. 2004. Geobacter sulfurreducens can grow with oxygen as a terminal electron acceptor. Appl Environ Microbiol 70(4):2525-2528.

Loeppert RH, Inskeep WP. 1996. Methods of soil analysis: part 3-chemical methods. Sparks DL, editor: Soil Science Society of America, Inc. and American Society of Agronomy, Inc., 677 South Segoe Road, Madison, WI 53711 USA.

Lohman EJ, Gardner, Halverson L, Macure RE, Peyton BM, Gerlach R. in-press. An efficient and scalable extraction and quantification method for algal derived biofuel. Journal of Microbiological Methods.

Lotka AJ. 1922a. Contribution to the energetics of evolution. Proc Natl Acad Sci USA 8(6):147-151.

Lotka AJ. 1922b. Natural selection as a physical principle. Proc Natl Acad Sci USA 8(6):151-154.

Macur RE, Langner HW, Kocar BD, Inskeep WP. 2004. Linking geochemical processes with microbial community analysis: successional dynamics in an arsenic-rich, acid-sulphate-chloride geothermal spring. Geobiology 2(3):163-177.

Majewski RA, Domach MM. 1990. Simple Constrained-Optimization View of Acetate Overflow in Escherichia-Coli. Biotechnology and Bioengineering 35(7):732-738.

McCleary WR, Stock JB, Ninfa AJ. 1993. Is acetyl phosphate a global signal in Escherichia coli? J Bacteriol 175(10):2793-8.

McInerney MJ, Sieber JR, Gunsalus RP. 2009. Syntrophy in anaerobic global carbon cycles. Current opinion in biotechnology 20(6):623-32.

McMahon KD, Martin HG, Hugenholtz P. 2007. Integrating ecology into biotechnology. Curr Opin Biotechnol 18(3):287-92.

Meyer-Dombard DR, Shock EL, Amend JP. 2005. Archaeal and bacterial communities in geochemically diverse hot springs of Yellowstone National Park, USA. Geobiology 3(3):211-227.

Miller JH. 1972. Experiments in molecular genetics. Cold Spring Harbor, N.Y.: Cold Spring Harbor Laboratory. xvi, 466 p. p.

Miller JH. 1992. A Short Course in Bacterial Genetics: A Laboratory Manual and Handbook for Escherichia coli and Related Bactera. Cold Spring Harbor, NY: Cold Spring Harbor Laboratory.

Miller TE, Burns JH, Munguia P, Walters EL, Kneitel JM, Richards PM, Mouquet N, Buckley HL. 2005. A critical review of twenty years' use of the resource ratio theory. American Naturalist 165(4):439-448.

Minty JJ, Lin X. Engineering A Synthetic Microbial Consortium for Efficient Production of Biofuels. Advances in Metabolic Engineering and Bioinformatics-Biofuels; 2010 November 10, 2010; Salt Lake City. AICHE.

Momeni B, Chen C-C, Hillesland K, Waite A, Shou W. 2011. Using artificial systems to explore the ecology and evolution of symbioses. Cell Mol Life Sci 68(8):1353-1368.

Mus F, Toussaint J-P, Cooksey KE, Fields MW, Gerlach R, Peyton BM, Carlson RP. 2013. Physiological and molecular analysis of carbon source supplementation and pH stress-induced lipid accumulation in the marine diatom Phaeodactylum tricornutum. Appl Microbiol Biotechnol:1-18.

Nevin KP, Zhang P, Franks AE, Woodard TL, Lovley DR. 2011. Anaerobes unleashed: Aerobic fuel cells of Geobacter sulfurreducens. J Power Sources 196(18):7514-7518.

Nicolaou SA, Gaida SM, Papoutsakis ET. 2010. A comparative view of metabolite and substrate stress and tolerance in microbial bioprocessing: From biofuels and chemicals, to biocatalysis and bioremediation. Metab Eng 12(4):307-31.

Niederholtmeyer H, Wolfstadter BT, Savage DF, Silver PA, Way JC. 2010. Engineering cyanobacteria to synthesize and export hydrophilic products. Appl Environ Microbiol 76(11):3462-6.

Nold SC, Ward DM. 1996. Photosynthate partitioning and fermentation in hot spring microbial mat communities. Applied and Environmental Microbiology 62(12):4598-4607.

Ogren WL. 1984. Photorespiration: pathways, regulation, and modification. Annu Rev Plant Physiol 35(1):415-442.

Ordog V, Stirk WA, Lenobel R, Bancirova M, Strnad M, van Staden J, Szigeti J, Nemeth L. 2004. Screening microalgae for some potentially useful agricultural and pharmaceutical secondary metabolites. J. Appl Phycol 16(4):309-314.

Orth JD, Thiele I, Palsson BO. 2010. What is flux balance analysis? Nat Biotech 28(3):245-248.

Ozkan A, Kinney K, Katz L, Berberoglu H. 2012. Reduction of water and energy requirement of algae cultivation using an algae biofilm photobioreactor. Bioresour Technol 114(0):542-548.

Park J, Kerner A, Burns MA, Lin XN. 2011. Microdroplet-enabled highly parallel co-cultivation of microbial communities. PLoS ONE 6(2):e17019.

Pfeiffer T, Sanchez-Valdenebro I, Nuno JC, Montero F, Schuster S. 1999. METATOOL: for studying metabolic networks. Bioinformatics 15(3):251-257.

Pokoo-Aikins G, Nadim A, El-Halwagi M, Mahalec V. 2010. Design and analysis of biodiesel production from algae grown through carbon sequestration. Clean Technol Environ Pol 12(3):239-254.

Pósfai G, Koob MD, Kirkpatrick HA, Blattner FR. 1997. Versatile insertion plasmids for targeted genome manipulations in bacteria: isolation, deletion, and rescue of the pathogenicity island LEE of the Escherichia coli O157:H7 genome. Journal of Bacteriology 179(13):4426-8.

Qu Y, Feng Y, Wang X, Logan BE. 2012. Using a co-culture to enable current production by Geobacter sulfurreducens. Appl Environ Microbiol.

Rawlings DE. 2002. Heavy metal mining using microbes. Annual Review of Microbiology 56:65-91.

Rawlings DE, Johnson DB. 2007. The microbiology of biomining: development and optimization of mineral-oxidizing microbial consortia. Microbiology 153(2):315-324.

Ren Z, Ward TE, Regan JM. 2007. Electricity Production from Cellulose in a Microbial Fuel Cell Using a Defined Binary Culture. Environ Sci Technol 41(13):4781-4786.

Revsbech NP. 1989. An oxygen microsensor with a guard cathode. Limnol Oceanograph 34(2):474-478.

Revsbech NP, Jorgensen BB. 1986. Microelectrodes - their use in microbial ecology. Adv Microb Ecol 9:293-352.

Revsbech NP, Jorgensen BB, Blackburn TH, Cohen Y. 1983. Microelectrode studies of the photosynthesis and O2, H2S, and pH profiles of a microbial mat. Limnol Oceanograph 28(6):1062-1074.

Rosche B, Li XZ, Hauer B, Schmid A, Buehler K. 2009. Microbial biofilms: a concept for industrial catalysis? Trends Biotechnol 27(11):636-643.

Rosenzweig RF, Sharp RR, Treves DS, Adams J. 1994. Microbial Evolution in a Simple Unstructured Environment - Genetic Differentiation in Escherichia-Coli. Genetics 137(4):903-917.

Roth JR, Lawrence JG, Bobik TA. 1996. Cobalamin (coenzyme B-12): Synthesis and biological significance. Annual Review of Microbiology 50:137-181.

Sabra W, Dietz D, Tjahjasari D, Zeng AP. 2010. Biosystems analysis and engineering of microbial consortia for industrial biotechnology. Engineering in Life Sciences 10(5):407-421.

Sambrook J, Russell DW. 2001. Molecular cloning : a laboratory manual. Cold Spring Harbor, N.Y.: Cold Spring Harbor Laboratory Press.

Schuster S, Dandekar T, Fell DA. 1999. Detection of elementary flux modes in biochemical networks: a promising tool for pathway analysis and metabolic engineering. Trends Biotechnol 17(2):53-60.

Sciubba E. 2011. What did Lotka really say? A critical reassessment of the "maximum power principle". Ecol Modell 222(8):1347-1353.

Senousy HH, Beakes GW, Hack E. 2004. Phylogenetic placement of Botryococcus braunii (Trebouxiophyceae and Botryococcus sudeticus isolate UTEX 2629 (Chlorophyceae). J. Phycol 40(2):412-423.

Shou W, Ram S, Vilar JMG. 2007. Synthetic cooperation in engineered yeast populations. Proc Natl Acad Sci USA 104(6):1877-1882.

Singer PC, Stumm W. 1970. Acidic mine drainage . rate-determining step. Science 167(3921):1121-&.

Sobolev D, Roden EE. 2001. Suboxic deposition of ferric iron by bacteria in opposing gradients of Fe(II) and oxygen at circumneutral pH. Appl Environ Microbiol 67(3):1328-34.

Stephenson AL, Dennis JS, Howe CJ, Scott SA, Smith AG. 2010. Influence of nitrogen-limitation regime on the production by Chlorella vulgaris of lipids for biodiesel feedstocks. Biofuels 1(1):47-58.

Stevens SE, Patterso.Co, Myers J. 1973. Production of Hydrogen-Peroxide by Blue-Green-Algae - Survey. Journal of Phycology 9(4):427-430.

Stewart PS. 1998. A review of experimental measurements of effective diffusive permeabilities and effective diffusion coefficients in biofilms. Biotechnol Bioeng 59(3):261-272.

Stewart PS. 2003. Diffusion in biofilms. J Bacteriol 185(5):1485-91.

Stewart PS, Franklin MJ. 2008. Physiological heterogeneity in biofilms. Nat Rev Microbiol 6(3):199-210.

Stewart PS, Raquepas JB. 1995. Implications of reaction-diffusion theory for the disinfection of microbial biofilms by reactive antimicrobial agents. Chemical Engineering Science 50(19):3099-3104.

Stolyar S, Van Dien S, Hillesland KL, Pinel N, Lie TJ, Leigh JA, Stahl DA. 2007. Metabolic modeling of a mutualistic microbial community. Mol Syst Biol 3.

Stookey LL. 1970. Ferrozine---a new spectrophotometric reagent for iron. Analytical Chemistry 42(7):779-781.

Swenson W, Arendt J, Wilson DS. 2000a. Artificial selection of microbial ecosystems for 3-chloroaniline biodegradation. Environ Microbiol 2(5):564-571.

Swenson W, Wilson DS, Elias R. 2000b. Artificial ecosystem selection. Proc Natl Acad Sci USA 97(16):9110-9114.

Taffs R, Aston J, Brileya K, Jay Z, Klatt C, McGlynn S, Mallette N, Montross S, Gerlach R, Inskeep W and others. 2009a. In silico approaches to study mass and energy flows in microbial consortia: a syntrophic case study. BMC Sys Biol 3(1):114.

Takahashi H, Miyake M, Tokiwa Y, Asada Y. 1998. Improved accumulation of poly-3-hydroxybutyrate by a recombinant cyanobacterium. Biotechnology Letters 20(2):183-186.

Terzer M, Stelling J. 2006. Accelerating the Computation of Elementary Modes Using Pattern Trees

Algorithms in Bioinformatics. In: Bücher P, Moret B, editors: Springer Berlin / Heidelberg. p 333-343.

Terzer M, Stelling J. 2008. Large-scale computation of elementary flux modes with bit pattern trees. Bioinformatics 24(19):2229-2235.

Thiele EW. 1939. Relation between catalytic activity and size of particle. Industrial and Engineering Chemistry 31:916-920.

Tilman D. 1982. Resource competition and community structure. Princeton, N.J.: Princeton University Press. xi, 296 p. p.

Trinh CT, Carlson R, Wlaschin A, Srienc F. 2006. Design, construction and performance of the most efficient biomass producing E-coli bacterium. Metabolic Engineering 8(6):628-638.

Trinh CT, Unrean P, Srienc F. 2008. Minimal Escherichia coli cell for the most efficient production of ethanol from hexoses and pentoses. Applied and Environmental Microbiology 74(12):3634-3643.

Tzamali E, Reczko M. The benefit of cooperation: Identifying growth-efficient interacting strains of Escherichia coli using metabolic flux balance models; 2008 8-10 Oct. 2008. p 1-6.

Uduman N, Qi Y, Danquah MK, Forde GM, Hoadley A. 2010. Dewatering of microalgal cultures: A major bottleneck to algae-based fuels. J Renew Sustain Energy 2(1).

Unden G, Bongaerts J. 1997. Alternative respiratory pathways of Escherichia coli: energetics and transcriptional regulation in response to electron acceptors. Biochimica et Biophysica Acta-Bioenergetics-Including Reviews on Bioenergetics 1320(3):217-234.

Unrean P, Srienc F. 2010. Continuous production of ethanol from hexoses and pentoses using immobilized mixed cultures of Escherichia coli strains. J of Biotechnol 150(2):215-223.

Valenzuela J, Mazurie A, Carlson RP, Gerlach R, Cooksey KE, Peyton BM, Fields MW. 2012. Potential role of multiple carbon fixation pathways during lipid accumulation in Phaeodactylum tricornutum. Biotechol biofuels 5(1):40.

Van Baalen C. 1962. Studies on Marine Blue-Green Algae. Botanica Marina. p 129.

Vazquez-Duhalt R, Greppin H. 1987. Growth and production of cell constituents in batch cultures of< i> botryococcus sudeticus</i>. Phytochem 26(4):885-889.

Vu TT, Stolyar SM, Pinchuk GE, Hill EA, Kucek LA, Brown RN, Lipton MS, Osterman A, Fredrickson JK, Konopka AE. 2012. Genome-scale modeling of light-driven reductant partitioning and carbon fluxes in diazotrophic unicellular cyanobacterium Cyanothece sp. ATCC 51142. PLoS computational biology 8(4):e1002460.

Wagner M, Loy A. 2002. Bacterial community composition and function in sewage treatment systems. Curr Opin Biotechnol 13(3):218-227.

Walters MC, Roe F, Bugnicourt A, Franklin MJ, Stewart PS. 2003. Contributions of antibiotic penetration, oxygen limitation, and low metabolic activity to tolerance of Pseudomonas aeruginosa biofilms to ciprofloxacin and tobramycin. Antimicrobial Agents and Chemotherapy 47(1):317-323.

Ward DM, Bateson MM, Ferris MJ, Kühl M, Wieland A, Koeppel A, Cohan FM. 2006. Cyanobacterial ecotypes in the microbial mat community of Mushroom Spring (Yellowstone National Park, Wyoming) as species-like units linking microbial community composition, structure and function. Philosophical Transactions of the Royal Society B: Biological Sciences 361(1475):1997-2008.

Watanabe K. 2001. Microorganisms relevant to bioremediation. Curr Opin Biotechnol 12(3):237-241.

Wilhelm SW, Trick CG. 1995. Effects of Vitamin-B-12 Concentration on Chemostat Cultured Synechococcus Sp Strain Pcc-7002. Canadian Journal of Microbiology 41(2):145-151.

Wilke CR, Chang P. 1955. Correlation of diffusion coefficients in dilute solutions. Aiche Journal 1(2):264-270.

Williamson K, Mccarty PL. 1976. Model of substrate utilization by bacterial films. Journal Water Pollution Control Federation 48(1):9-24.

Wimpenny JWT, Colasanti R. 1997. A unifying hypothesis for the structure of microbial biofilms based on cellular automaton models. FEMS Microbiol Ecol 22(1):1-16.

Wintermute EH, Silver PA. 2010a. Dynamics in the mixed microbial concourse. Genes Dev 24(23):2603-14.

Wintermute EH, Silver PA. 2010b. Emergent cooperation in microbial metabolism. Mol Syst Biol 6:407.

Wolfe AJ. 2005. The acetate switch. Microbiology and Molecular Biology Reviews 69(1):12-+.

Xu KD, Stewart PS, Xia F, Huang CT, McFeters GA. 1998. Spatial physiological heterogeneity in Pseudomonas aeruginosa biofilm is determined by oxygen availability. Appl Environ Microbiol 64(10):4035-9.

Xu L, Tschirner U. 2011. Improved ethanol production from various carbohydrates through anaerobic thermophilic co-culture. Bioresour Technol 102(21):10065-10071.

Yang YT, Aristidou AA, San KY, Bennett GN. 1999. Metabolic flux analysis of Escherichia coli deficient in the acetate production pathway and expressing the Bacillus subtilis acetolactate synthase. Metab Eng 1(1):26-34.

Zeidan AA, Radstrom P, van Niel EWJ. 2010. Stable coexistence of two Caldicellulosiruptor species in a de novo constructed hydrogen-producing co-culture. Microbial Cell Factories 9.

Zhang J, Hu B. 2012. A novel method to harvest microalgae via co-culture of filamentous fungi to form cell pellets. Bioresour Technol 114(0):529-535.

Zhuang K, Izallalen M, Mouser P, Richter H, Risso C, Mahadevan R, Lovley DR. 2011. Genome-scale dynamic modeling of the competition between Rhodoferax and Geobacter in anoxic subsurface environments. ISME J 5(2):305-316.

Zomorrodi AR, Maranas CD. 2012. OptCom: a multi-level optimization framework for the metabolic modeling and analysis of microbial communities. PLoS Comput Biol 8(2):e1002363.

Zuroff TR, Bernstein H, Lloyd-Randolfi J, Jimenez-Taracido L, Stewart PS, Carlson RP. 2010. Robustness analysis of culturing perturbations on Escherichia coli colony biofilm beta-lactam and aminoglycoside antibiotic tolerance. BMC Microbiol 10:185.

Zuroff TR, Curtis WR. 2012. Developing symbiotic consortia for lignocellulosic biofuel production. Applied Microbiology and Biotechnology 93(4):1423-35.